NASA Technical Paper 1233

Static Aerodynamic Characteristics of a Winged Single-Stage-to-Orbit Vehicle at Mach Numbers From 0.3 to 4.63

Delma C. Freeman, Jr., and Roger H. Fournier

AUGUST 1978

NASA

NASA Technical Paper 1233

Static Aerodynamic Characteristics of a Winged Single-Stage-to-Orbit Vehicle at Mach Numbers From 0.3 to 4.63

Delma C. Freeman, Jr., and Roger H. Fournier
Langley Research Center
Hampton, Virginia

NASA
National Aeronautics
and Space Administration

Scientific and Technical
Information Office

1978

SUMMARY

An investigation has been conducted in the Langley 8-foot transonic pressure tunnel and the Langley Unitary Plan wind tunnel to determine the longitudinal and lateral-directional aerodynamic characteristics of a winged single-stage-to-orbit vehicle. The model was tested over a Mach number range from 0.3 to 4.63 for an angle-of-attack range from -4° to 30° at both 0° and 5° sideslip. Tests were made to determine the static longitudinal stability and trim, the static lateral-directional stability, the aileron control effectiveness, and the base pressures of the model.

The results of the investigation showed the model had a pitch-up at an angle of attack of 12° for all Mach numbers below 1.2. For the supersonic Mach numbers the variation of pitching moment with lift coefficient was linear. Large elevon deflections were required to trim the model at transonic and low supersonic Mach numbers, and the subsonic trimmed lift-drag ratio was low. The model exhibited directional stability at low Mach numbers, but at Mach numbers of 0.9 and 1.2 the model became unstable throughout the test angle-of-attack range for the supersonic Mach numbers. The aileron control effectiveness was nonlinear with angle of attack at subsonic and transonic Mach numbers and generated adverse yaw for all test conditions.

INTRODUCTION

The Space Shuttle Program is currently in the final development stages, and initial flight tests have been completed. Studies project that a follow-on earth orbital transportation system could be required in the 1995 timeframe, provided that this new system offers significant cost/performance advantages over the then current system. Based upon these projections there is a continuing effort within NASA to study these advanced transportation systems. (See ref. 1.)

A vertical take-off and horizontal landing concept has evolved and is of interest because of potential weight savings associated with some unique structures and systems design techniques incorporated in the vehicle (refs. 1 and 2). In this approach the primary structural arrangement provides an efficient, lightweight design for accommodating propellant and subsystems, crew and payload compartment, and for reacting loads from the engines, aerodynamic surfaces, and landing gear. The fuselage structure consists of aluminum tanks and advanced composite nontank shells. The wing, fin, and thrust structures use advanced composite materials (ref. 2).

Tests were conducted on a model of this vehicle design over the subsonic, transonic, and supersonic Mach number range for angles of attack from -4^{o} to 30^{o}. Results include the static longitudinal stability and trim, the static lateral-directional stability, aileron control effectiveness, and the base pressures of the model. The results of these tests are presented herein.

SYMBOLS

The longitudinal data are referred to the stability system of axes, and the lateral-directional data are referred to the body system of axes. (See fig. 1.) The moment center was located at 71 percent of the body length as indicated in figure 2.

b	reference wing span, 45.54 cm
C_D	drag coefficient, $\frac{\text{Drag}}{qS}$
C_L	lift coefficient, $\frac{\text{Lift}}{qS}$
C_{L_α}	lift-curve slope, per deg
C_l	rolling-moment coefficient, $\frac{M_X}{qSb}$
C_{l_β}	$= \frac{\Delta C_l}{\Delta \beta}$, $\beta = 0^{o}$ and 5^{o}
$C_{l_{\delta_a}}$	$= \frac{\Delta C_l}{\Delta \delta_a}$, per deg
C_m	pitching-moment coefficient, $\frac{M_Y}{qS\ell}$
$C_{m,0}$	pitching-moment coefficient at $C_L = 0$
C_n	yawing-moment coefficient, $\frac{M_Z}{qSb}$

C_{n_β} $= \frac{\Delta C_n}{\Delta \beta}$, $\beta = 0^o$ and 5^o

$C_{n_{\delta_a}}$ $= \frac{\Delta C_n}{\Delta \delta_a}$, per deg

$C_{p,b}$ base pressure coefficient, $\frac{p_\infty - p_b}{q}$

C_Y side-force coefficient, $\frac{\text{Side force}}{qS}$

C_{Y_β} $= \frac{\Delta C_Y}{\Delta \beta}$, $\beta = 0^o$ and 5^o

$C_{Y_{\delta_a}}$ $= \frac{\Delta C_Y}{\Delta \delta_a}$, per deg

D drag force, N

L lift force, N

ℓ reference body length, 54.22 cm

M_X rolling moment, m-N

M_Y pitching moment, m-N

M_Z yawing moment, m-N

p_b base pressure, Pa

p_∞ free-stream static pressure, Pa

q dynamic pressure, Pa

R Reynolds number based on body length

S	reference wing area, 0.064 m^2
X,Y,Z	body reference axes
y	spanwise distance from vehicle center line, cm
α	angle of attack, deg
β	angle of sideslip, deg
δ_a	$= \frac{\delta_{e,r} - \delta_{e,\ell}}{2}$
δ_e	elevon deflection, positive when trailing edge is down, deg

Subscripts:

b	base
ℓ	left
r	right
s	stability axes

Model components:

B	body
V	vertical tail
W	wing

MODEL AND APPARATUS

A drawing of the 0.01-scale model used in the investigation is presented in figure 2. The model is a distinct wing body design having a swept wing with an aft vertical tail, a rudder on the vertical tail, and elevon surfaces on the wing. The flat-bottom wing section

had a 10-percent constant thickness ratio. (See ref. 2.) Photographs of the model are presented in figure 3.

The experimental results were obtained in the Langley 8-foot transonic pressure tunnel and in the Langley Unitary Plan wind tunnel. Data were obtained over a Mach number range from 0.3 to 1.2 in the 8-foot tunnel and from 2.36 to 4.63 in the Unitary Plan tunnel. The operating characteristics of both facilities are presented in reference 3.

TESTS

Static wind-tunnel tests were conducted to determine the longitudinal stability and trim, the lateral-directional stability and control, and the base pressures of the model over a Mach number range from 0.3 to 4.63. For the subsonic and transonic Mach numbers (0.3 to 1.2) the model was tested over an angle-of-attack range from approximately -2° to 21°, and for the supersonic Mach numbers (M = 2.36 to 4.63) the angle-of-attack range was from approximately -4° to 30°. The static lateral-directional stability characteristics were determined from incremental differences in C_n, C_l, and C_Y measured over the angle-of-attack range at fixed angles of sideslip of 0° and 5°. The test conditions were as follows:

Mach number	Dynamic pressure, Pa	Stagnation temperature, K	Reynolds number
0.3	5.98	---	3.25×10^6
.6	20.01	---	5.66
.9	34.04	---	7.08
1.2	21.11	---	3.77
2.36	21.45	339	3.56
2.86	18.91	339	3.56
3.95	14.22	339	3.56
4.63	11.16	339	3.56

For all tests, boundary-layer transition strips were applied to the model in the form of bands of sparsely distributed carborundum grains, 0.16 cm wide, located 1.27 cm streamwise from the leading edge of all lifting surfaces and 3.05 cm aft of the nose. The size of the carborundum grains, determined using the sizing methods of reference 4 and used in the tests at the various Mach numbers, is presented in the following table:

Mach number	Grain size
0.3 to 1.2	No. 120
2.36 to 4.63	No. 45

Angles of attack have been adjusted for tunnel airflow misalignment and model deflection due to aerodynamic loads. All drag data represent total drag in that the base pressure has not been subtracted out.

INDEX OF RESULTS

An outline of the contents of the figures presented in this report follows:

RESULTS AND DISCUSSION

Static Longitudinal Stability Characteristics

The static longitudinal stability characteristics and elevon effectiveness of the model over the test Mach number range from 0.3 to 4.63 are presented in figures 4 to 19. Summary plots of various parameters as a function of Mach number are presented in figure 20.

Longitudinal stability.- The static longitudinal stability characteristics of the body and wing-body combination for zero elevon deflection are presented in figures 4 to 11. These results show that the body alone was unstable at a moment center of 0.71ℓ with the aerodynamic center of pressure located at approximately 37 percent of the body length for a Mach number of 0.3, at 41 percent for a Mach number of 1.2, and at 51 percent for all of the supersonic Mach numbers. These center-of-pressure locations are consistent with the results of reference 5 which are for somewhat similar blunt bodies. The addition of the small wing to the body had a stabilizing effect at the lower lift coefficients throughout the test Mach number range, but for all Mach numbers below 1.2 the wing-body combination has a nonlinear variation of pitching moment with lift coefficient resulting in a serious pitch-up at an angle of attack as low as 8°. For the supersonic Mach numbers the variation of pitching moment with lift coefficient is linear and the model exhibited neutral stability or slight instability for the test moment center (0.71ℓ). The reason for the nonlinearity in the pitching-moment curve at subsonic and transonic speeds is the high sweep of the wing quarter chord. This highly swept wing causes separation on the outboard wing panels resulting in a nose-up moment. This characteristic is described in reference 6.

The results of tests to determine the elevon effectiveness and longitudinal trim characteristics are presented in figures 12 to 19. Presented in figure 20(a) is C_m/C_L for several angles of attack as a function of Mach number. These results show that at an angle of attack of 10° the model is quite unstable at subsonic Mach numbers and approaches neutral stability through the rest of the Mach number range. These instabilities at the higher angles of attack at transonic and subsonic conditions are the results of the pitch-up previously discussed. The variation of lift-curve slope at various angles of attack is presented as a function of Mach number in figure 20(b). These results show the characteristic increase in C_{L_α} as transonic Mach numbers are approached. At supersonic speeds there is a decrease in C_{L_α} as Mach number increases except at $\alpha = 20^{\circ}$ where stall greatly decreased the slope at subsonic and transonic Mach numbers.

The elevon deflection required for trim at various angles of attack is presented as a function of Mach number in figure 20(c). Since the maximum negative elevon deflection of 20° was not sufficient to trim the model over the entire Mach number range, linear extrapolation was used to approximate elevon deflection and trim characteristics at elevon deflections larger than -20°. The elevon deflections required to trim in pitch are quite large at transonic and low supersonic Mach numbers (M = 1.2 and 2.36). These large deflections are required to offset the large negative $C_{m,0}$ of the model.

The trimmed lift coefficient and lift-drag ratio are presented as a function of Mach number in figures 20(d) and 20(e), respectively. The results show that even with the small wing, because of the relatively high C_{L_α}, the configuration as tested has sufficient

trim lift coefficient for reasonable landing speed at an angle of attack of 15°. The performance data (lift-drag ratio) presented in figure 20(e) show the model has subsonic trimmed lift-drag ratios of approximately 4.

Base pressures.- The base-pressure data measured during the tests are presented in figure 21. These results are presented for information, and no discussion of these results is included.

Static Lateral-Directional Stability Characteristics

Lateral-directional stability.- The static lateral-directional stability characteristics of the model with and without the vertical tail are presented in figure 22. These results show that for the lowest test Mach numbers (M = 0.3 and 0.6) the model was directionally stable (vertical tail on) throughout the test angle-of-attack range. At Mach numbers of 0.9 and 1.2, the model became unstable at high angles of attack. At all of the supersonic Mach numbers the vertical tail was not effective enough to overcome the large instability of the wing-body combination, and the model was unstable throughout the test angle-of-attack range.

Also presented in figure 22 is the effective dihedral parameter C_{l_β} measured in the tests. These results show that the model has positive effective dihedral $\left(-C_{l_\beta}\right)$ throughout the test angle-of-attack range except at low angles of attack at Mach numbers of 0.9, 2.36, 2.86, 3.95, and 4.63. At these Mach numbers C_{l_β} became negative as lift began to develop on the model at positive angles of attack.

Aileron control effectiveness.- Because of cross-coupling concerns due to the swept hinge line of the elevon, tests were made to determine the aileron control effectiveness of the model. The results of these tests are presented in figure 23. The data show that for the subsonic and transonic Mach numbers $C_{l_{\delta_a}}$ was nonlinear with a significant decrease in effectiveness at angles of attack above 12°. This loss of effectiveness results from the flow separation on the wing tip at angles of attack in excess of 8°. For the supersonic Mach numbers the data show that $C_{l_{\delta_a}}$ is linear throughout the Mach number range from 2.36 to 4.63. For all test conditions, the aileron control generated adverse yaw with an increase in $C_{n_{\delta_a}}$ with increased angle of attack.

SUMMARY OF RESULTS

An investigation has been conducted to determine the subsonic, transonic, and supersonic aerodynamic characteristics of a winged single-stage-to-orbit vehicle. The results of these tests are summarized as follows:

1. The model had pitch-up at an angle of attack as low as 8^{o} for all Mach numbers below 1.2. For the supersonic Mach numbers the variation of pitching moment with lift coefficient was linear and exhibited neutral or slight instability for the test moment center.

2. Large elevon deflections were required to trim at transonic and low supersonic Mach numbers because of large negative pitching moment at zero lift.

3. Subsonic trimmed lift-drag ratios were approximately 4.

4. At the lowest test Mach numbers the model was directionally stable throughout the test angle-of-attack range, and at Mach numbers of 0.9 and 1.2 the model became unstable at high angles of attack. The model was unstable throughout the angle-of-attack range for the supersonic Mach numbers.

5. The aileron control effectiveness was nonlinear with a loss of effectiveness at angles of attack above 8^{o} at the subsonic and transonic Mach numbers. The ailerons generated adverse yaw throughout the test Mach number range.

Langley Research Center
National Aeronautics and Space Administration
Hampton, VA 23665
June 6, 1978

REFERENCES

1. Henry, Beverly Z.; and Decker, John P.: Future Earth Orbit Transportation Systems/ Technology Implications. Astronaut. & Aeronaut., vol. 14, no. 9, Sept. 1976, pp. 18-28.

2. Haefeli, Rudolph C.; Littler, Ernest G.; Hurley, John B.; and Winter, Martin G.: Technology Requirements for Advanced Earth-Orbital Transportation Systems – Final Report. NASA CR-2866, 1977.

3. Schaefer, William T., Jr.: Characteristics of Major Active Wind Tunnels at the Langley Research Center. NASA TM X-1130, 1965.

4. Braslow, Albert L.; Hicks, Raymond M.; and Harris, Roy, V., Jr.: Use of Grit-Type Boundary-Layer-Transition Trips on Wind-Tunnel Models. NASA TN D-3579, 1966.

5. Spencer, Bernard, Jr.; and Fox, Charles H., Jr.: Hypersonic Aerodynamic Performance of Minimum-Wave-Drag Bodies. NASA TR R-250, 1966.

6. Spreeman, Kenneth P.: Design Guide for Pitch-Up Evaluation and Investigation at High Subsonic Speeds of Possible Limitations Due to Wing-Aspect-Ratio Variations. NASA TM X-26, 1959.

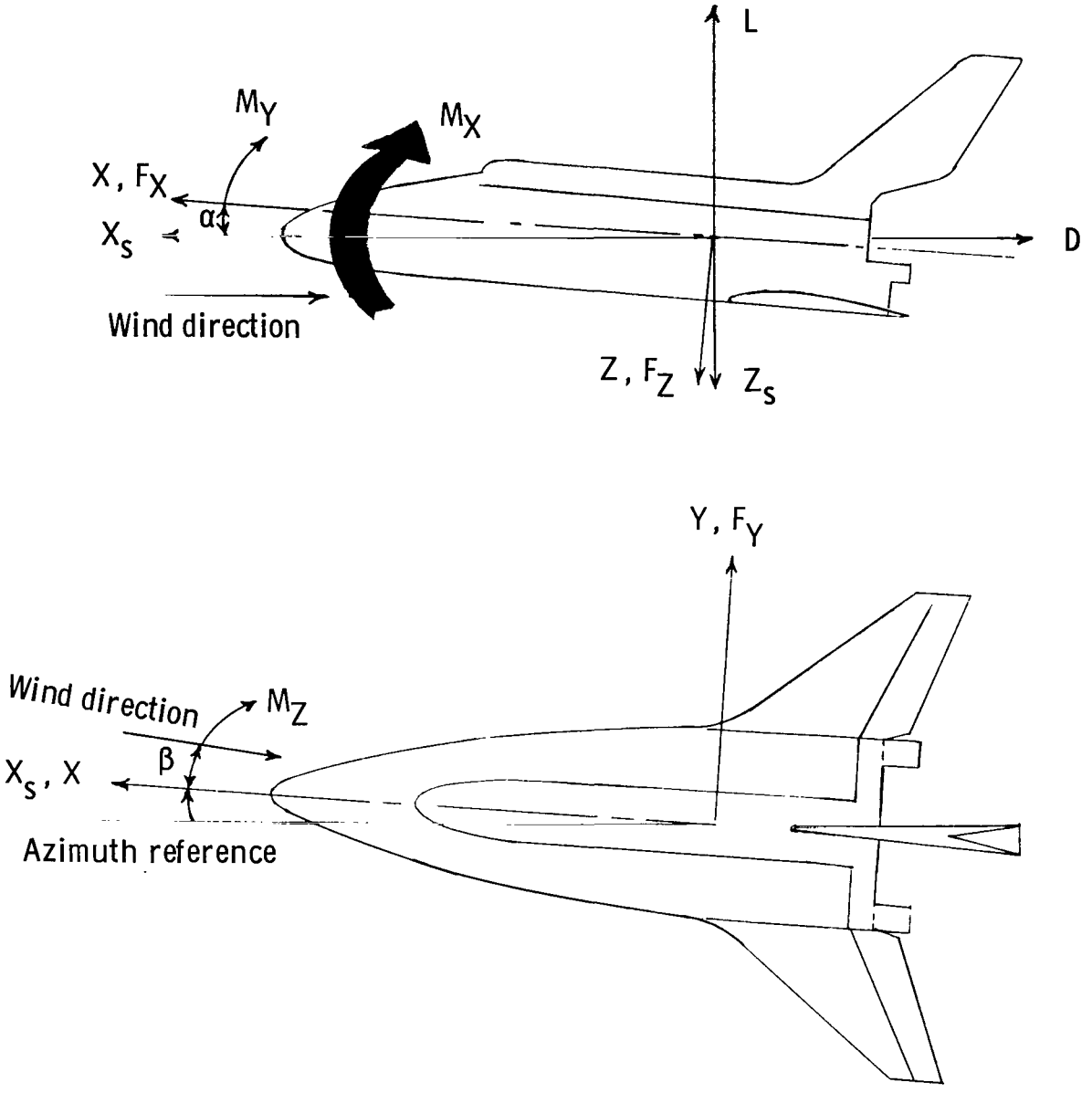

Figure 1.- System of axes used in investigation. Arrows indicate positive direction of moments, forces, and angles.

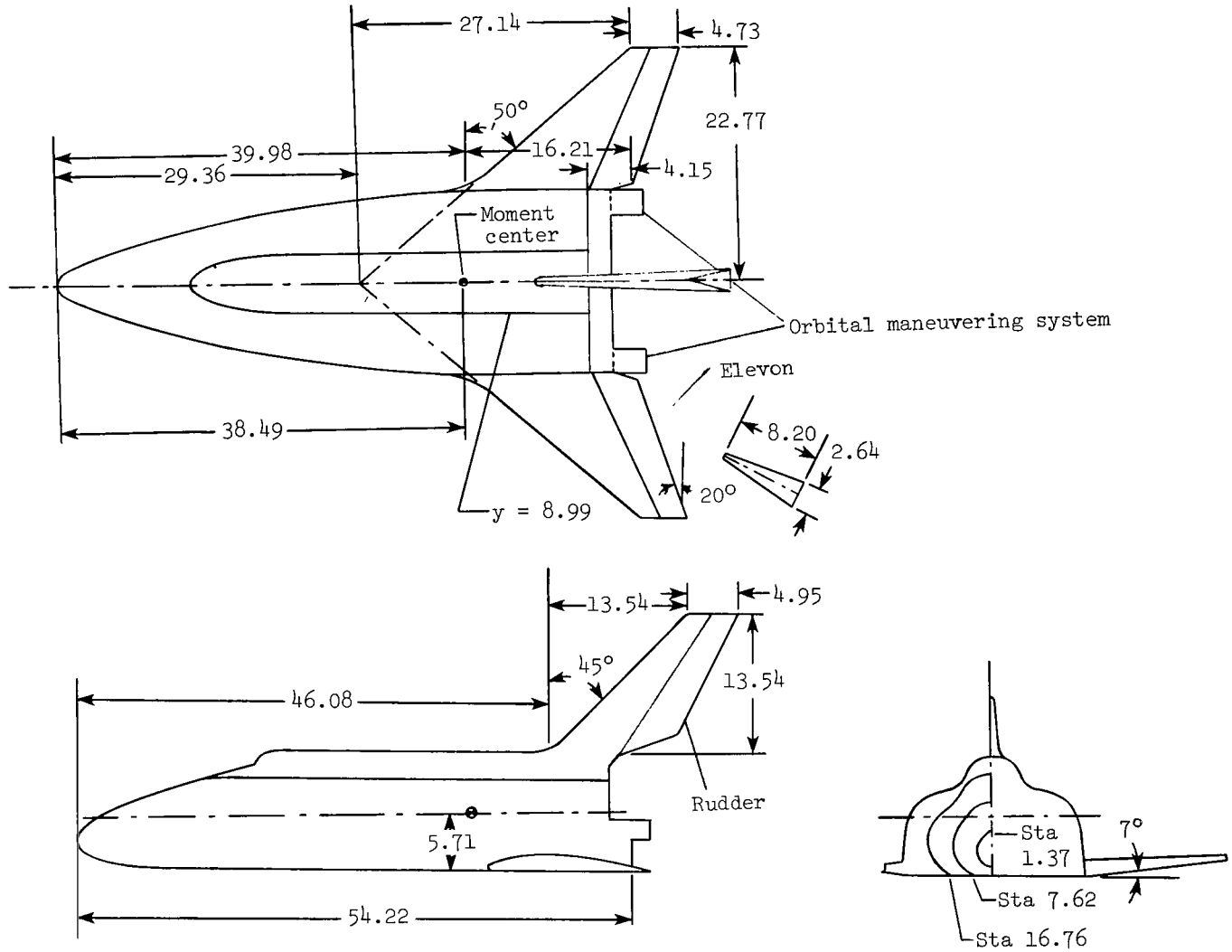

Figure 2.- Drawing of the model used in the investigation. All dimensions are in centimeters.

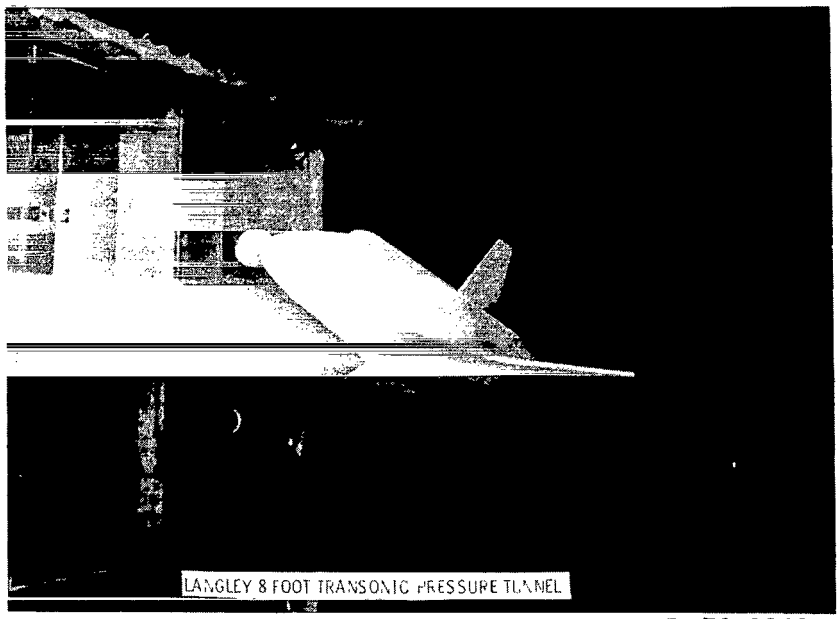

L-76-8263.1

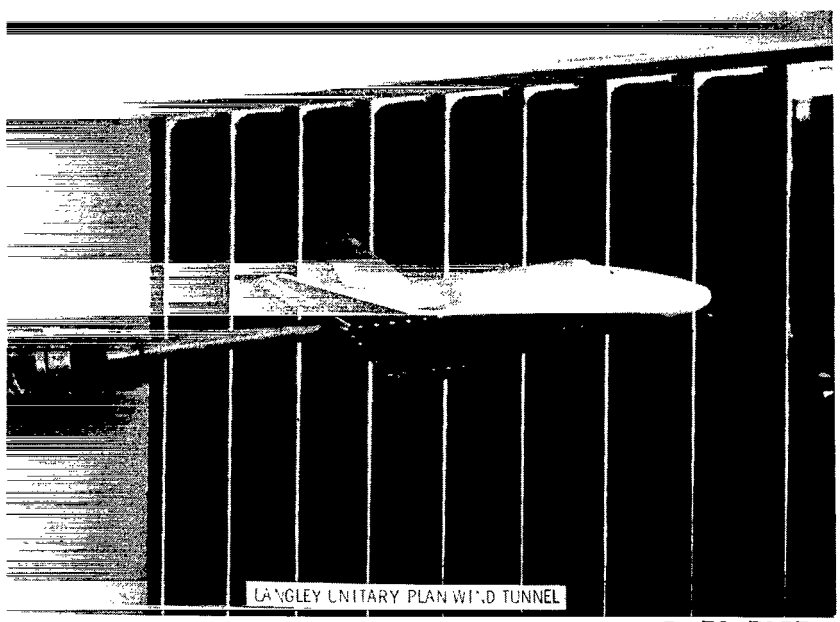

L-76-7957.1

Figure 3.- Photographs of the model mounted for tests.

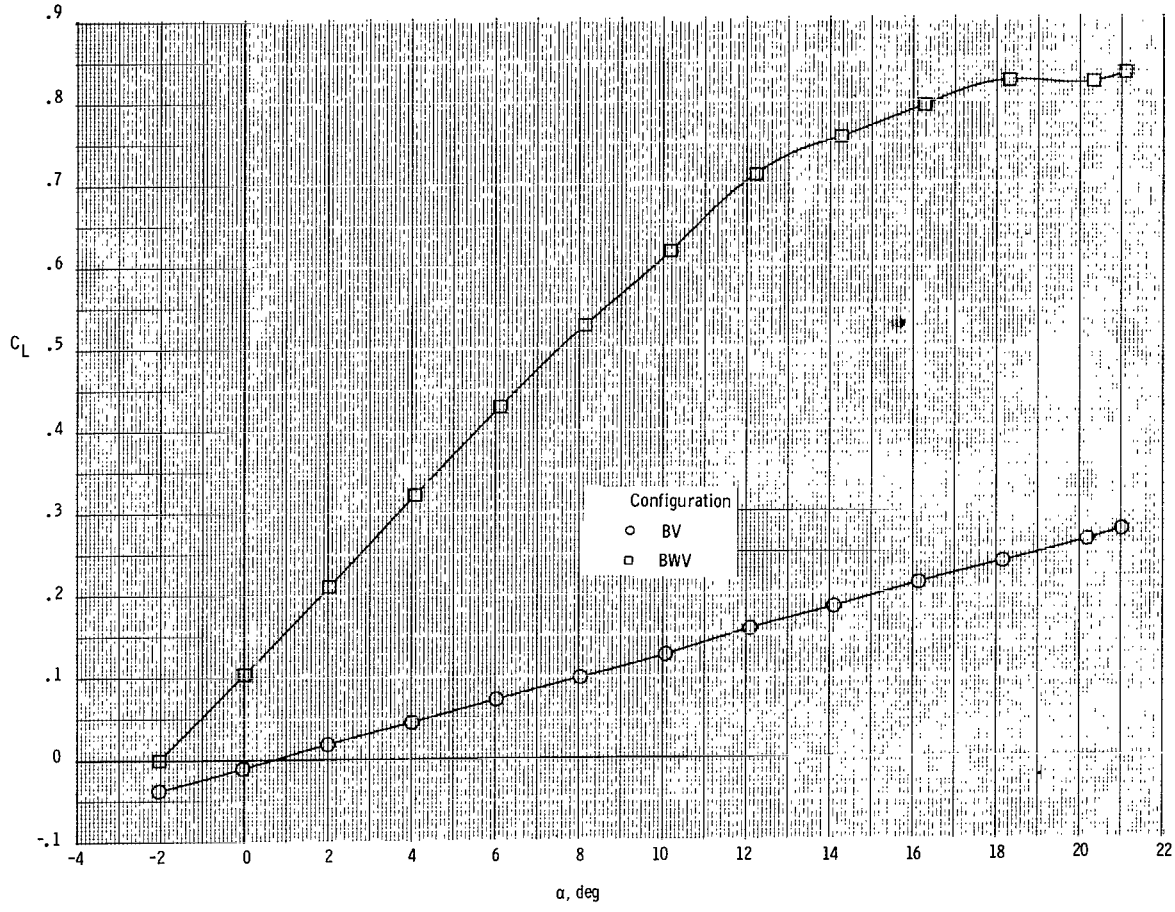

(a) C_L as a function of α.

Figure 4.- Effect of body buildup on the static longitudinal stability characteristics of the model at $M = 0.3$.

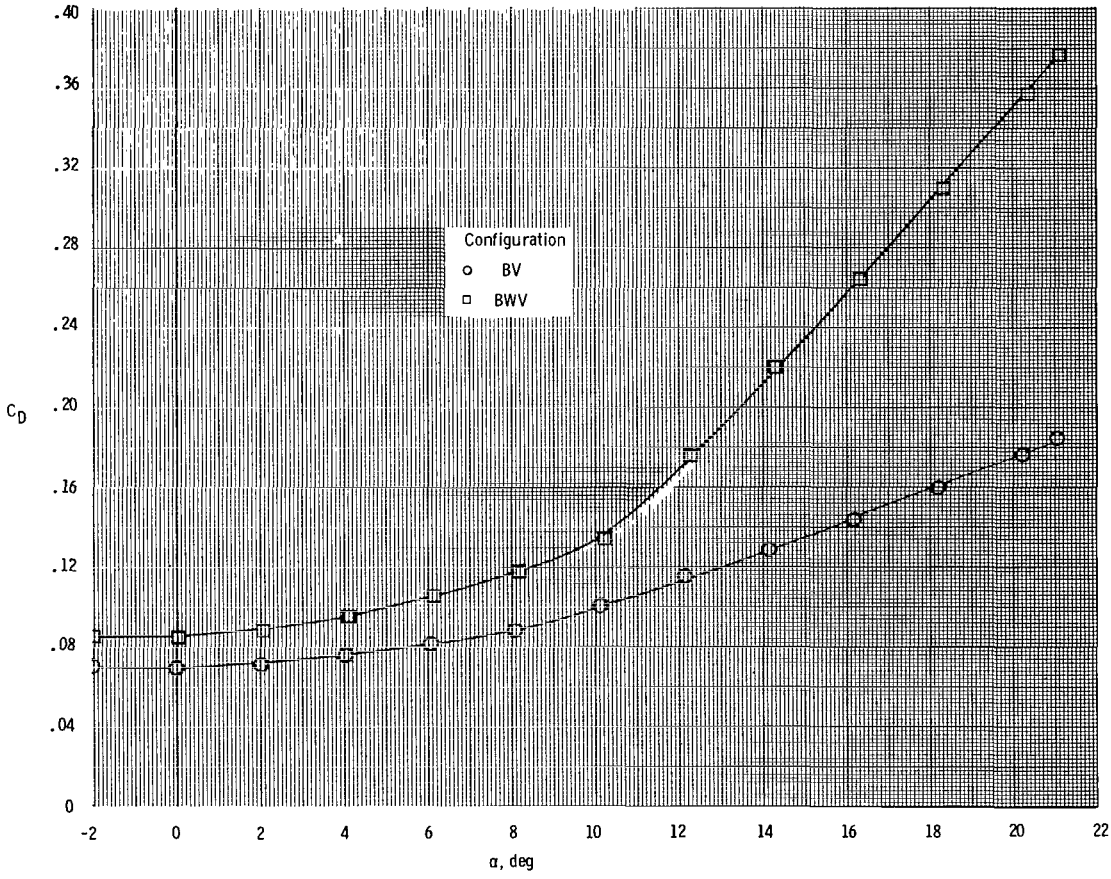

(b) C_D as a function of α.

Figure 4.- Continued.

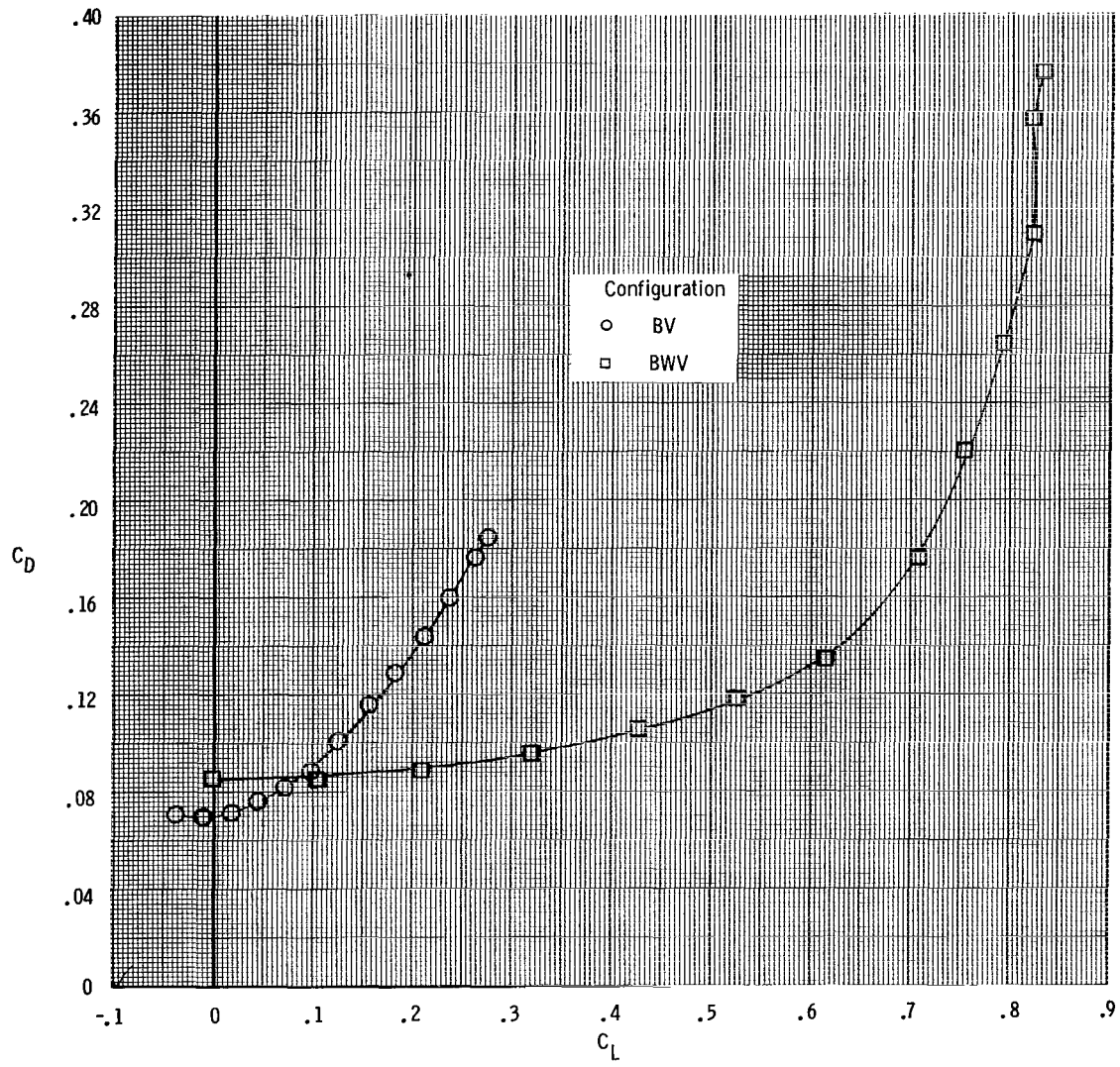

(c) C_D as a function of C_L.

Figure 4.- Continued.

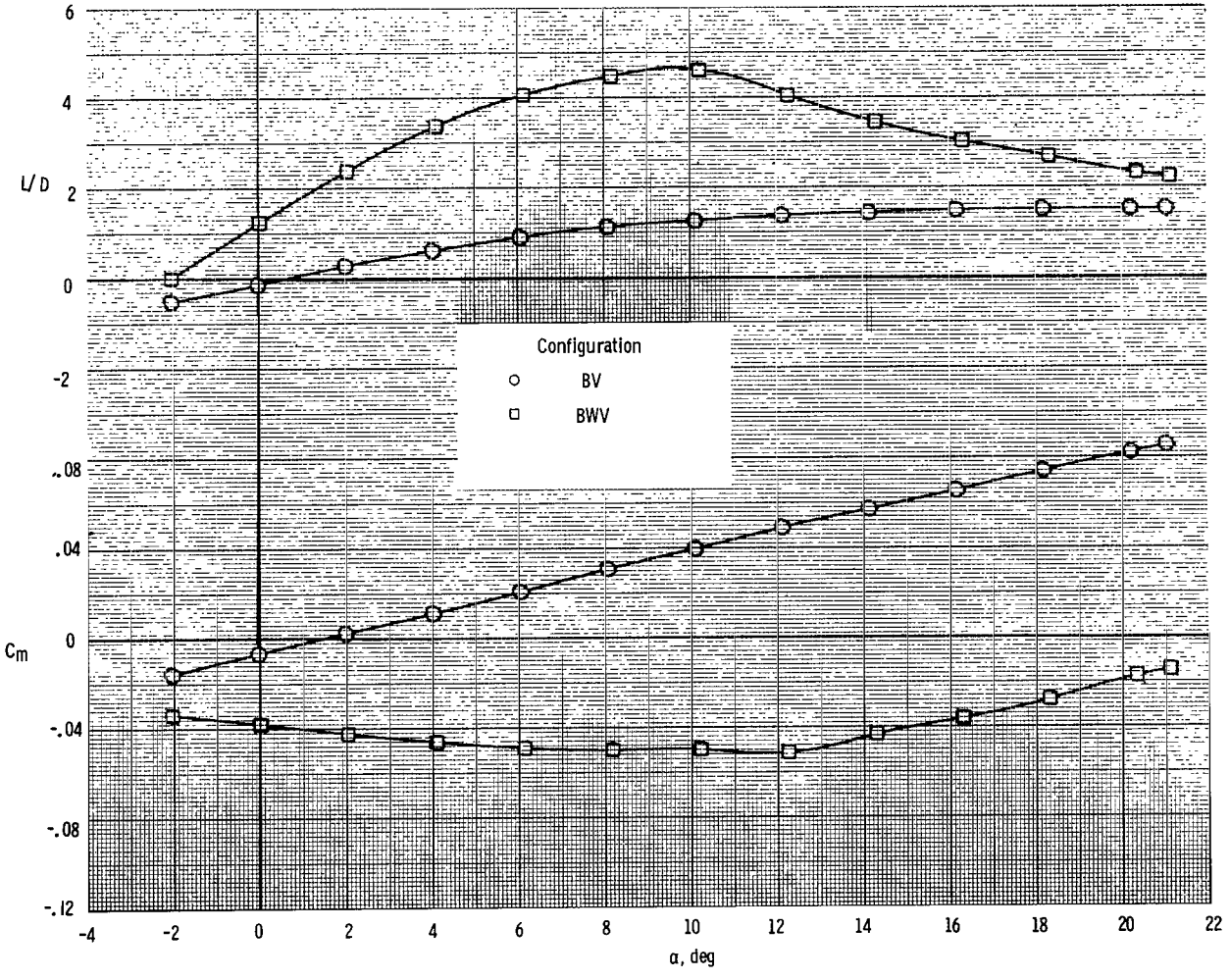

(d) C_m and L/D as a function of α.

Figure 4.- Continued.

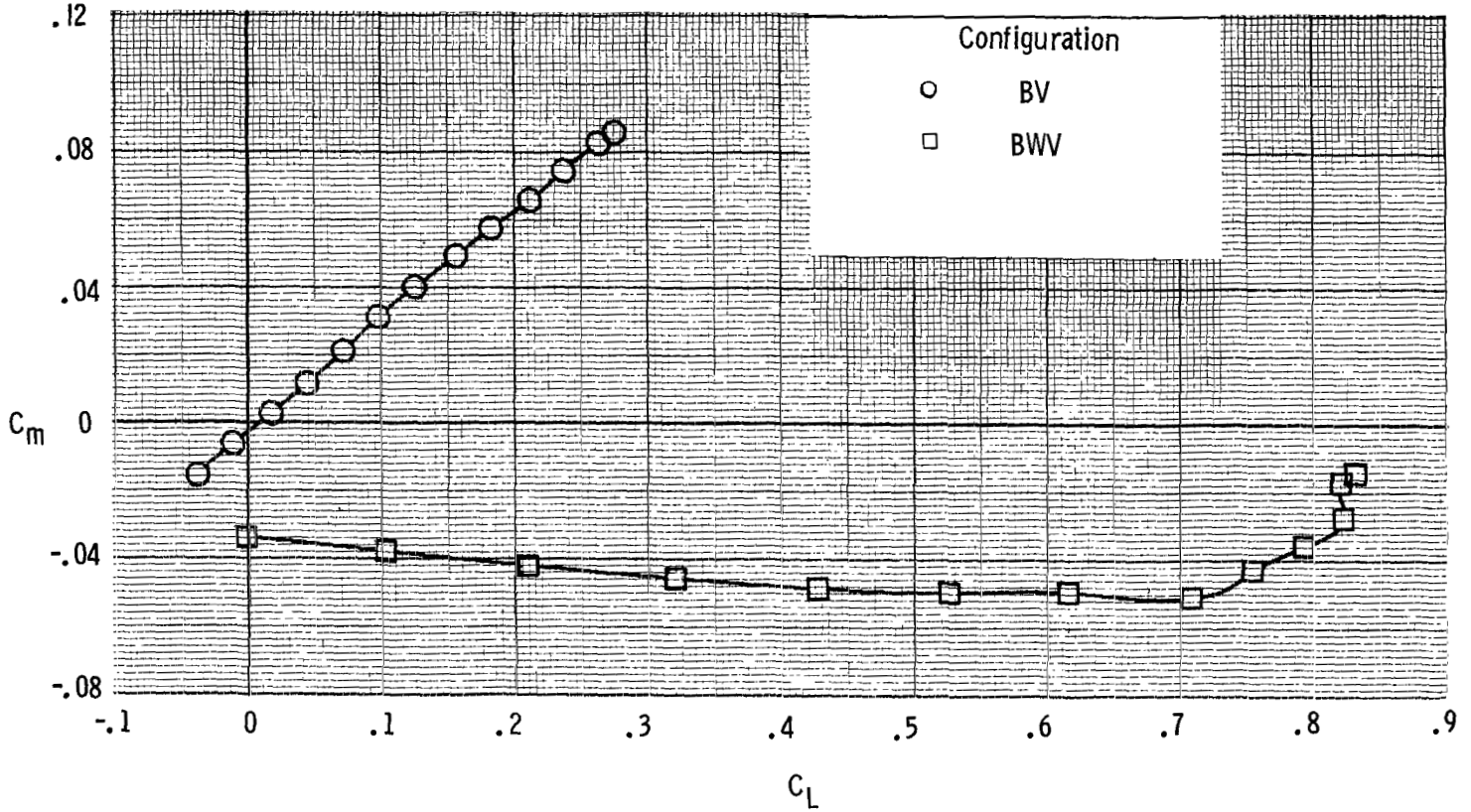

(e) C_m as a function of C_L.

Figure 4.- Concluded.

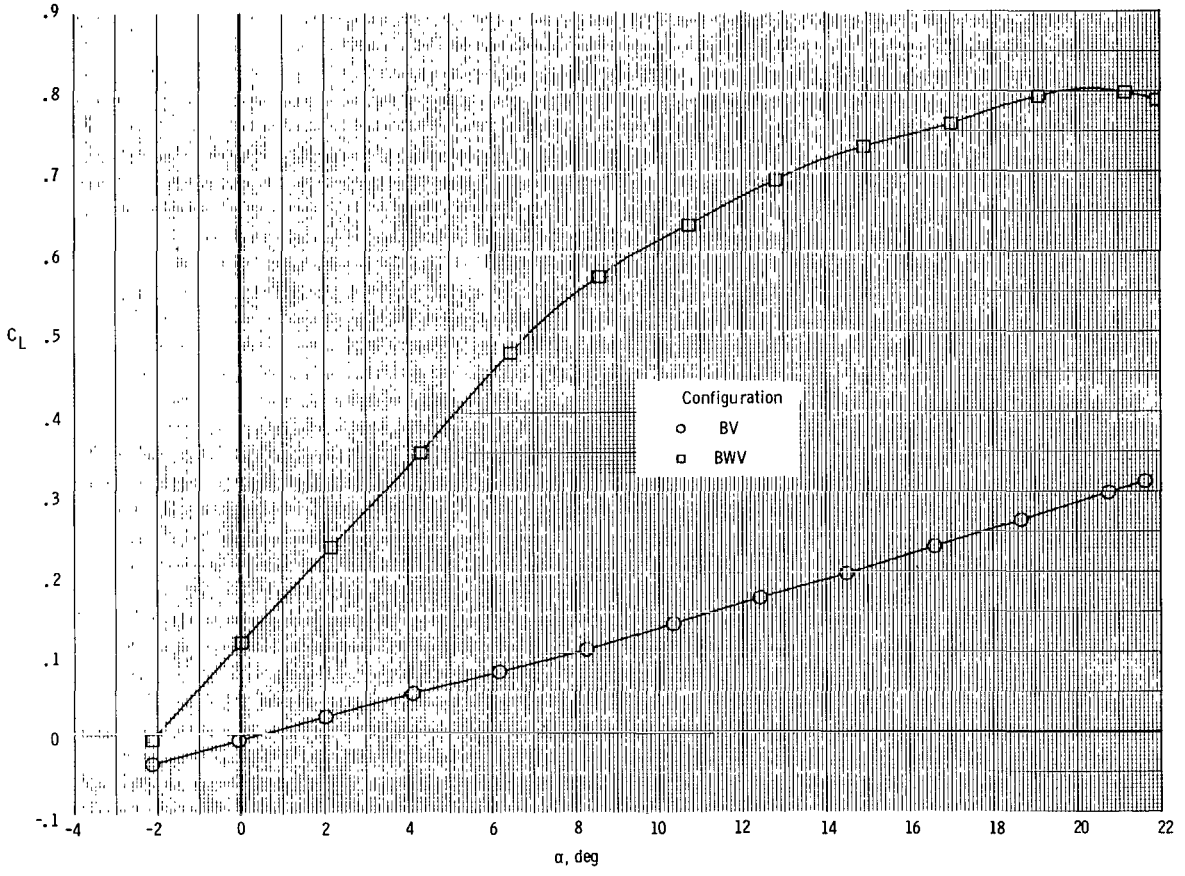

(a) C_L as a function of α.

Figure 5.- Effect of body buildup on the static longitudinal stability characteristics of the model at M = 0.6.

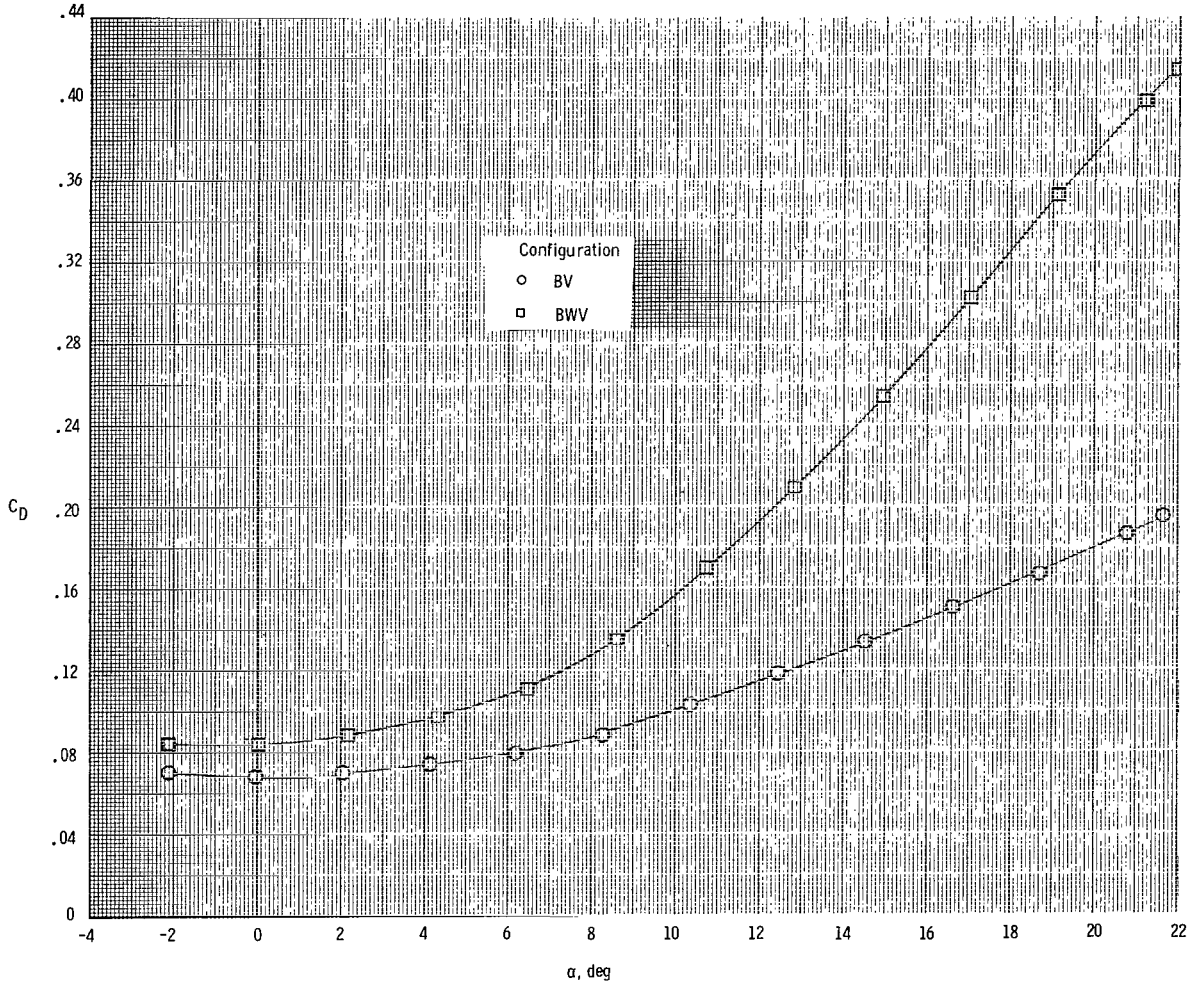

(b) C_D as a function of α.

Figure 5.- Continued.

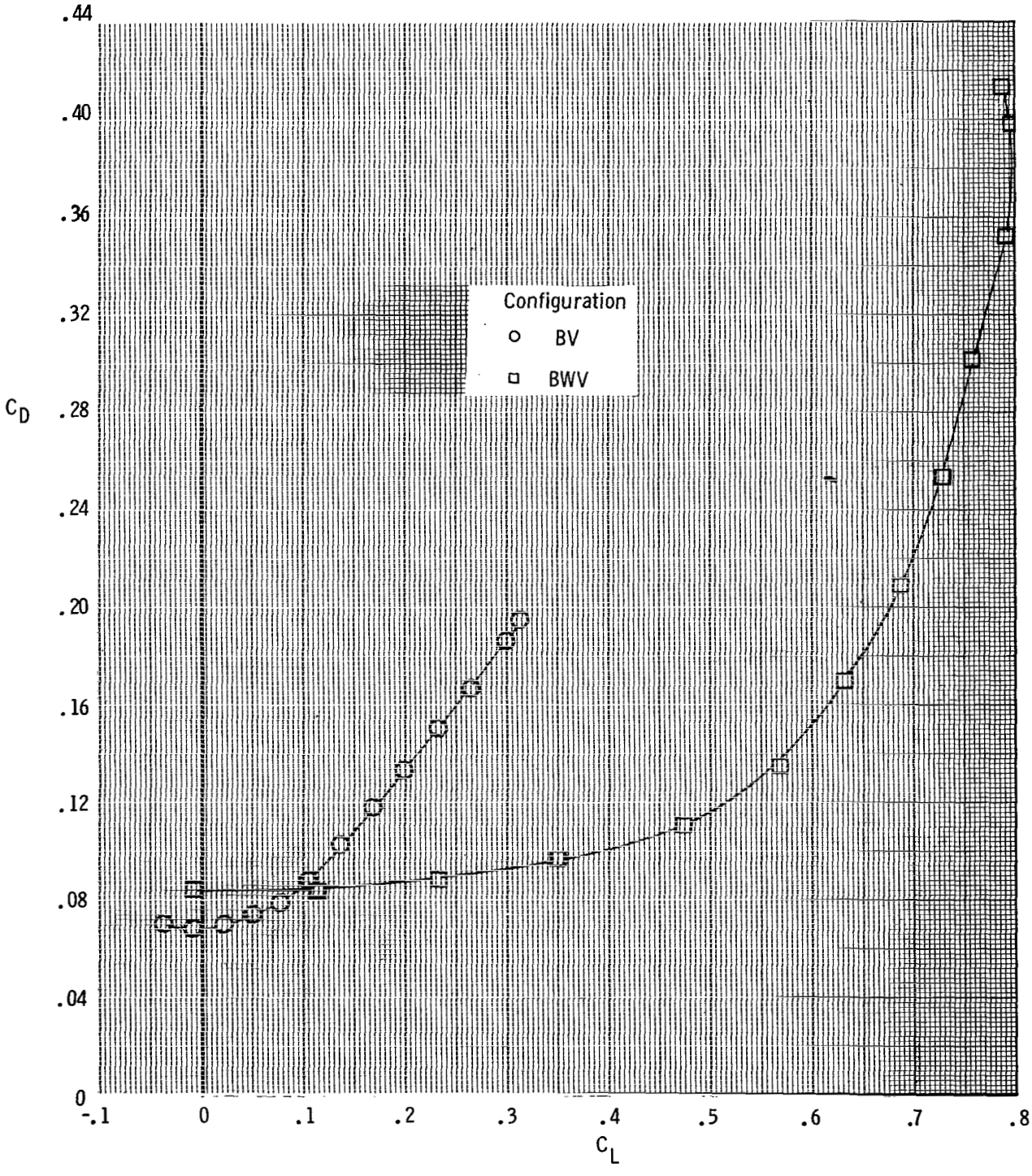

(c) C_D as a function of C_L.

Figure 5.- Continued.

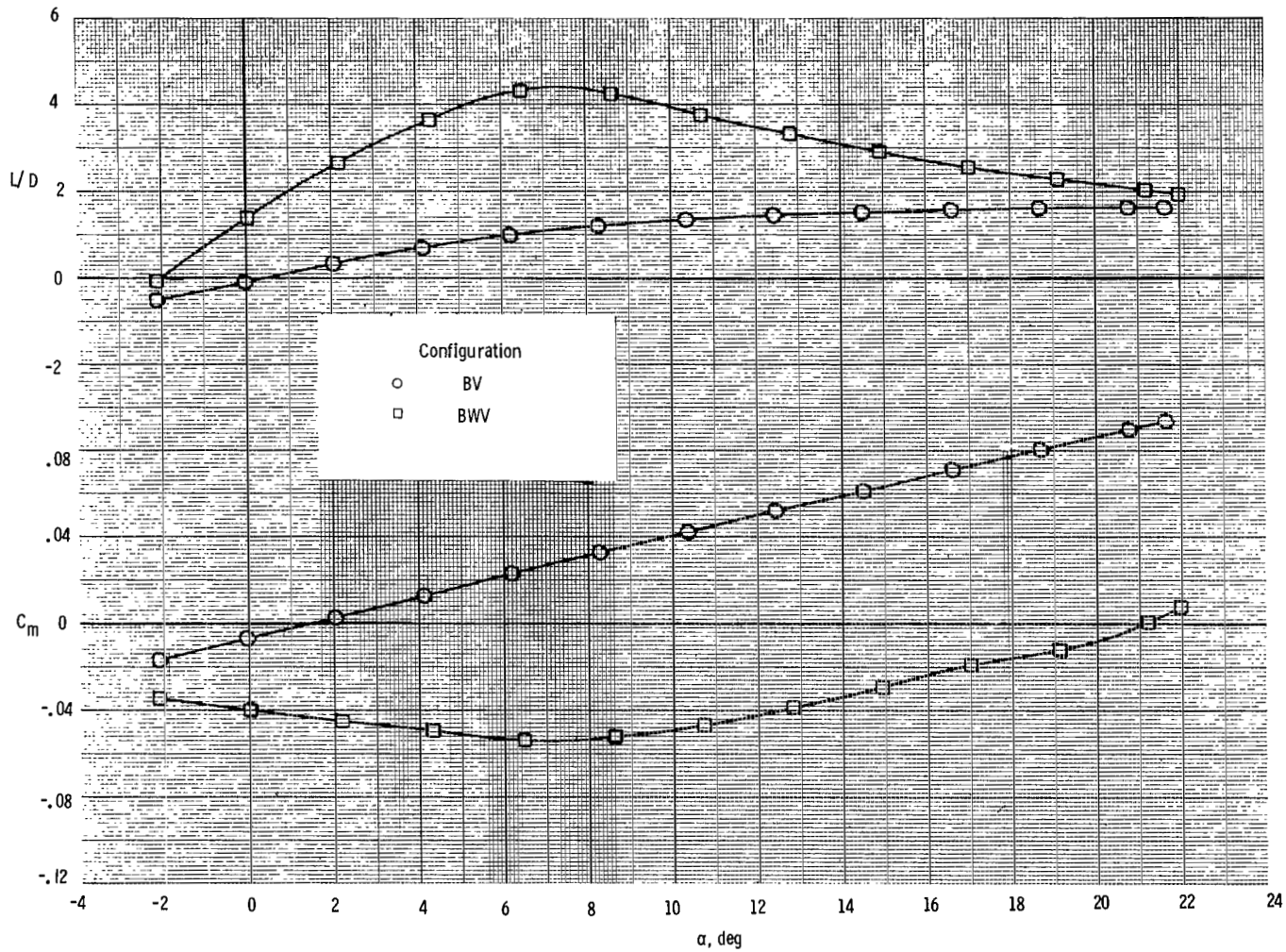

(d) C_m and L/D as a function of α.

Figure 5.- Continued.

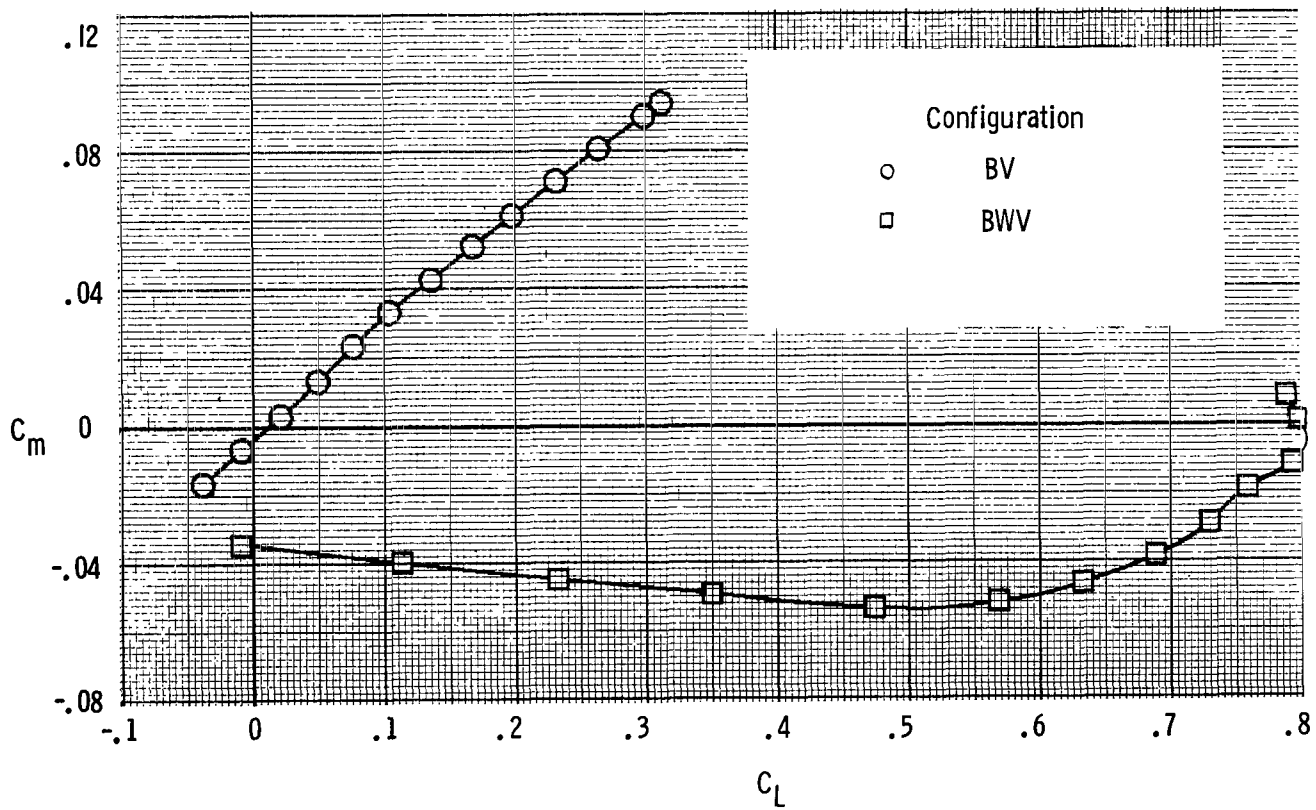

(e) C_m as a function of C_L.

Figure 5.- Concluded.

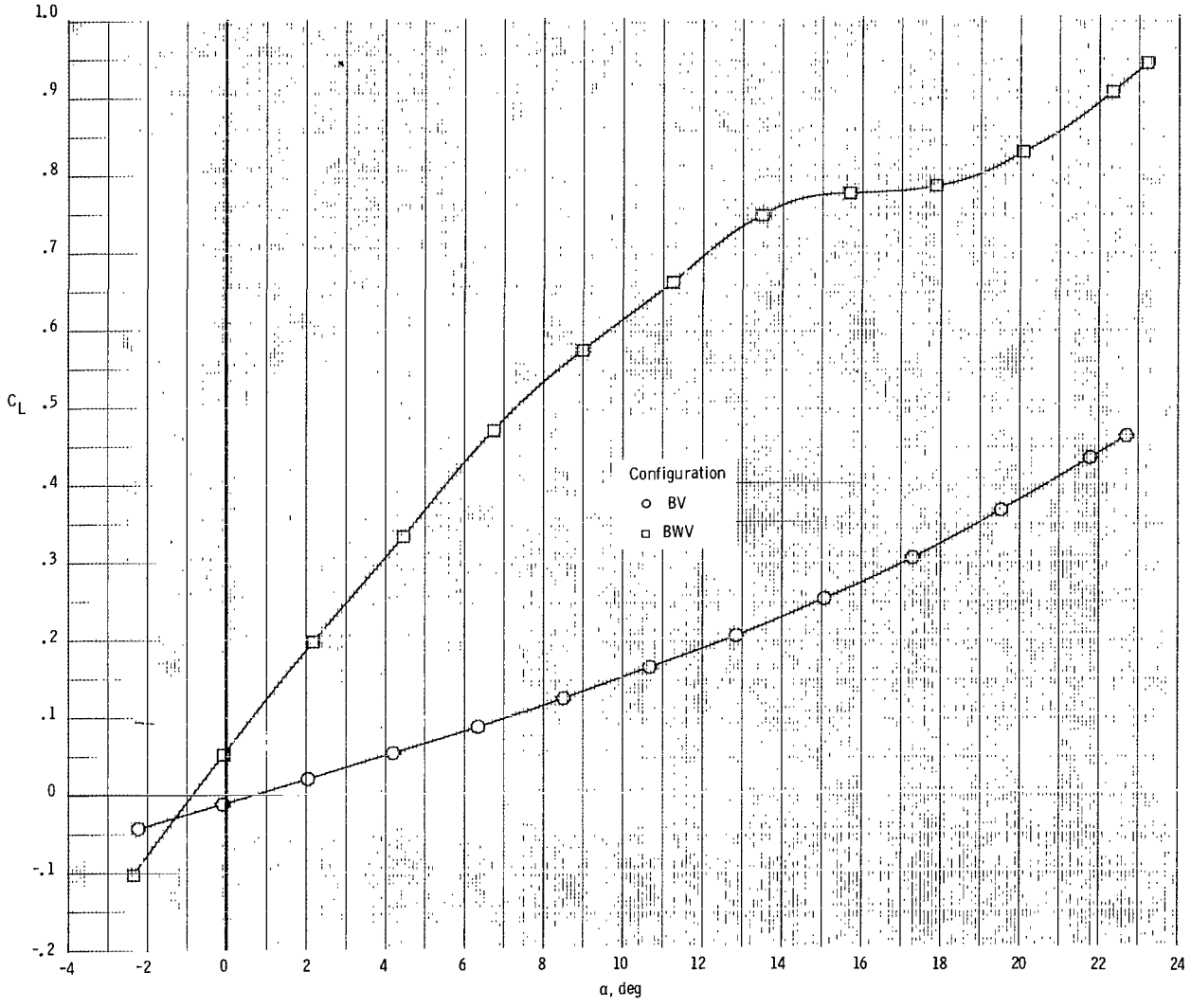

(a) C_L as a function of α.

Figure 6.- Effect of body buildup on the static longitudinal stability characteristics of the model at M = 0.9.

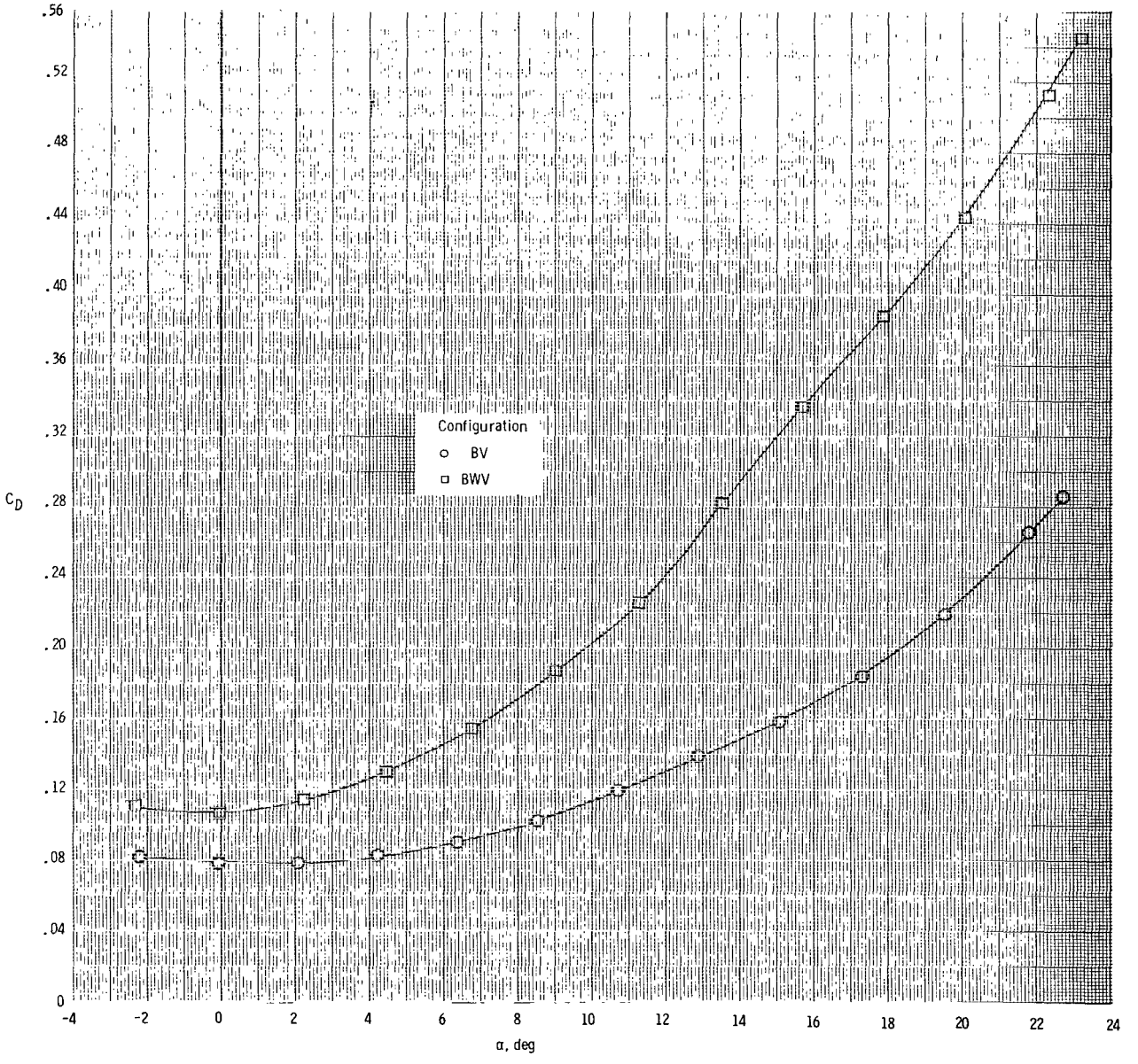

(b) C_D as a function of α.

Figure 6.- Continued.

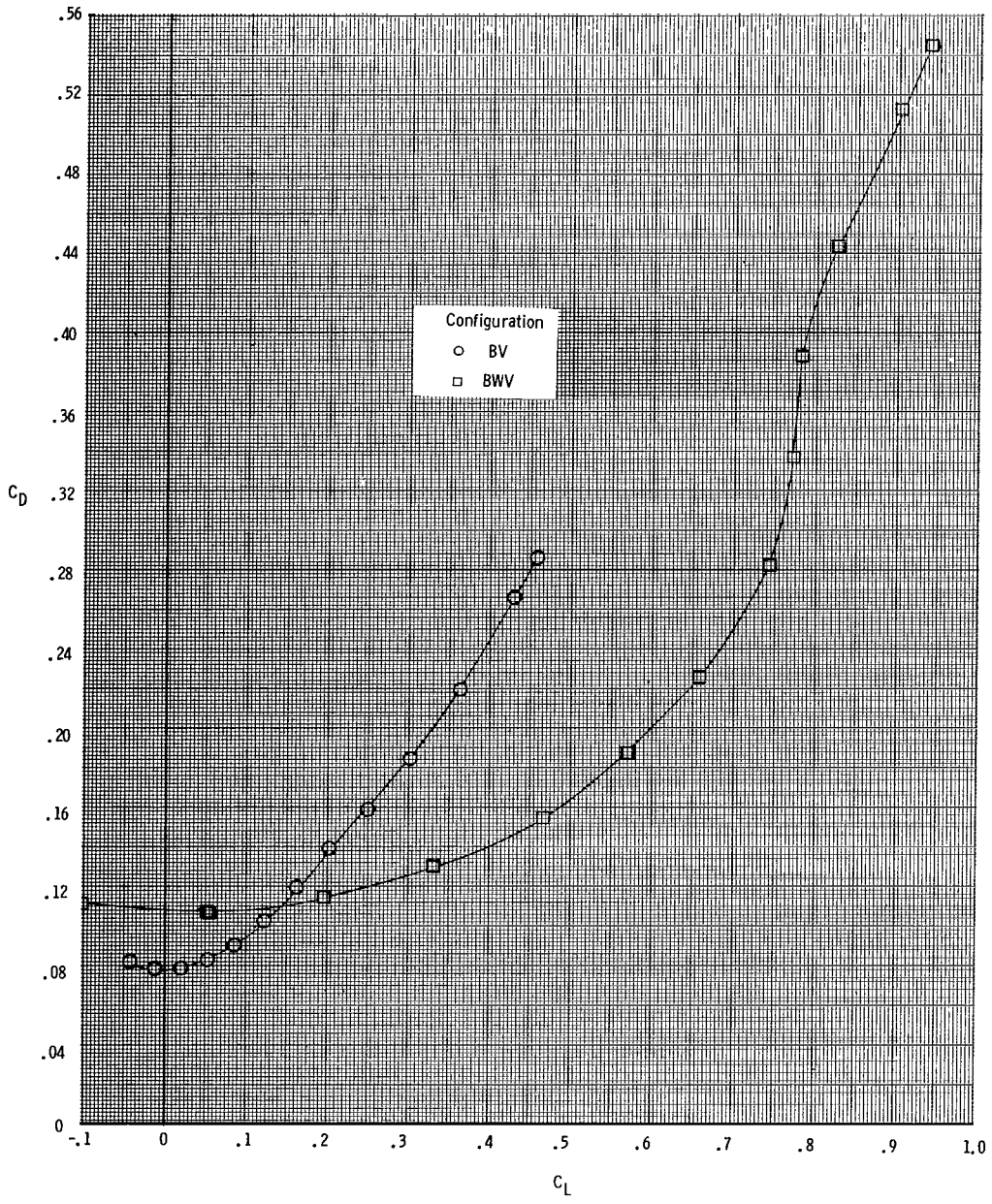

(c) C_D as a function of C_L.

Figure 6.- Continued.

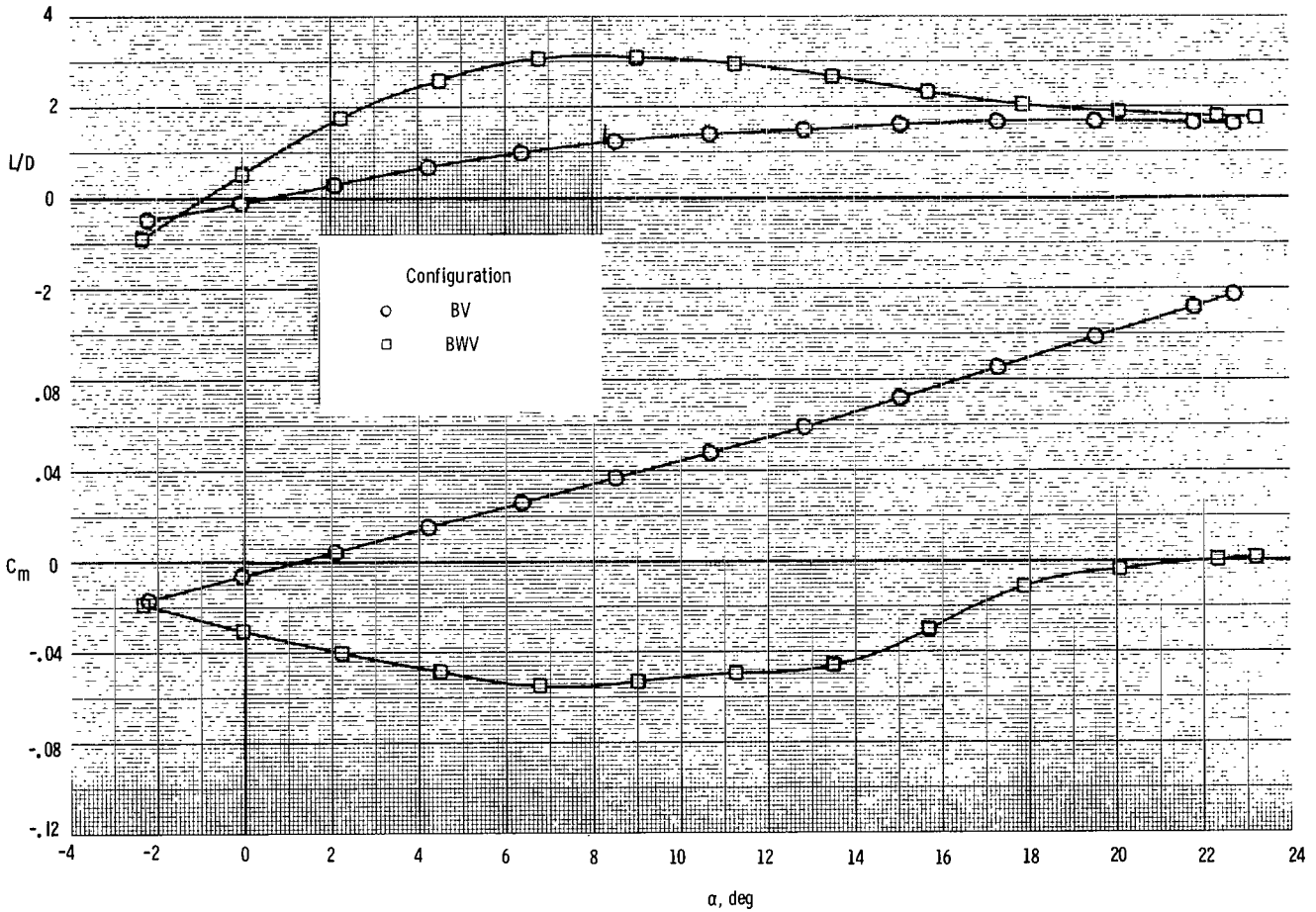

(d) C_m and L/D as a function of α.

Figure 6.- Continued.

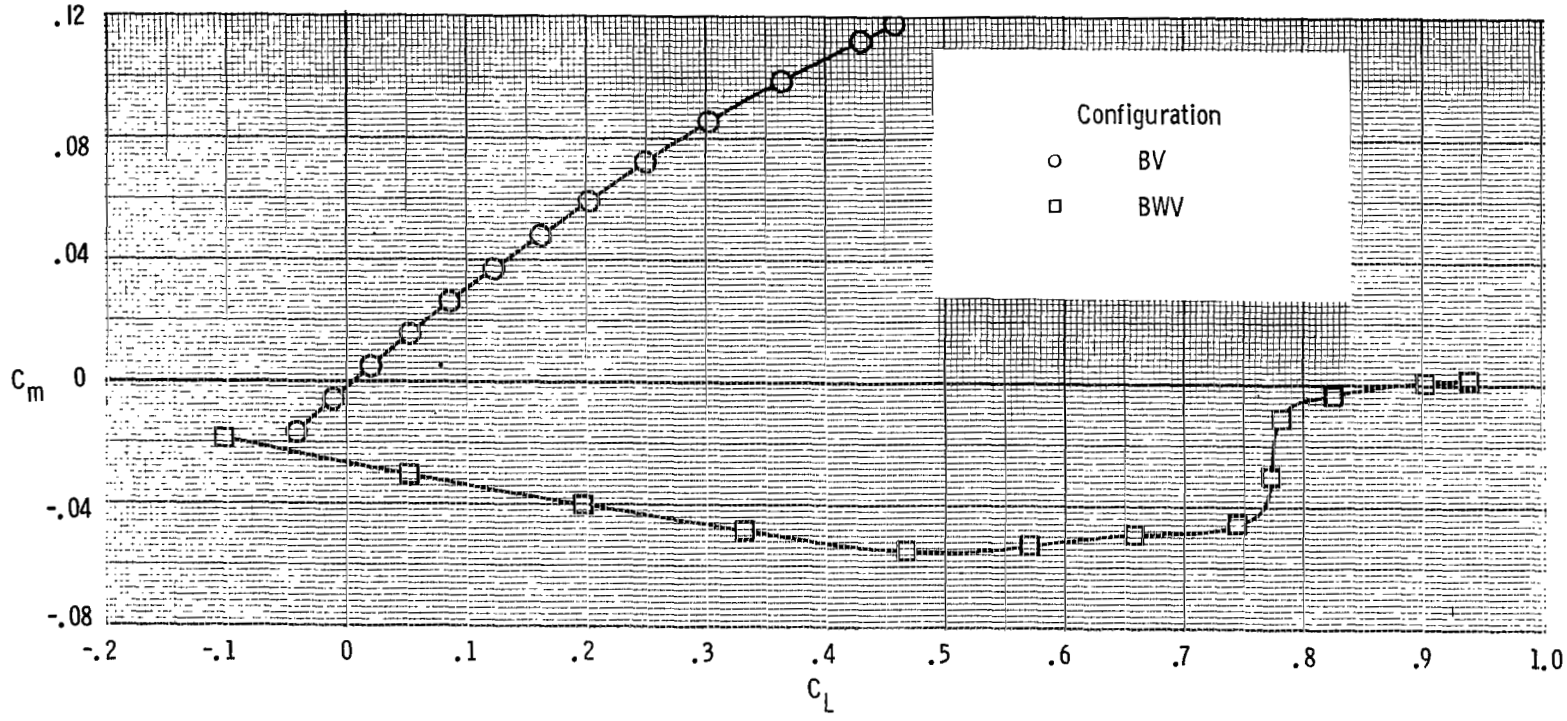

(e) C_m as a function of C_L.

Figure 6.- Concluded.

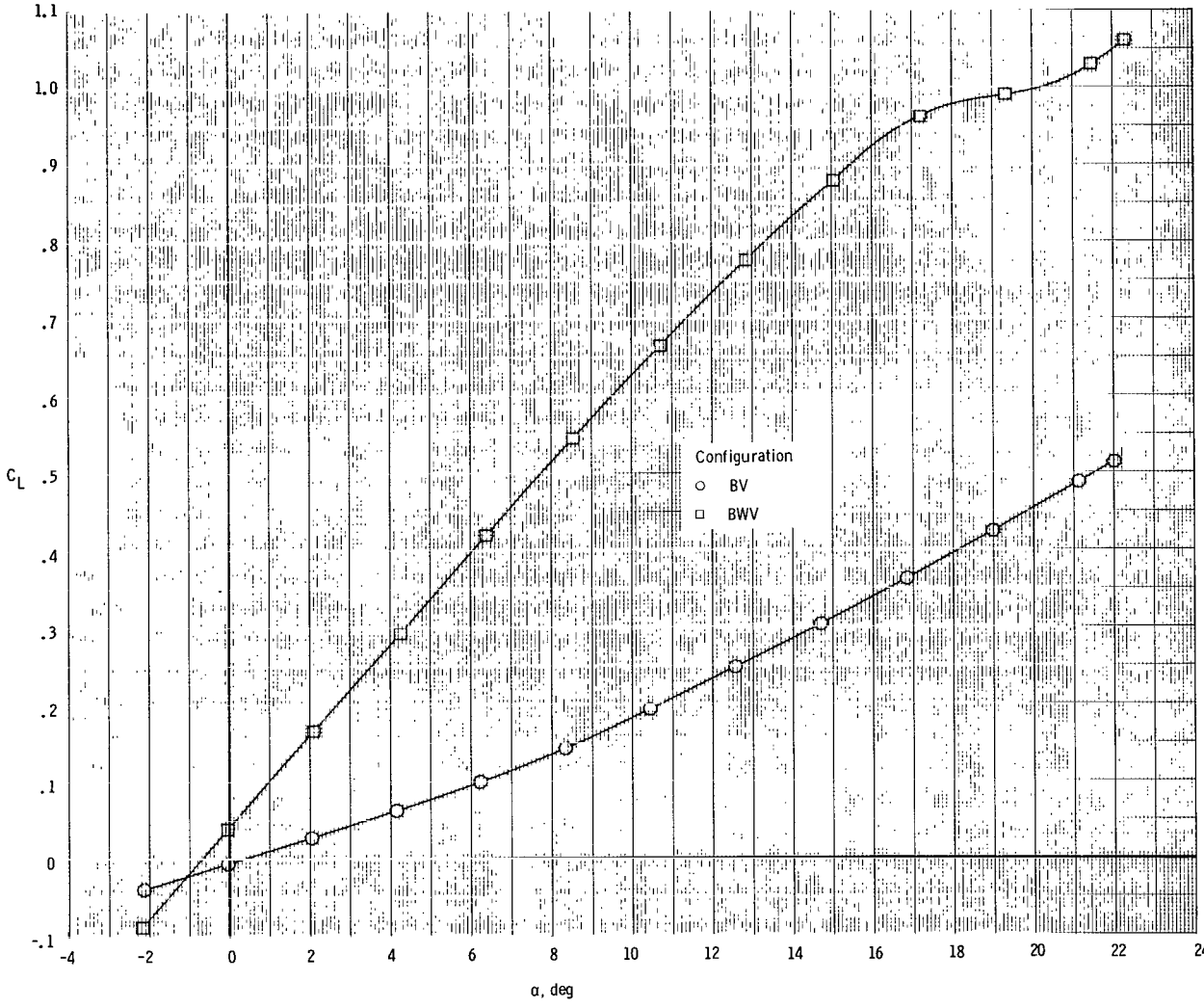

(a) C_L as a function of α.

Figure 7.- Effect of body buildup on the static longitudinal stability characteristics of the model at M = 1.2.

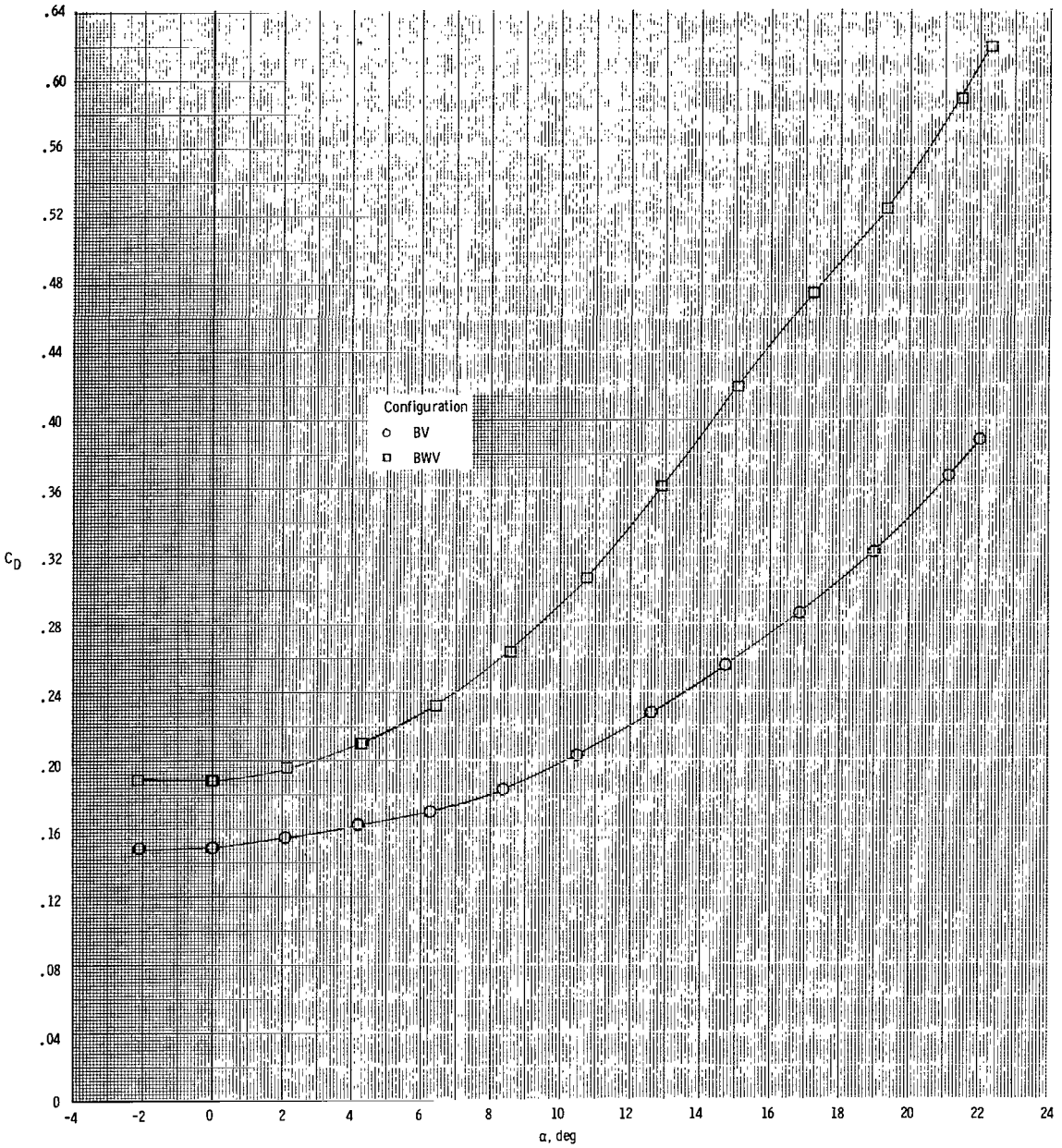

(b) C_D as a function of α.

Figure 7.- Continued.

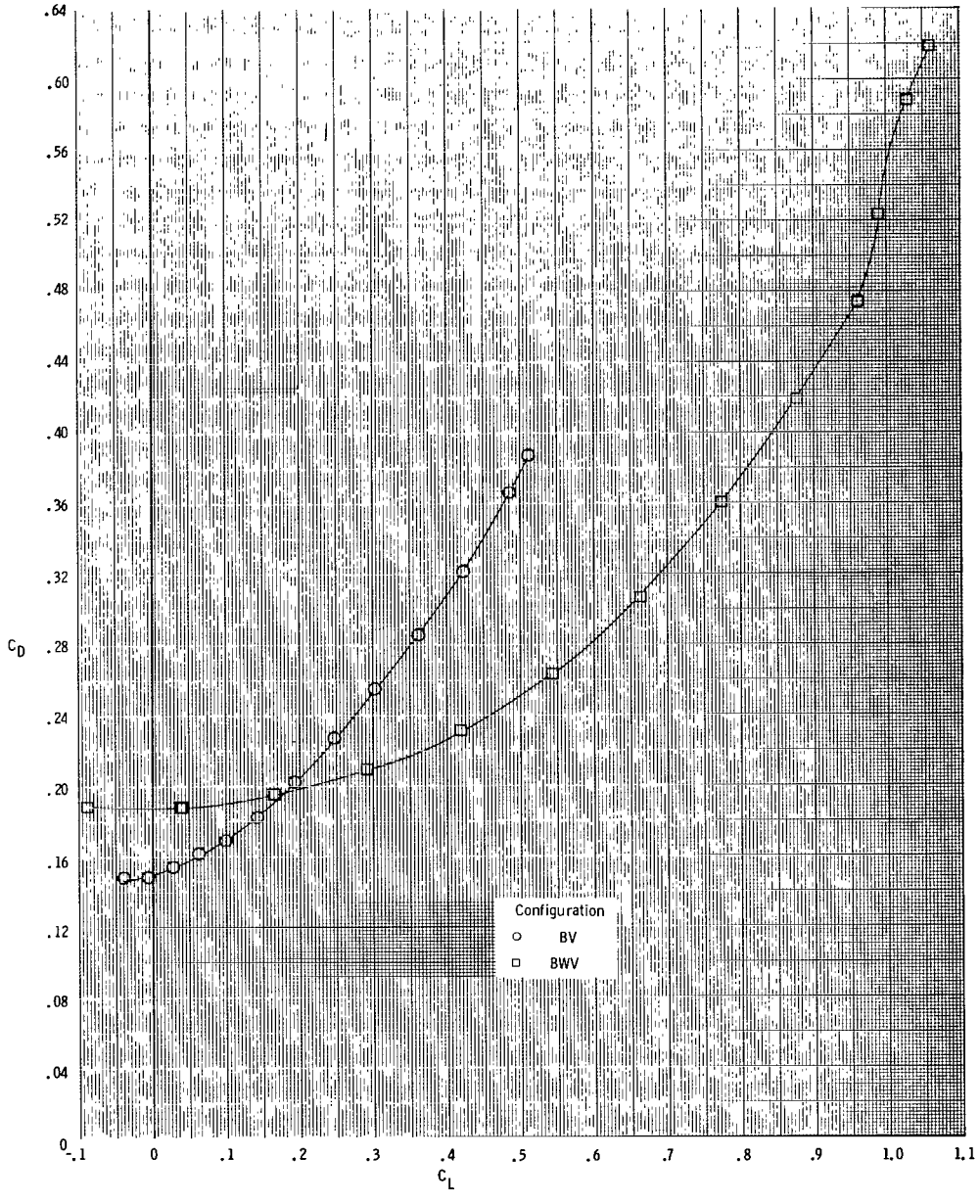

(c) C_D as a function of C_L.

Figure 7.- Continued.

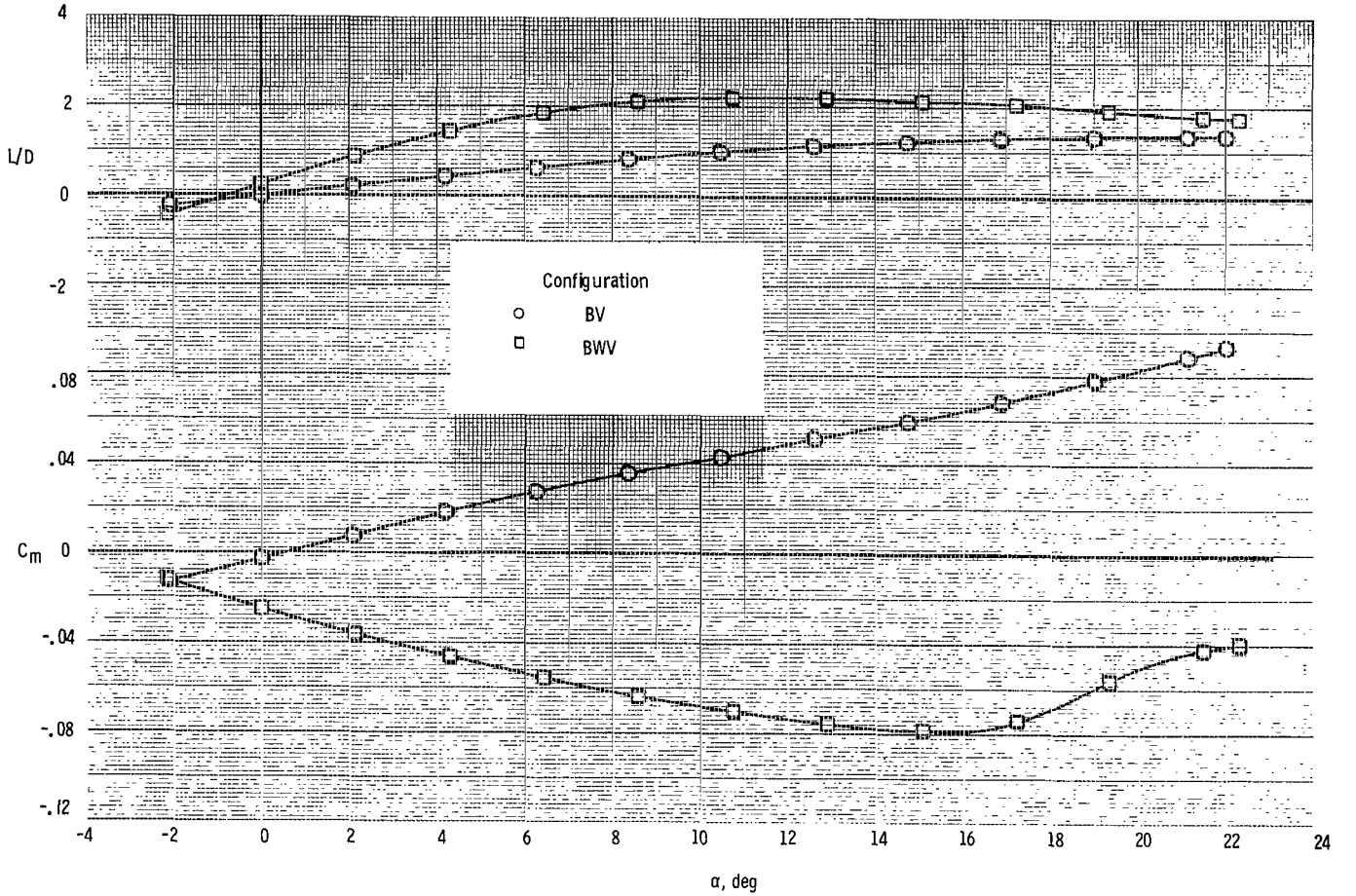

(d) C_m and L/D as a function of α.

Figure 7.- Continued.

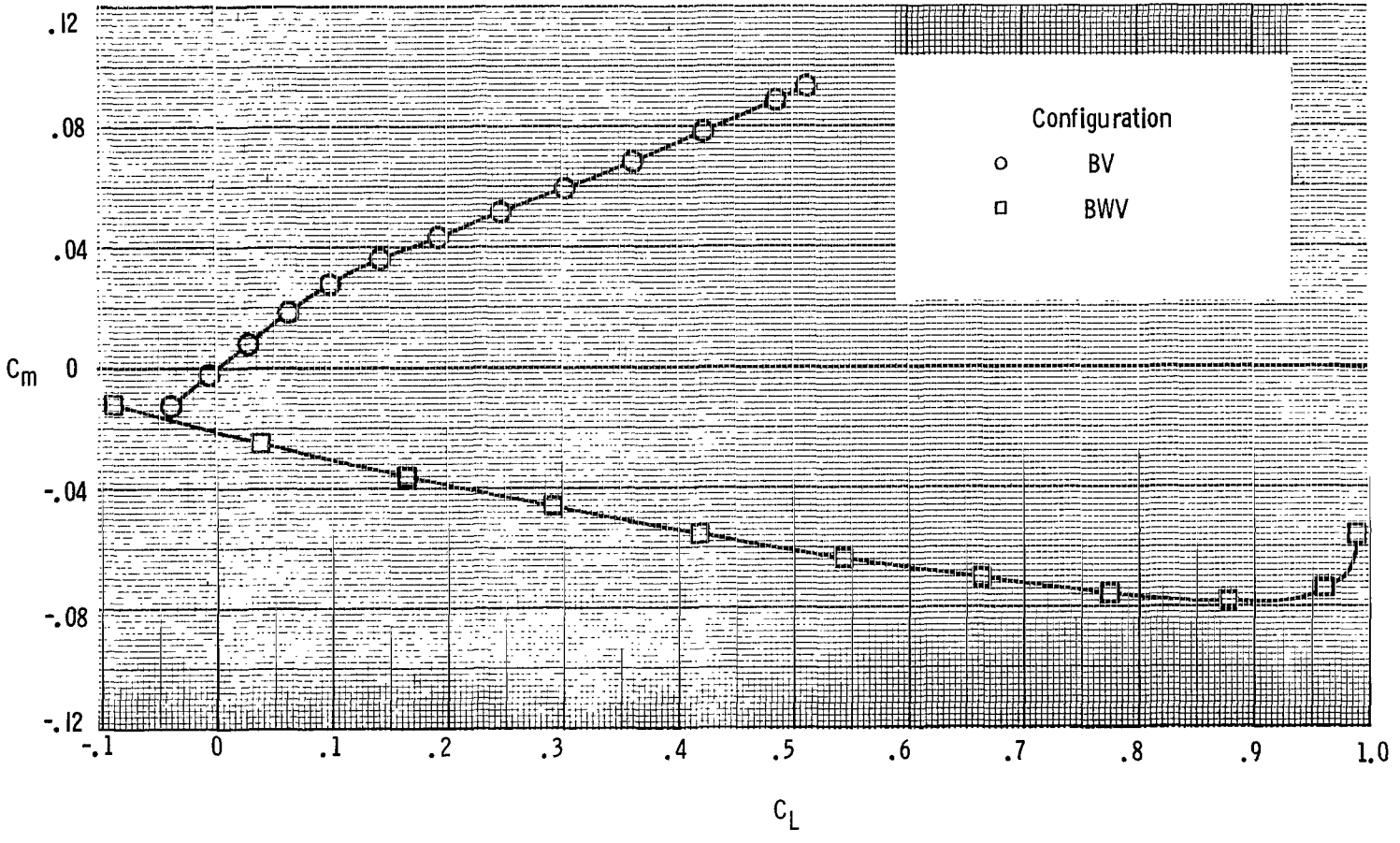

(e) C_m as a function of C_L.

Figure 7.- Concluded.

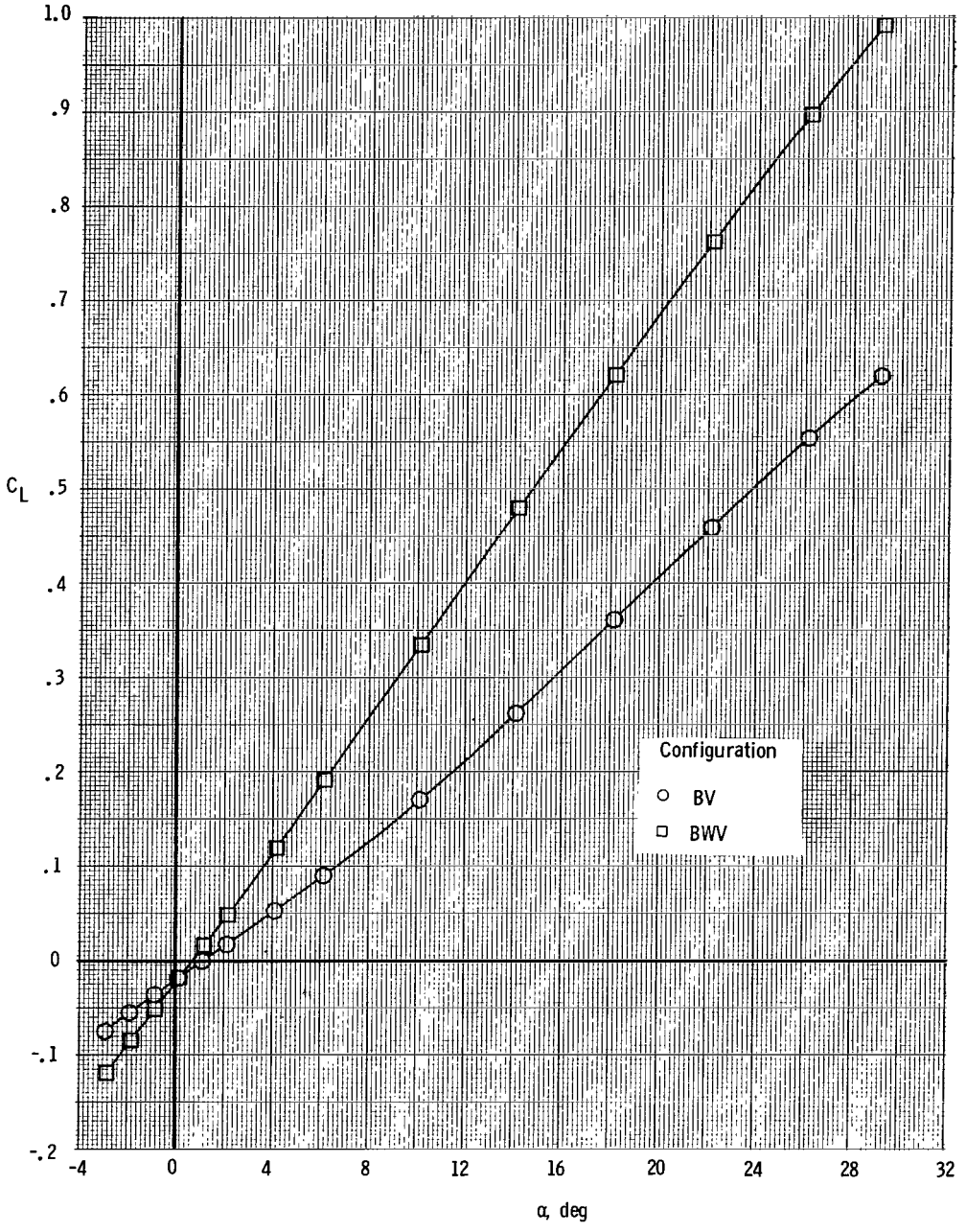

(a) C_L as a function of α.

Figure 8.- Effect of body buildup on the static longitudinal stability characteristics of the model at M = 2.36.

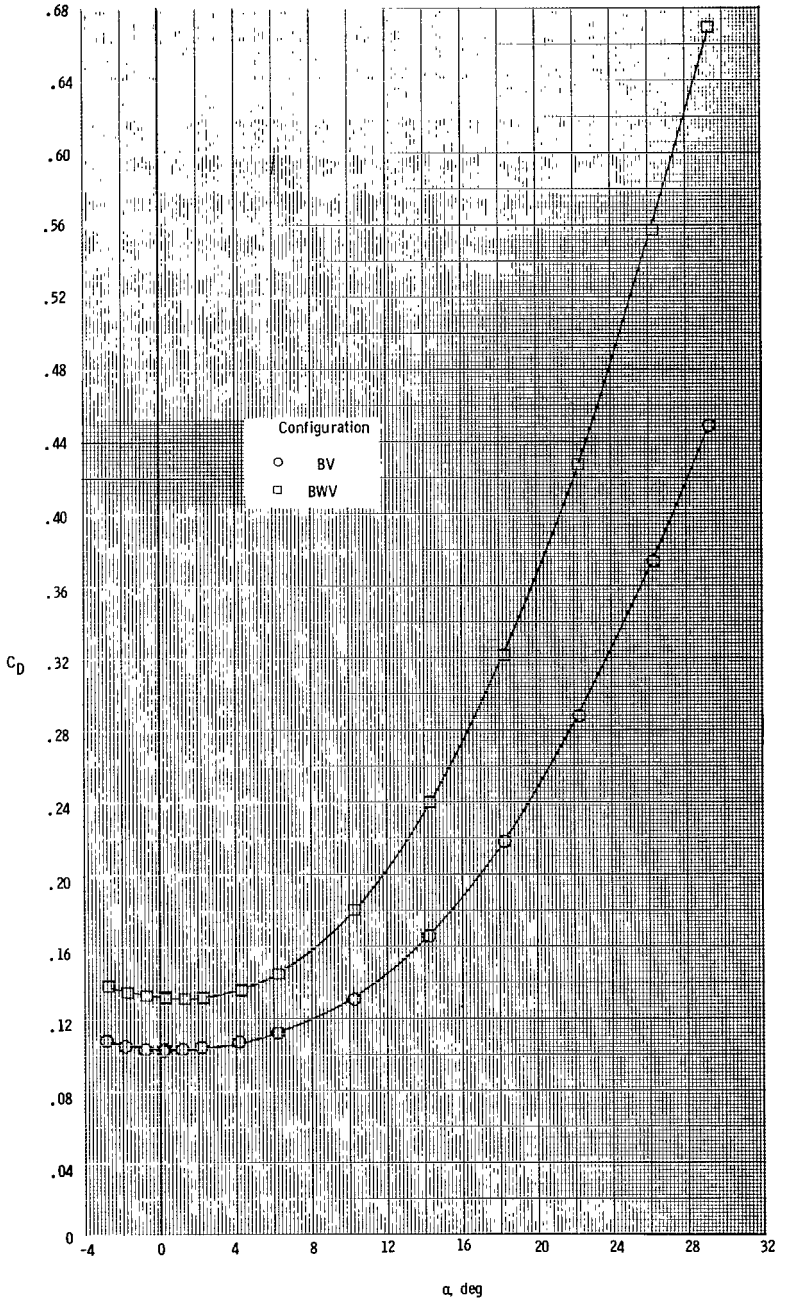

(b) C_D as a function of α.

Figure 8.- Continued.

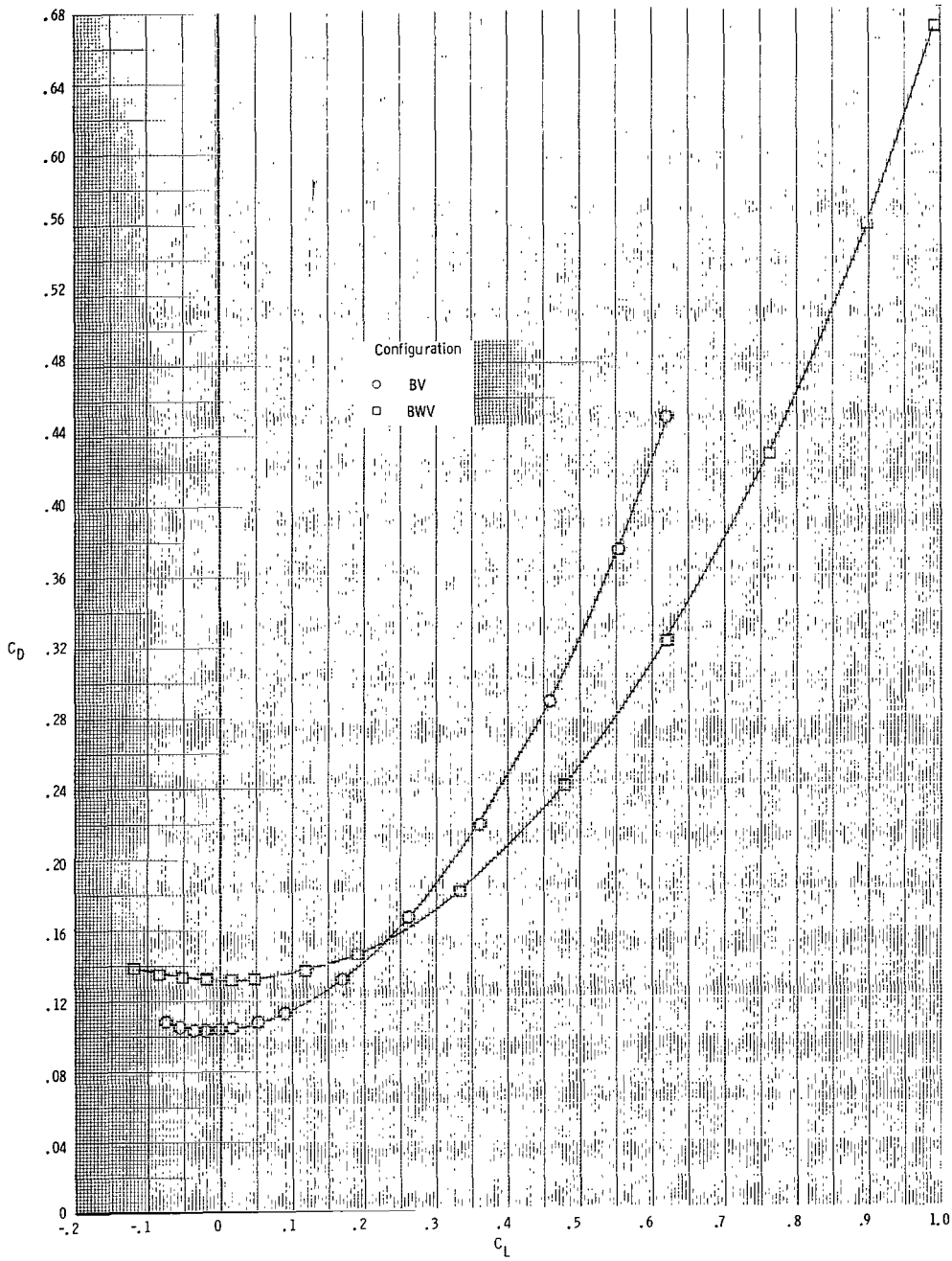

(c) C_D as a function of C_L.

Figure 8.- Continued.

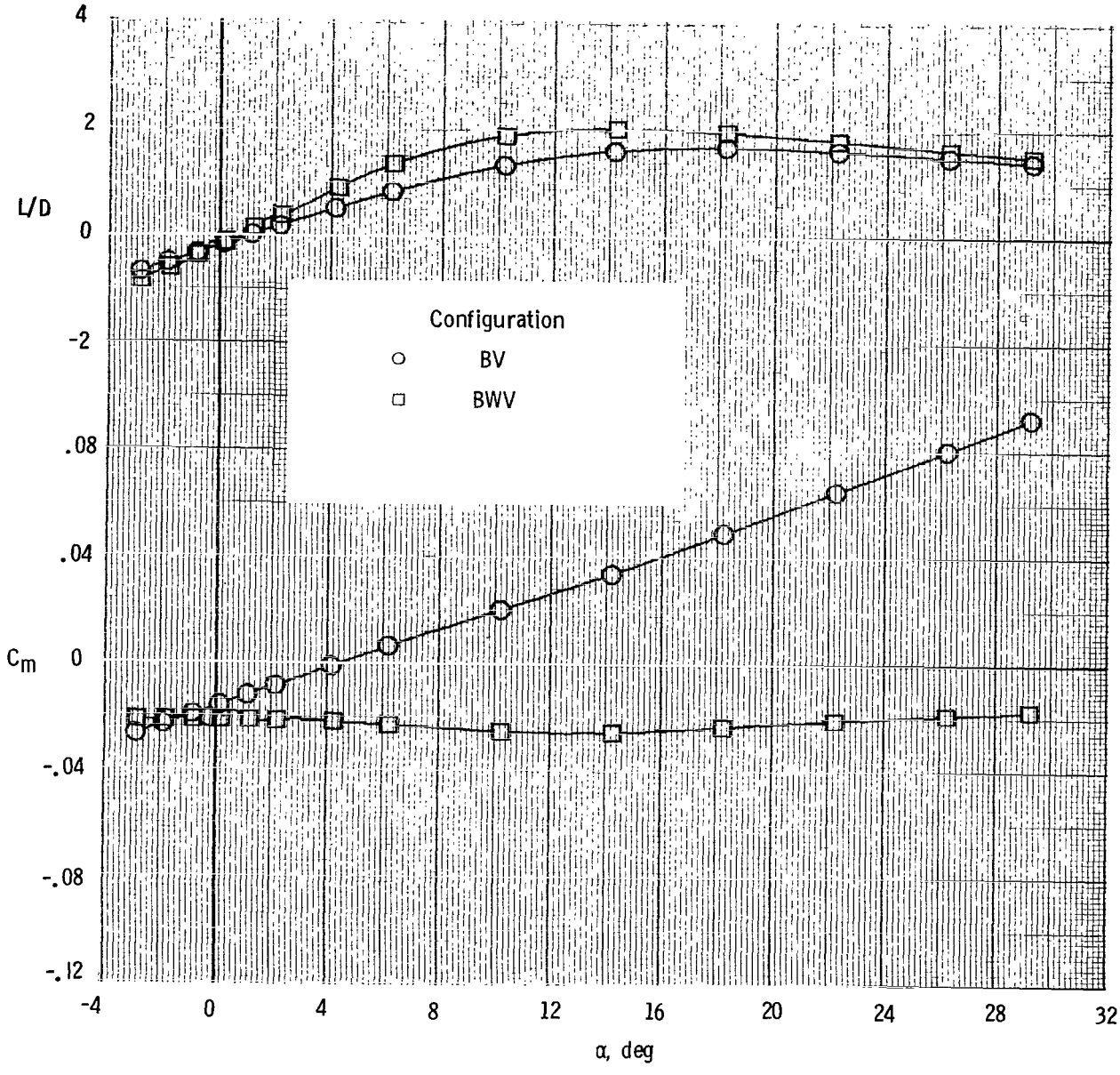

(d) C_m and L/D as a function of α.

Figure 8.- Continued.

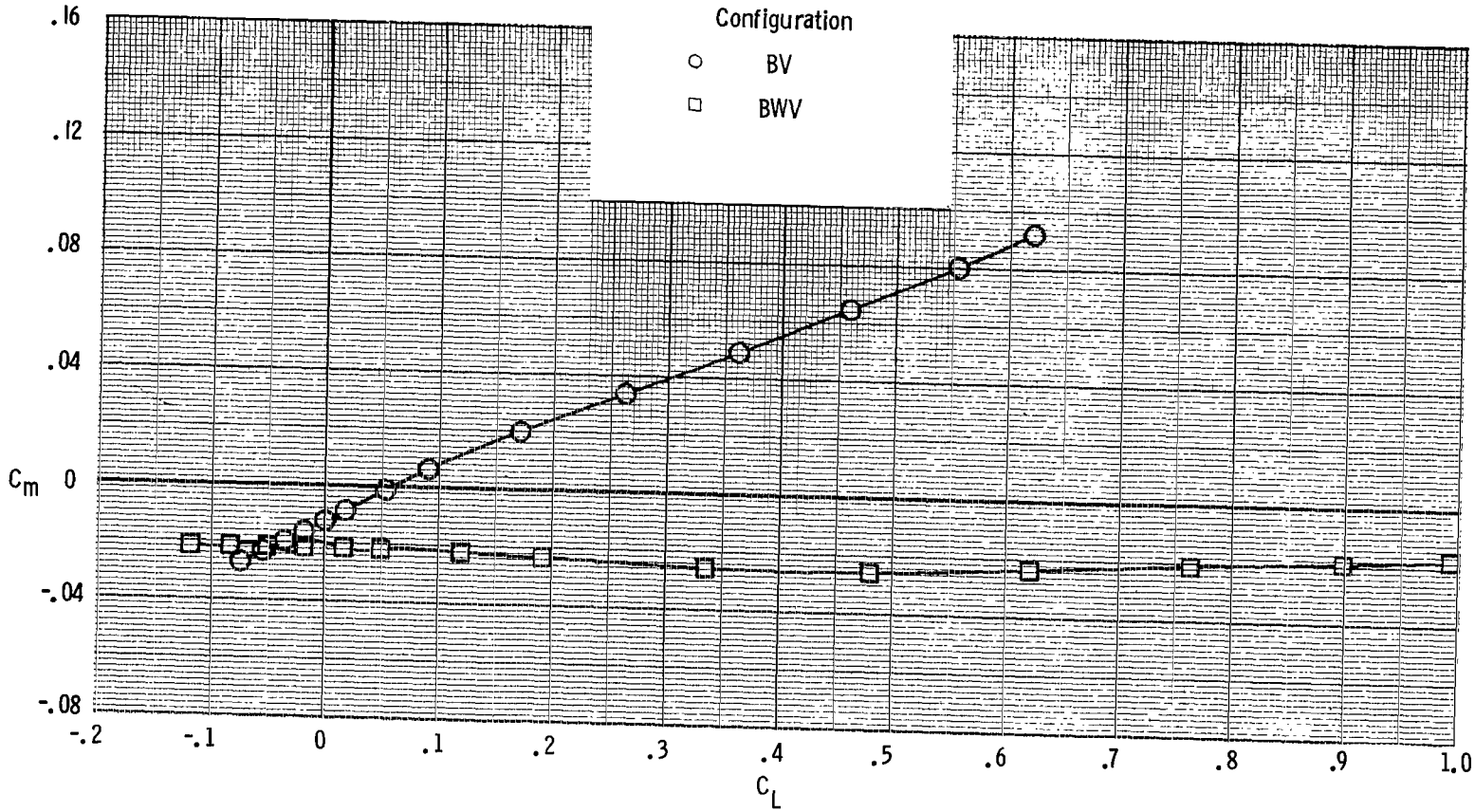

(e) C_m as a function of C_L.

Figure 8.- Concluded.

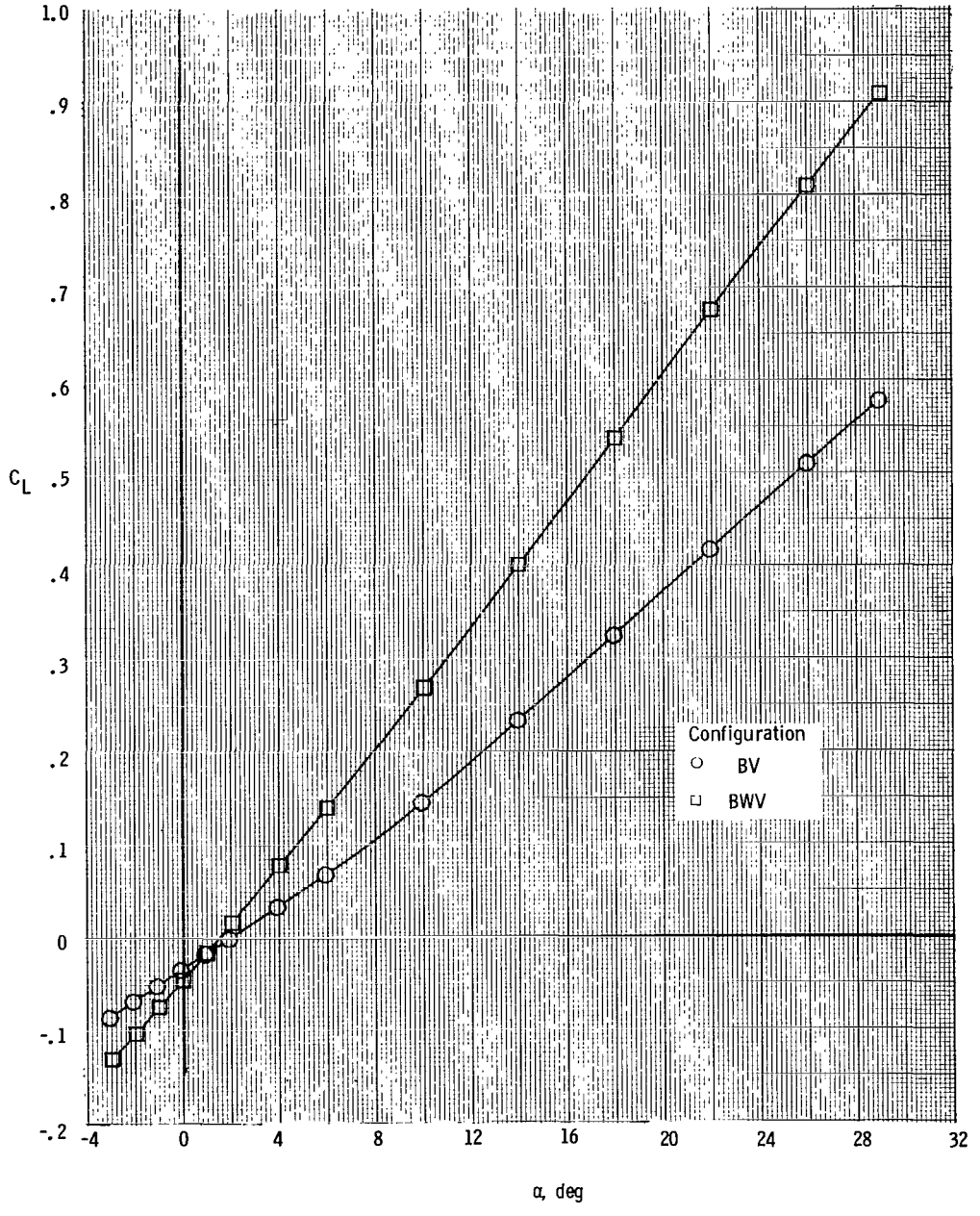

(a) C_L as a function of α.

Figure 9.- Effect of body buildup on the static longitudinal stability characteristics of the model at M = 2.86.

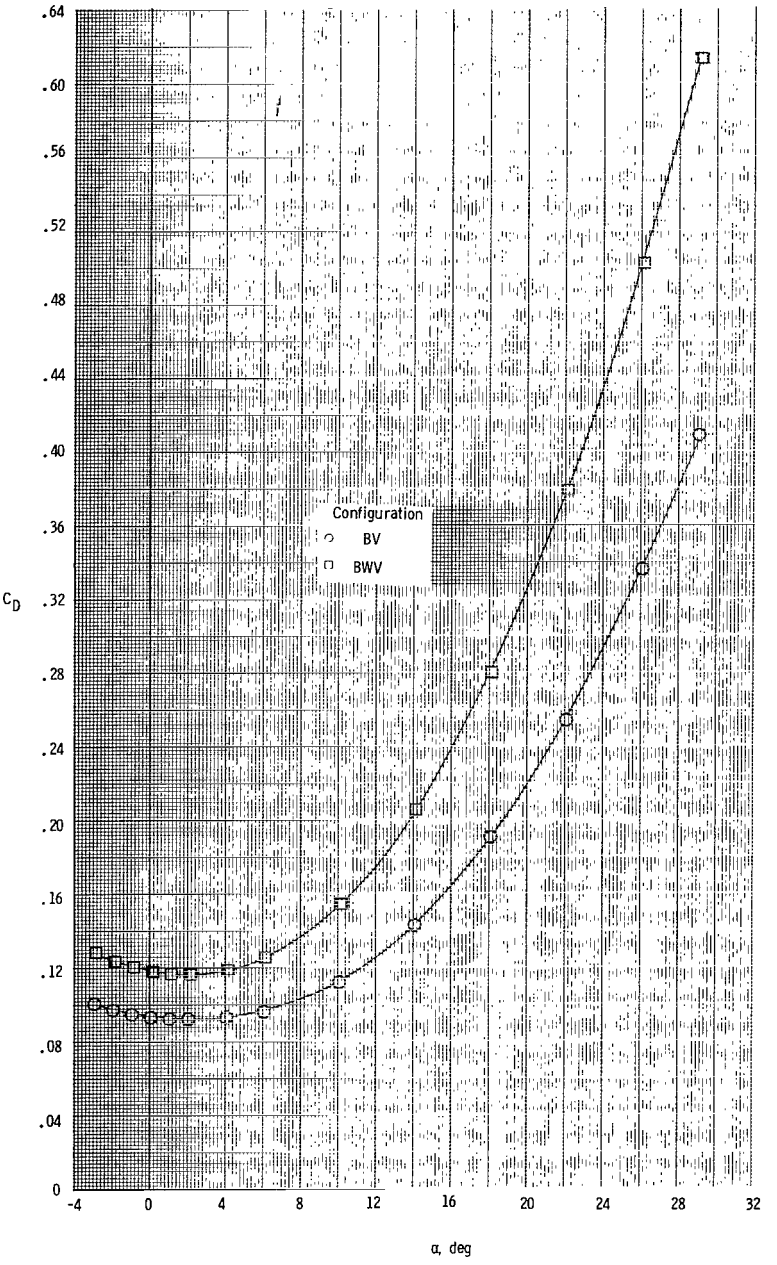

(b) C_D as a function of α.

Figure 9.- Continued.

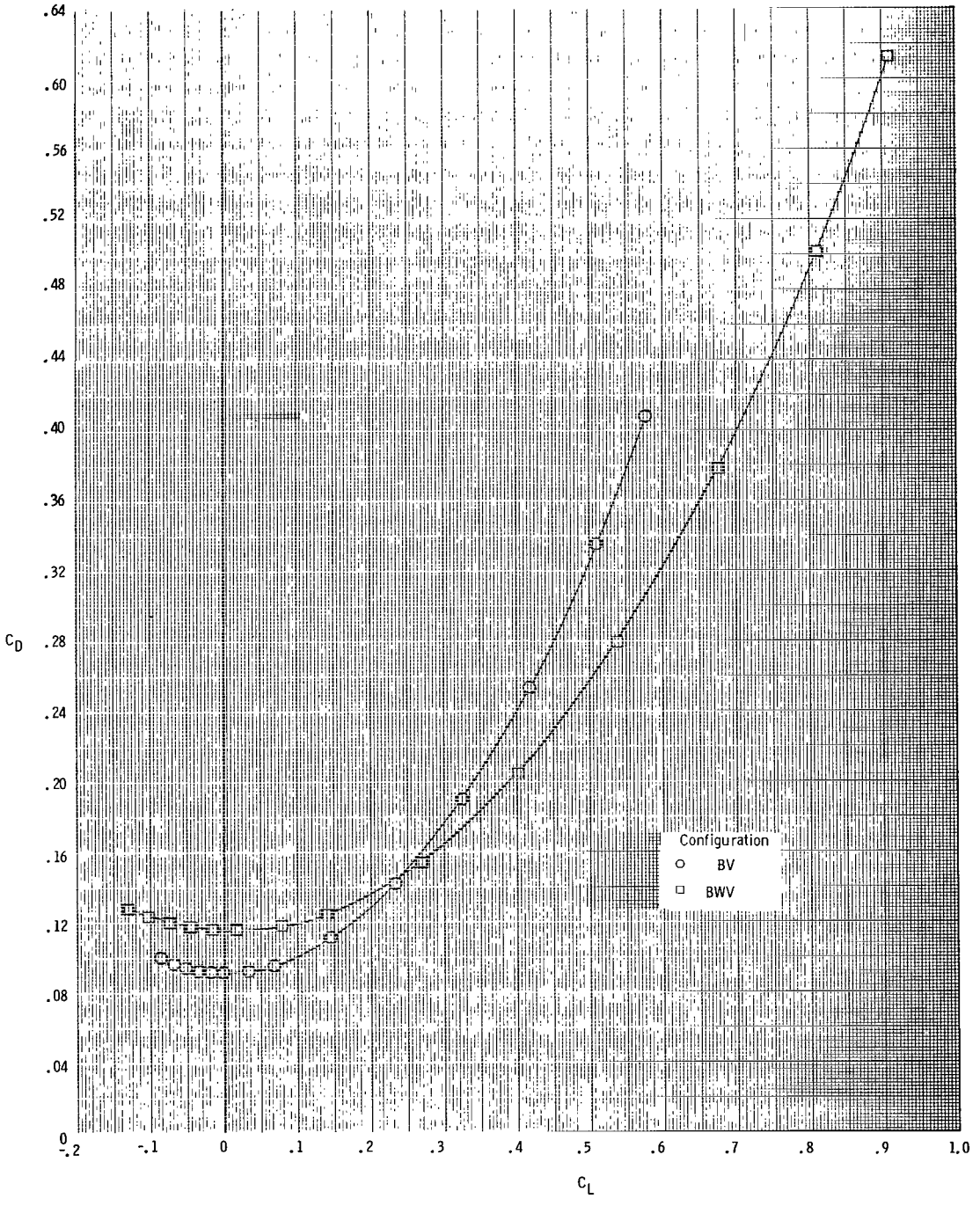

(c) C_D as a function of C_L.

Figure 9.- Continued.

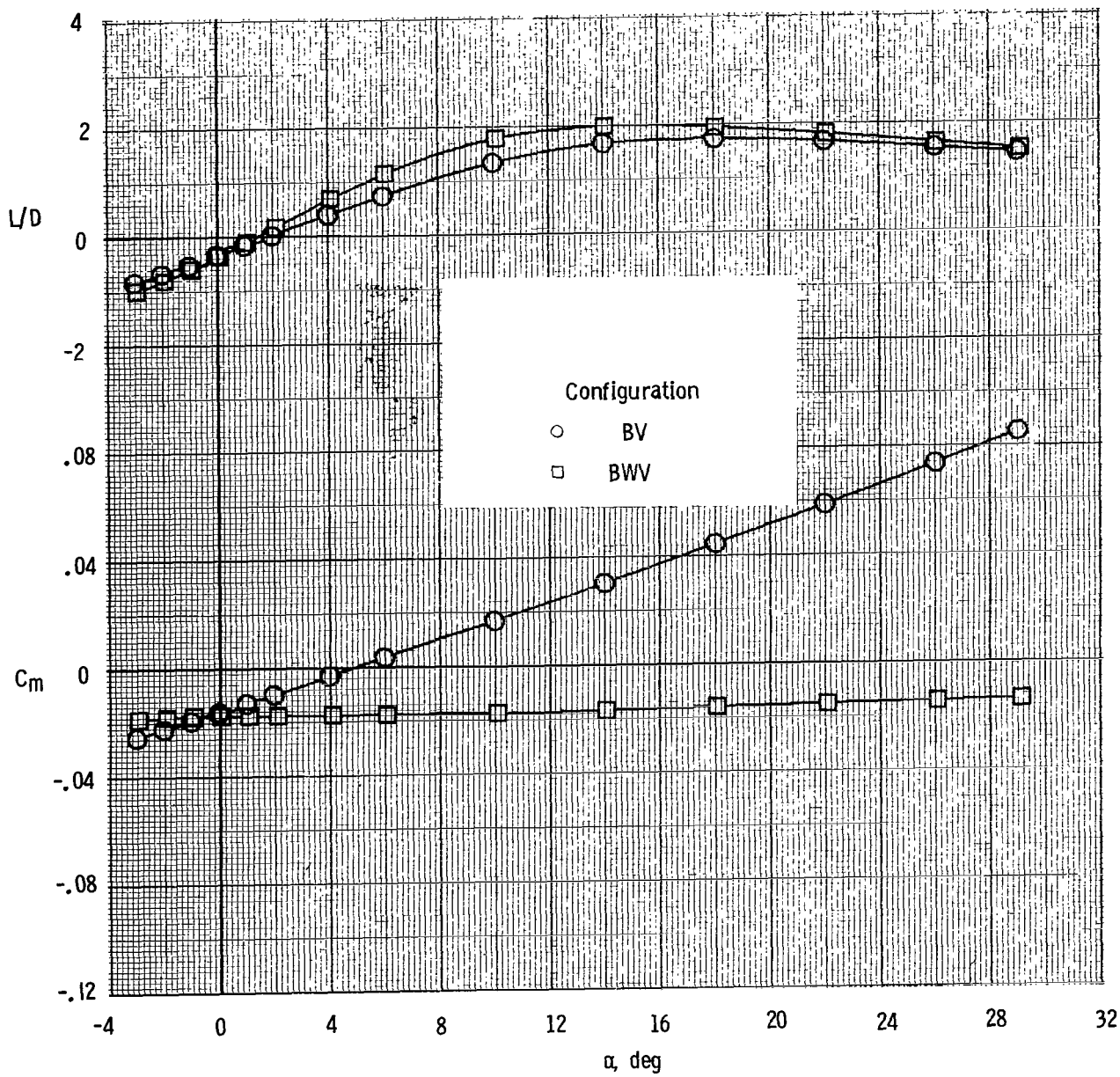

(d) C_m and L/D as a function of α.

Figure 9.- Continued.

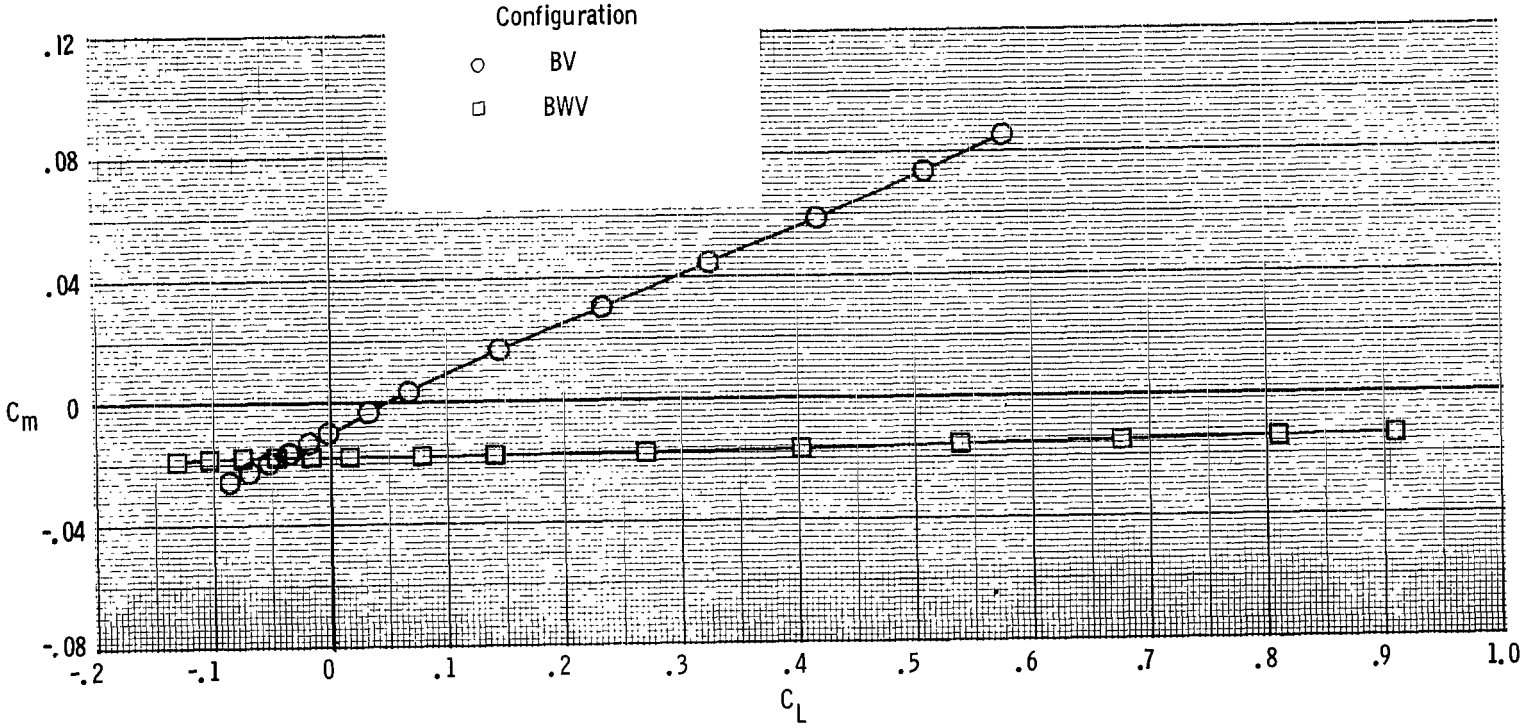

(e) C_m as a function of C_L.

Figure 9.- Concluded.

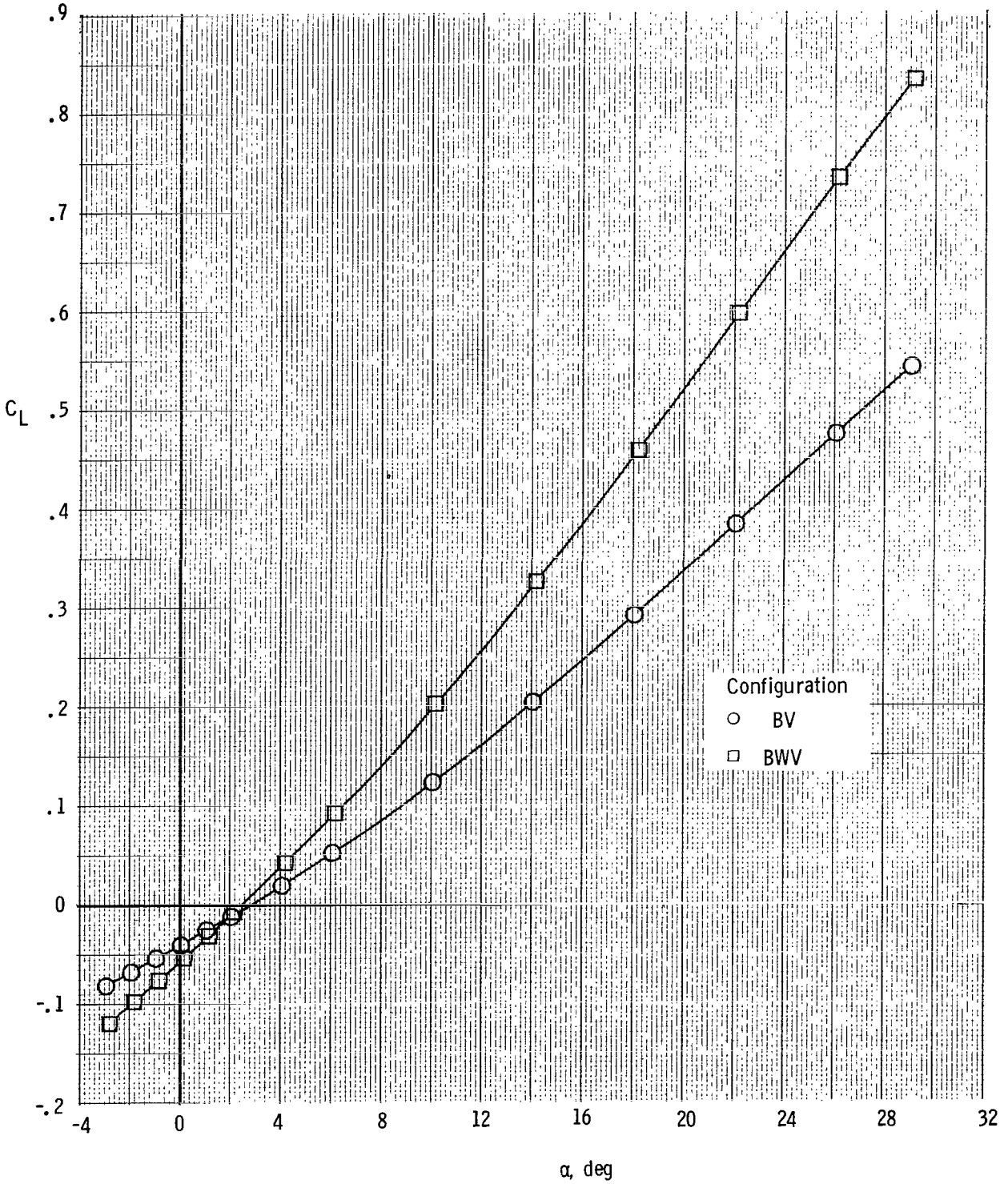

(a) C_L as a function of α.

Figure 10.- Effect of body buildup on the static longitudinal stability characteristics of the model at M = 3.95.

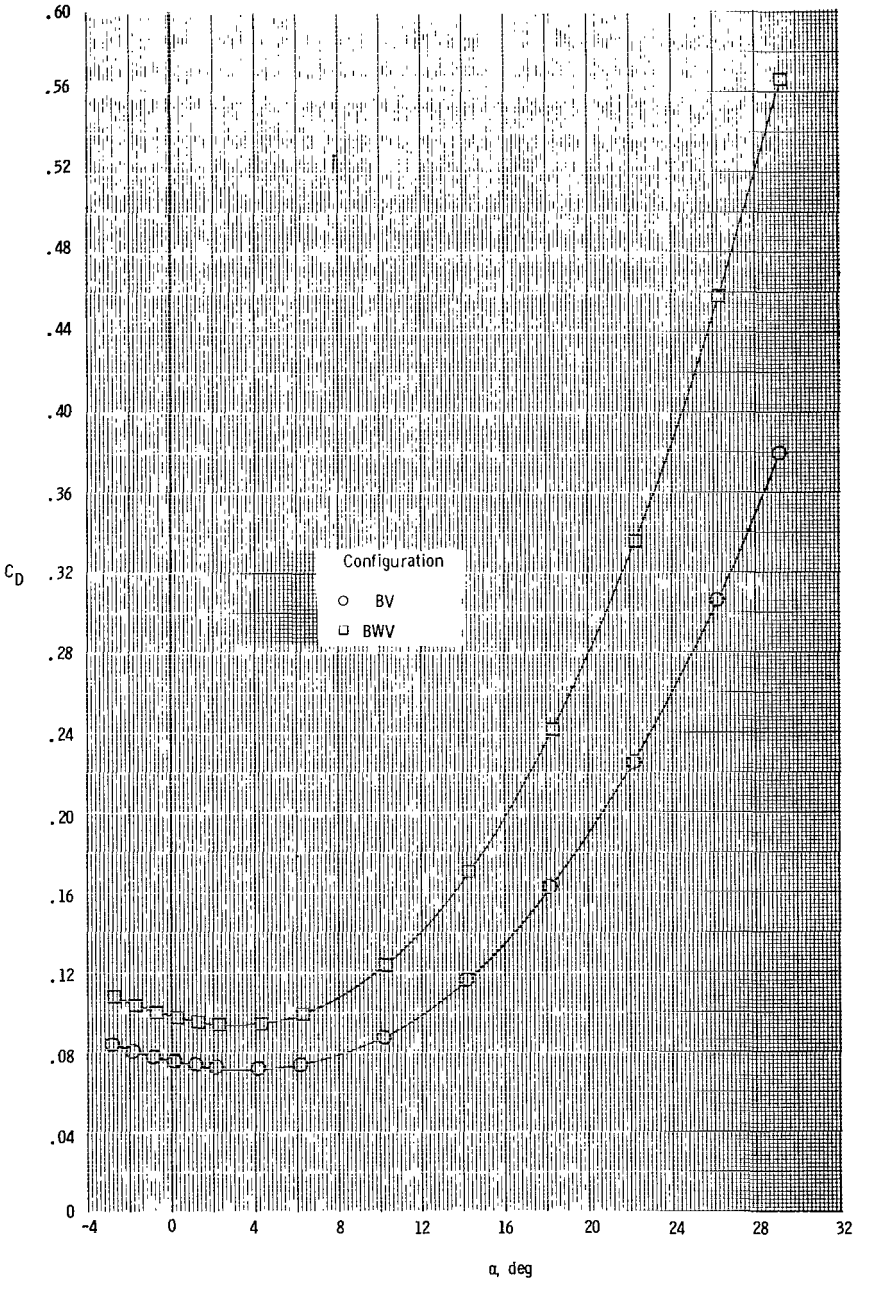

(b) C_D as a function of α.

Figure 10.- Continued.

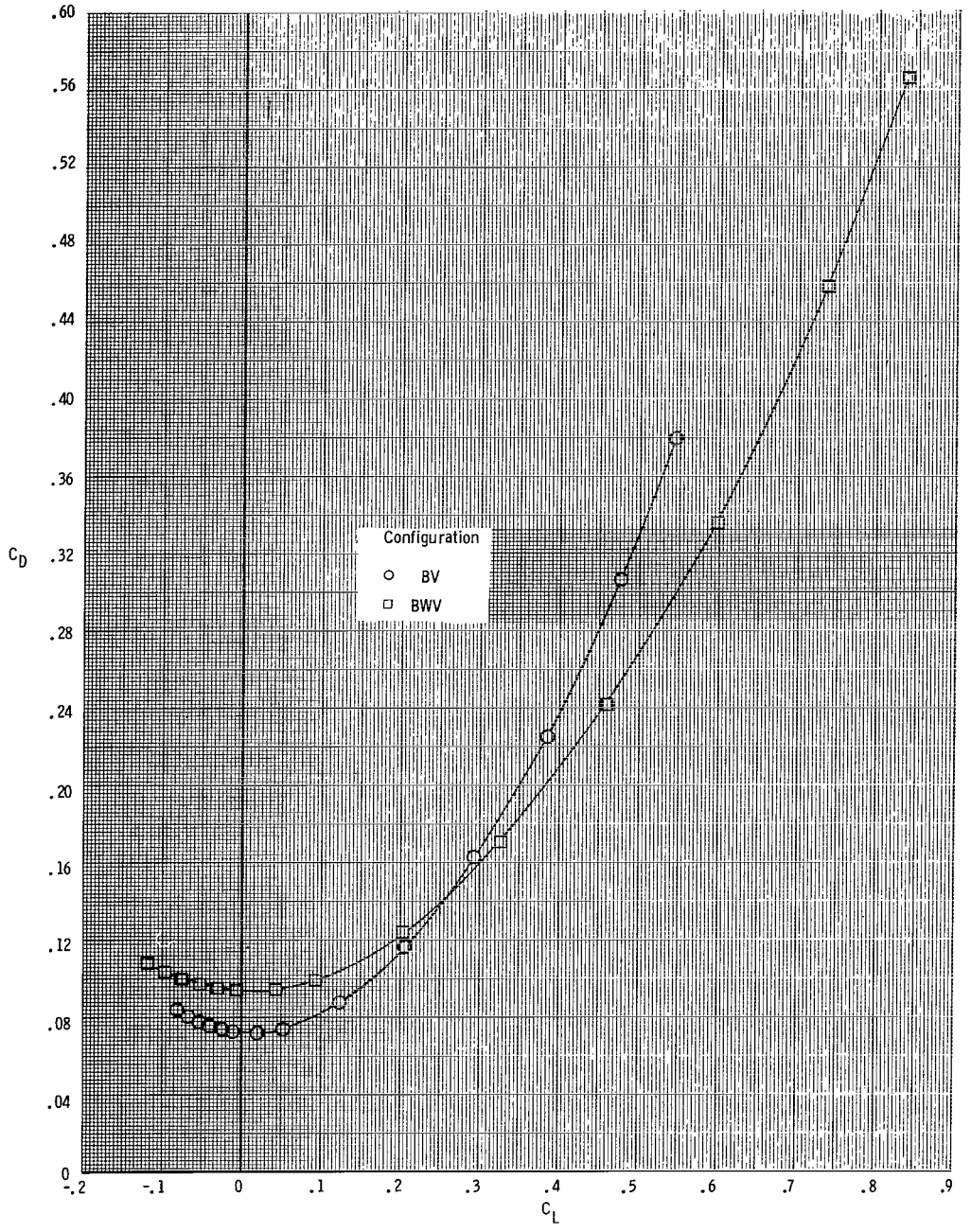

(c) C_D as a function of C_L.

Figure 10.- Continued.

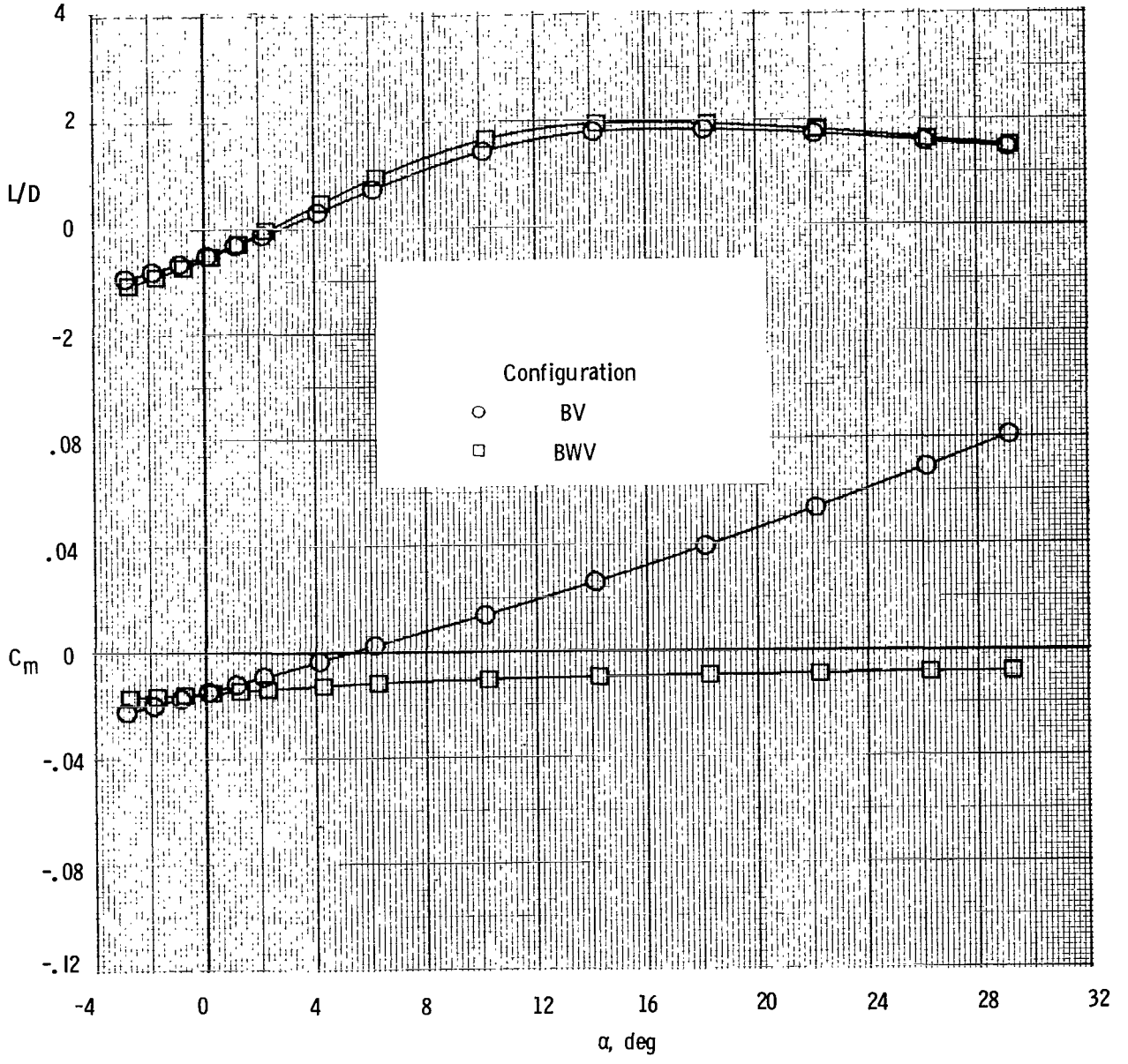

(d) C_m and L/D as a function of α.

Figure 10.- Continued.

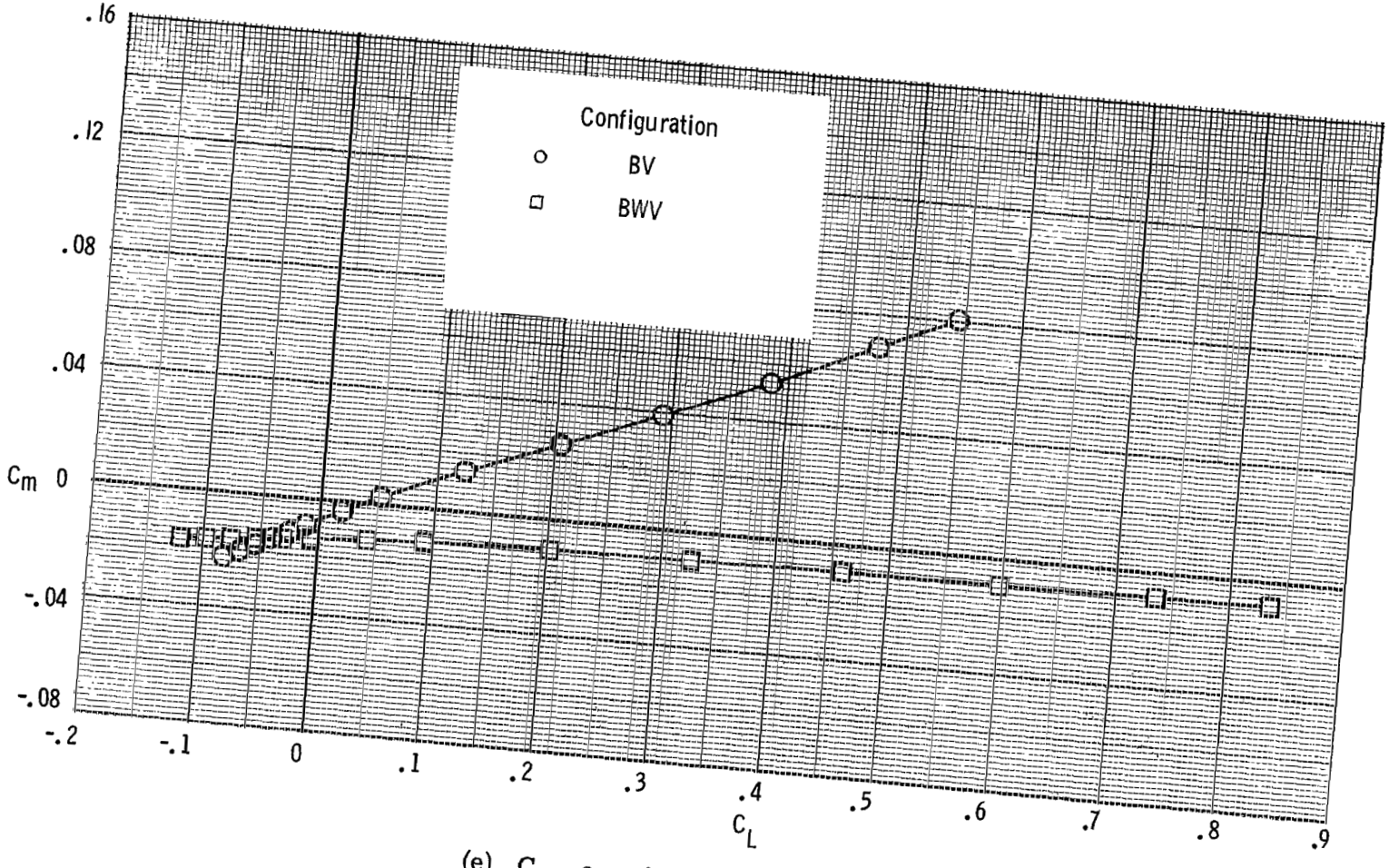

(e) C_m as a function of C_L.

Figure 10.- Concluded.

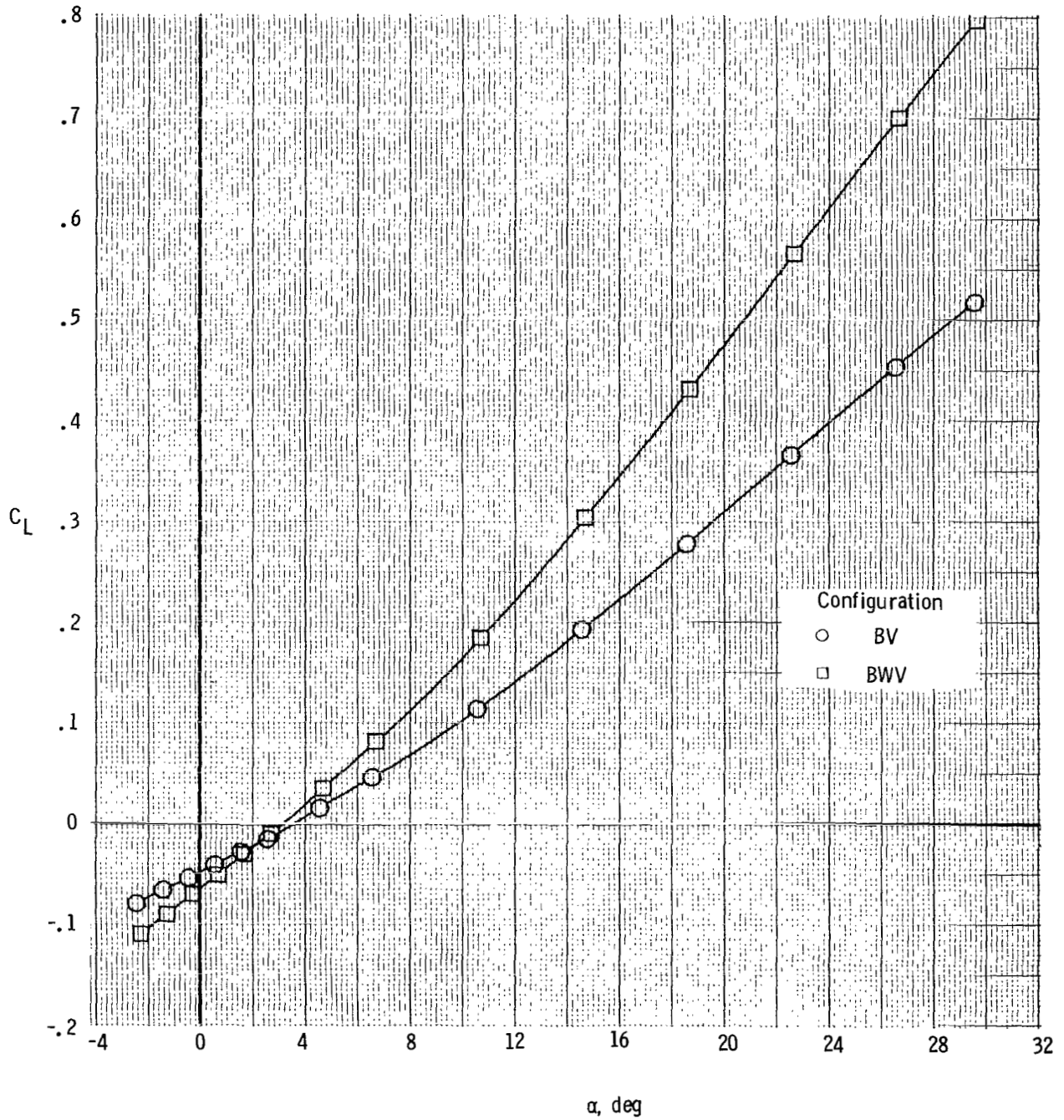

(a) C_L as a function of α.

Figure 11.- Effect of body buildup on the static longitudinal stability characteristics of the model at M = 4.63.

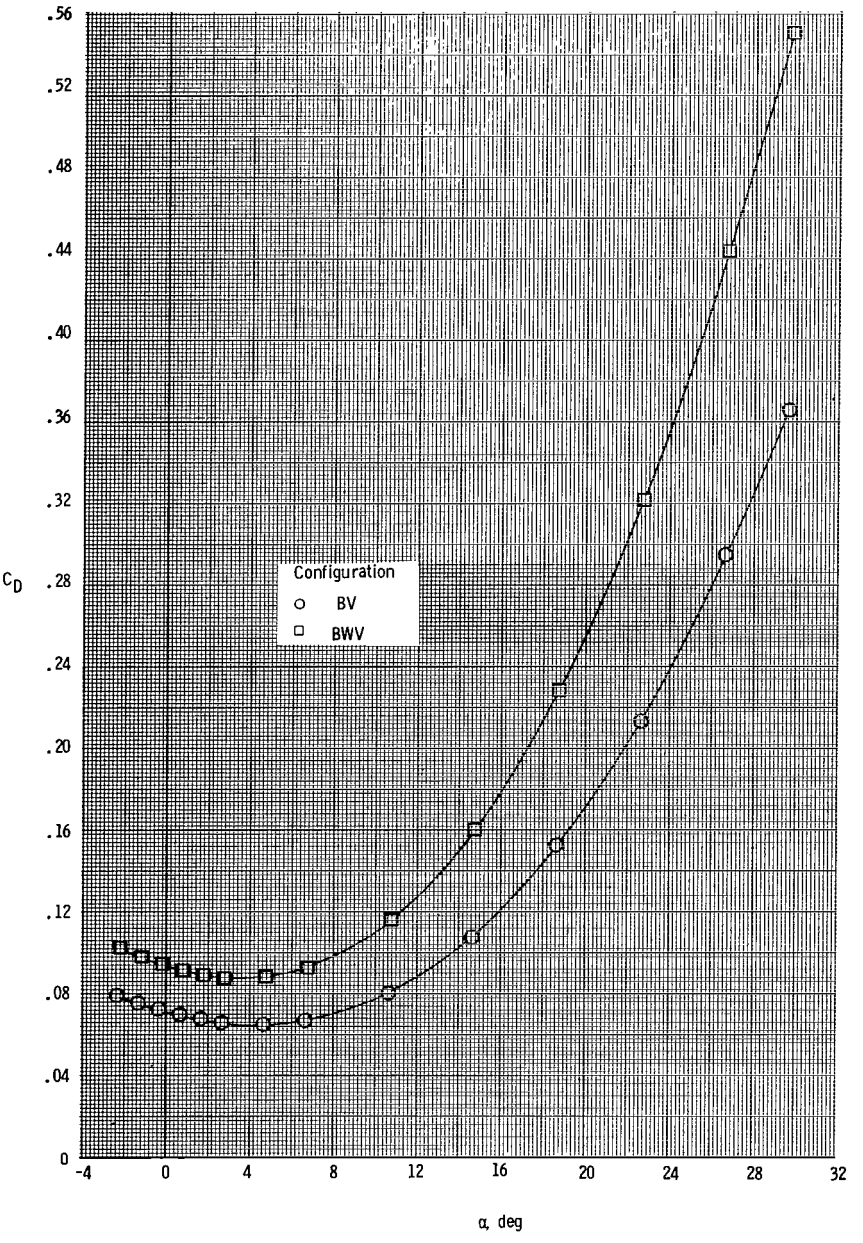

(b) C_D as a function of α.

Figure 11.- Continued.

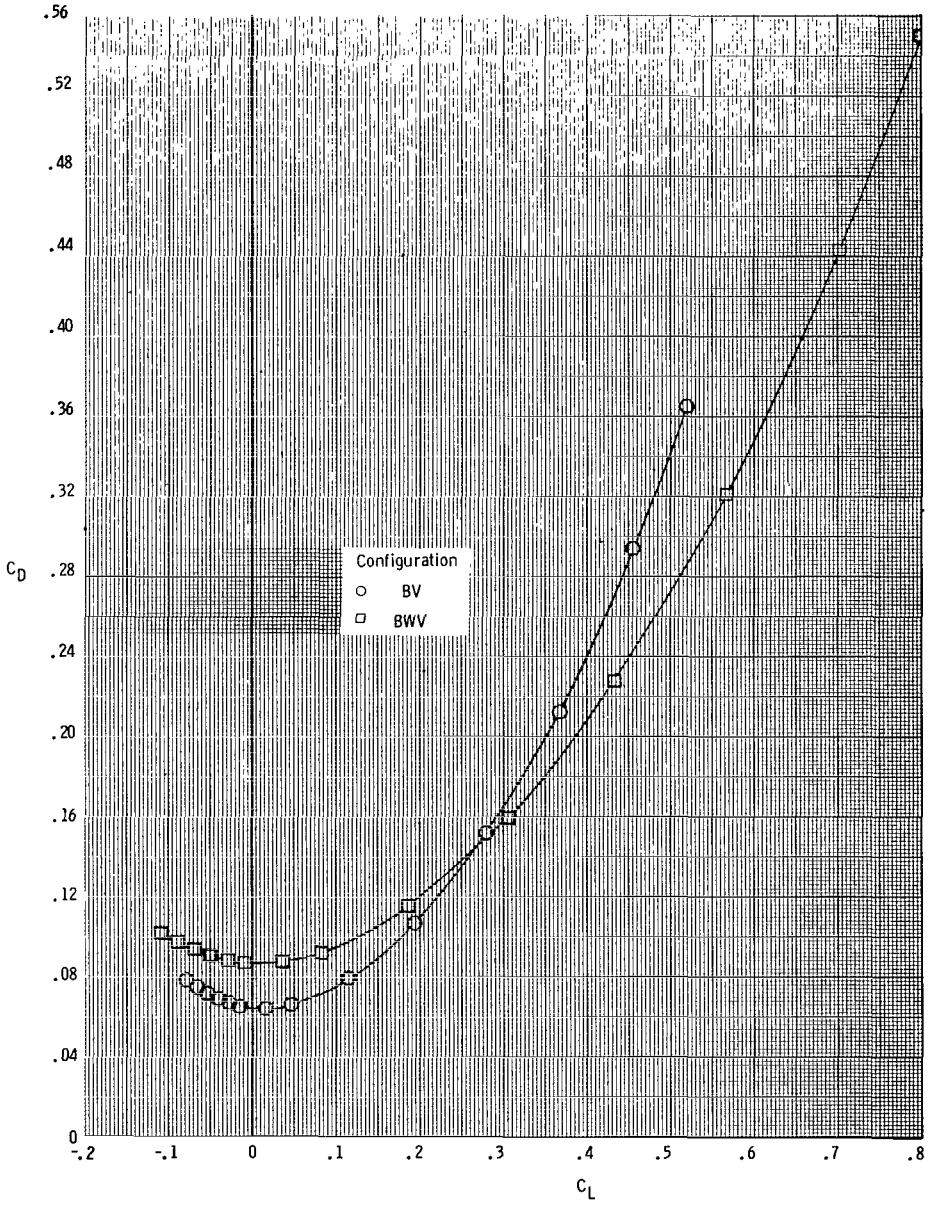

(c) C_D as a function of C_L.

Figure 11.- Continued.

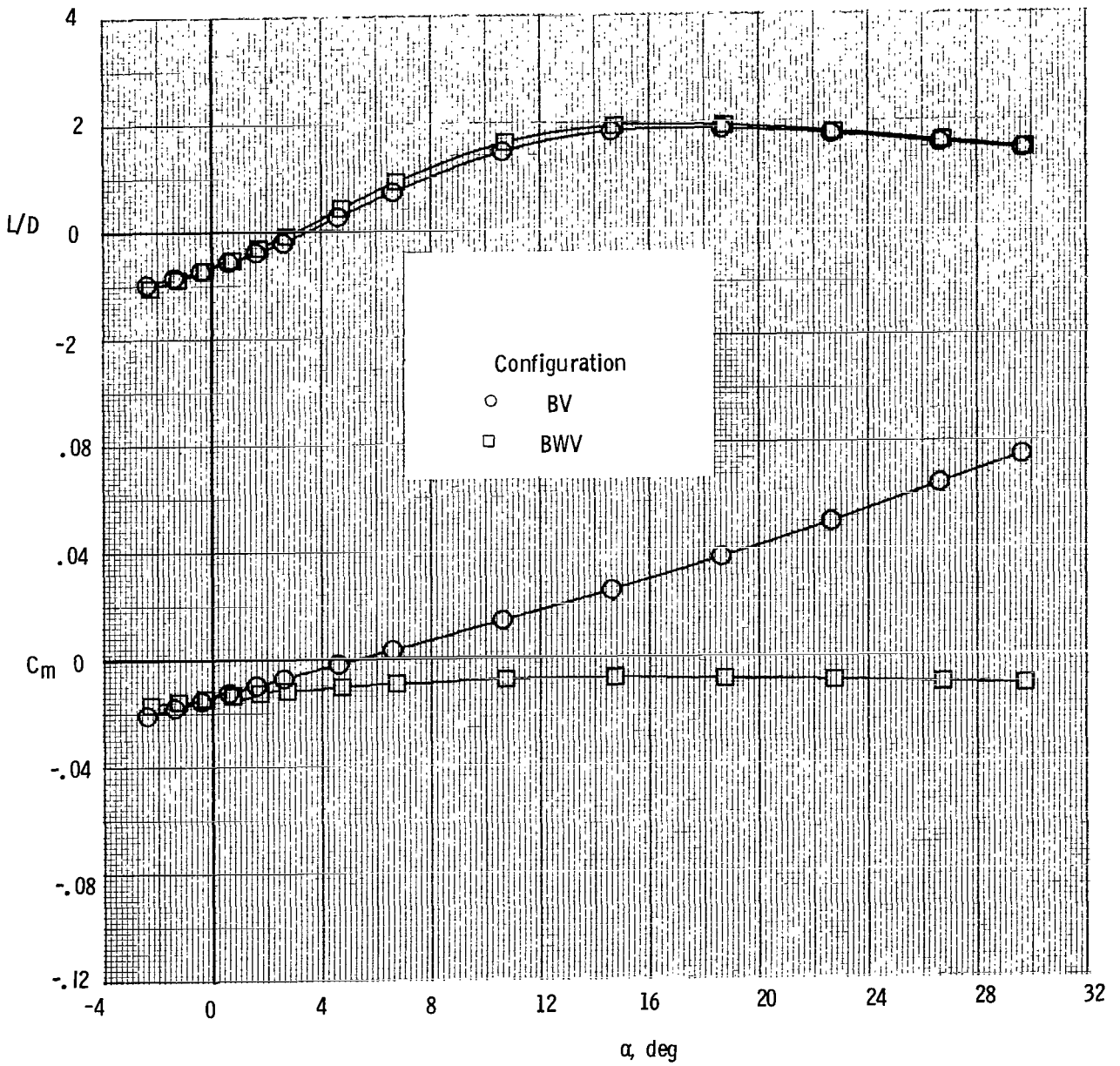

(d) C_m and L/D as a function of α.

Figure 11.- Continued.

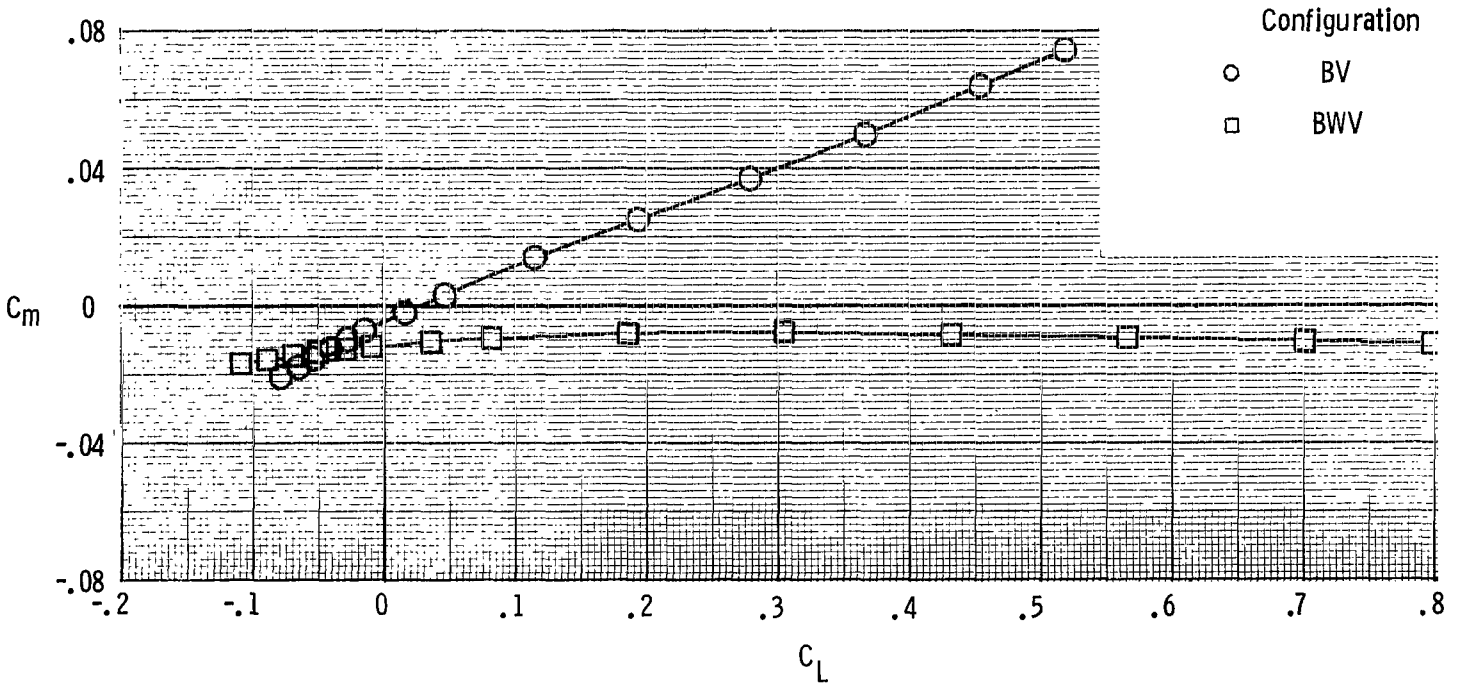

(e) C_m as a function of C_L.

Figure 11.- Concluded.

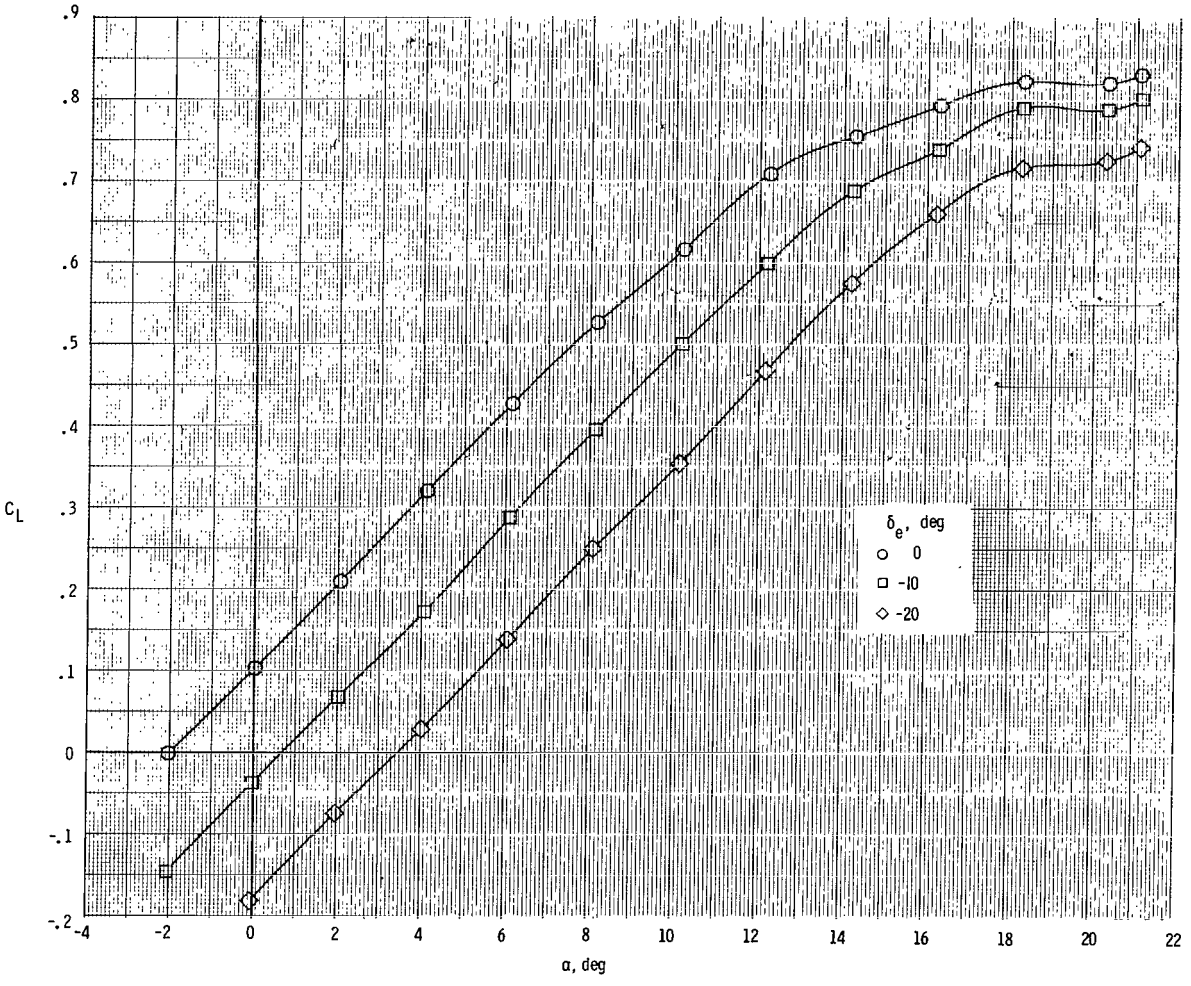

(a) C_L as a function of α.

Figure 12.- Elevon effectiveness of the model at M = 0.3.

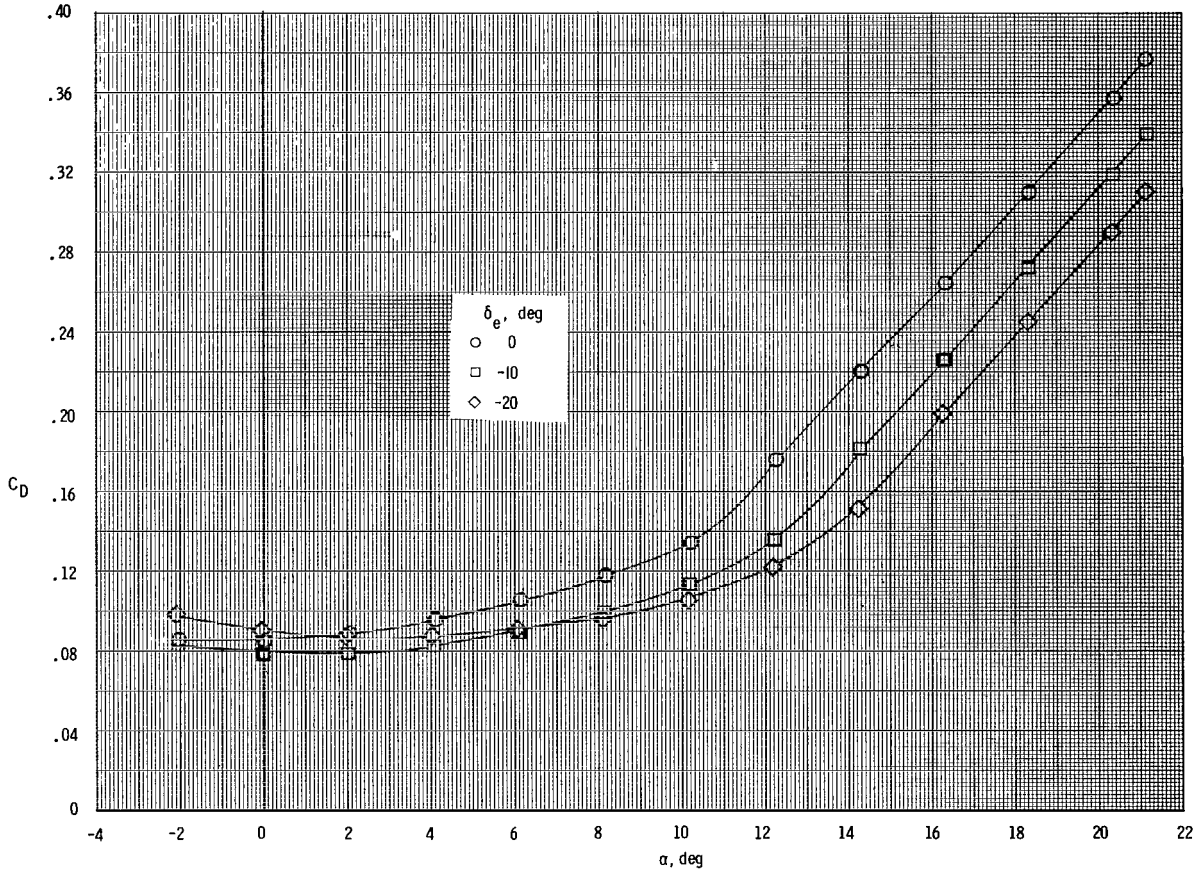

(b) C_D as a function of α.

Figure 12.- Continued.

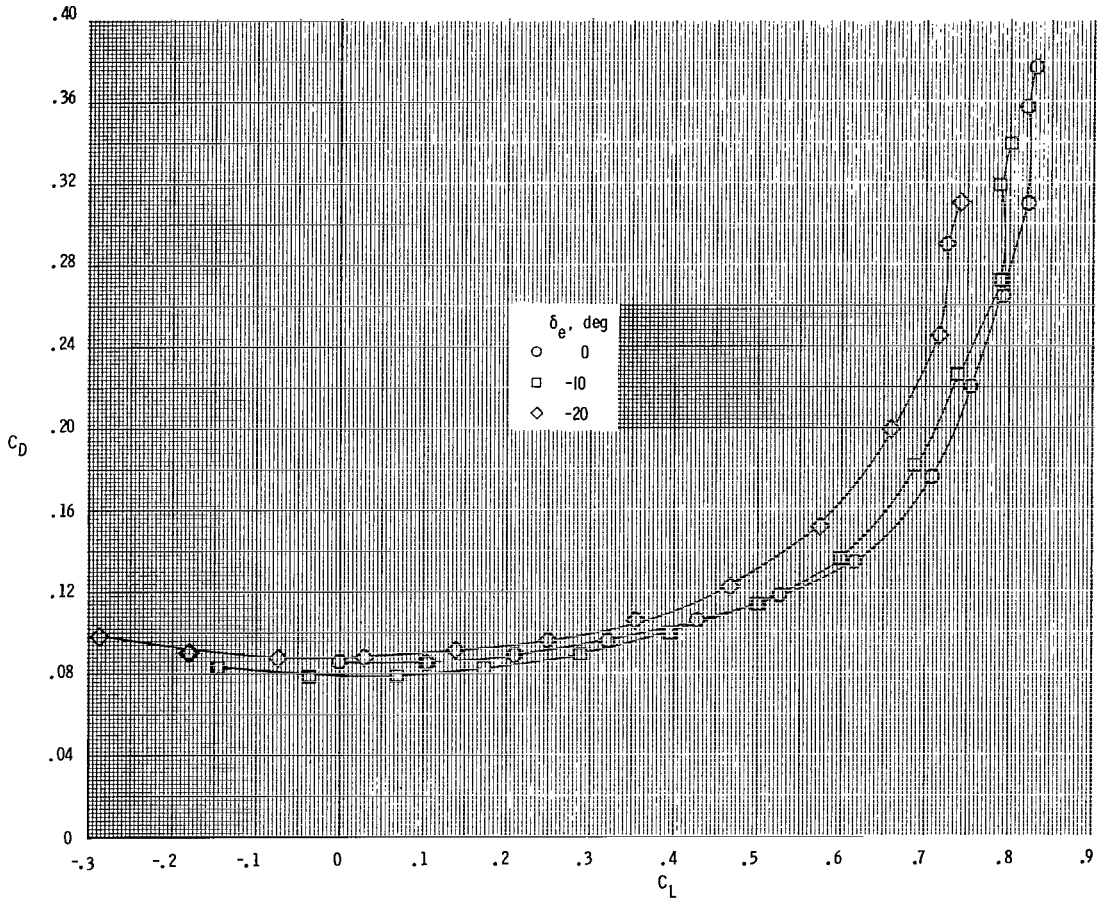

(c) C_D as a function of C_L.

Figure 12.- Continued.

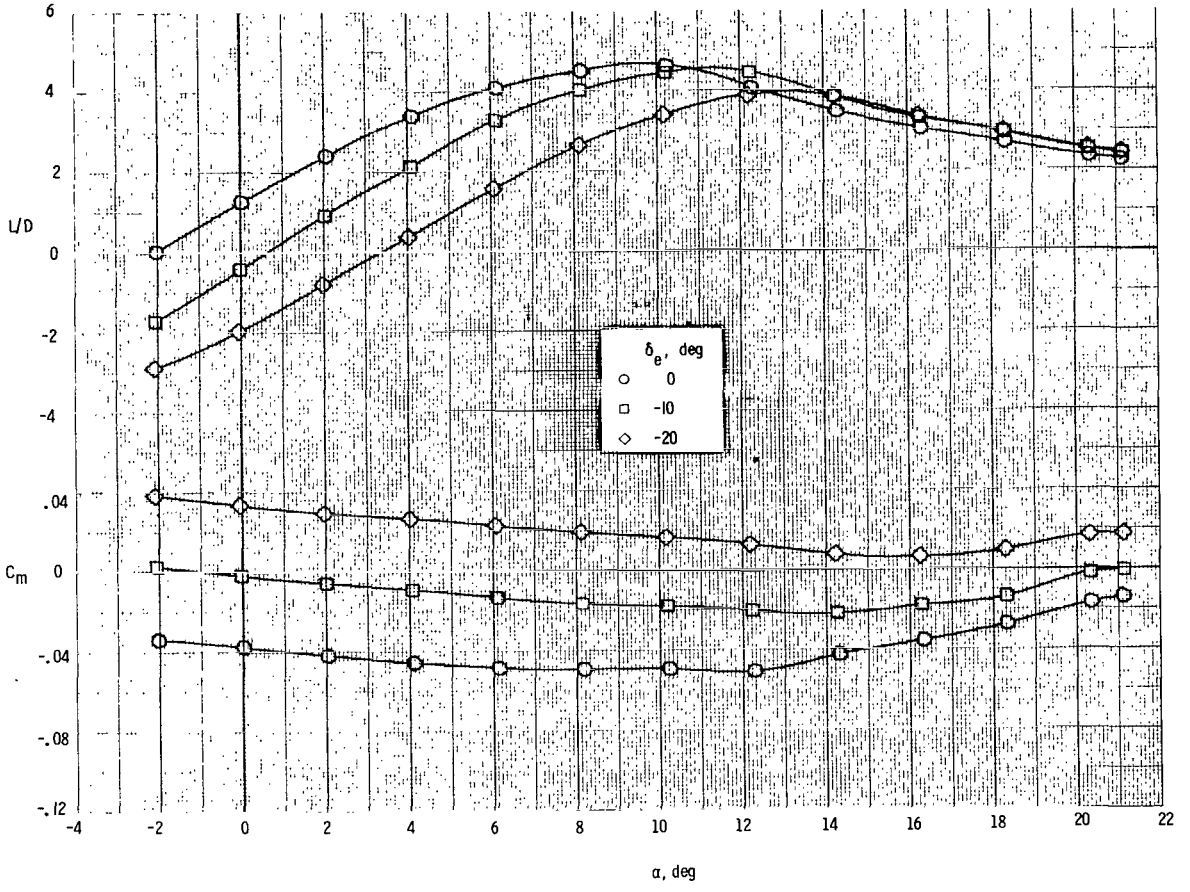

(d) C_m and L/D as a function of α.

Figure 12.- Continued.

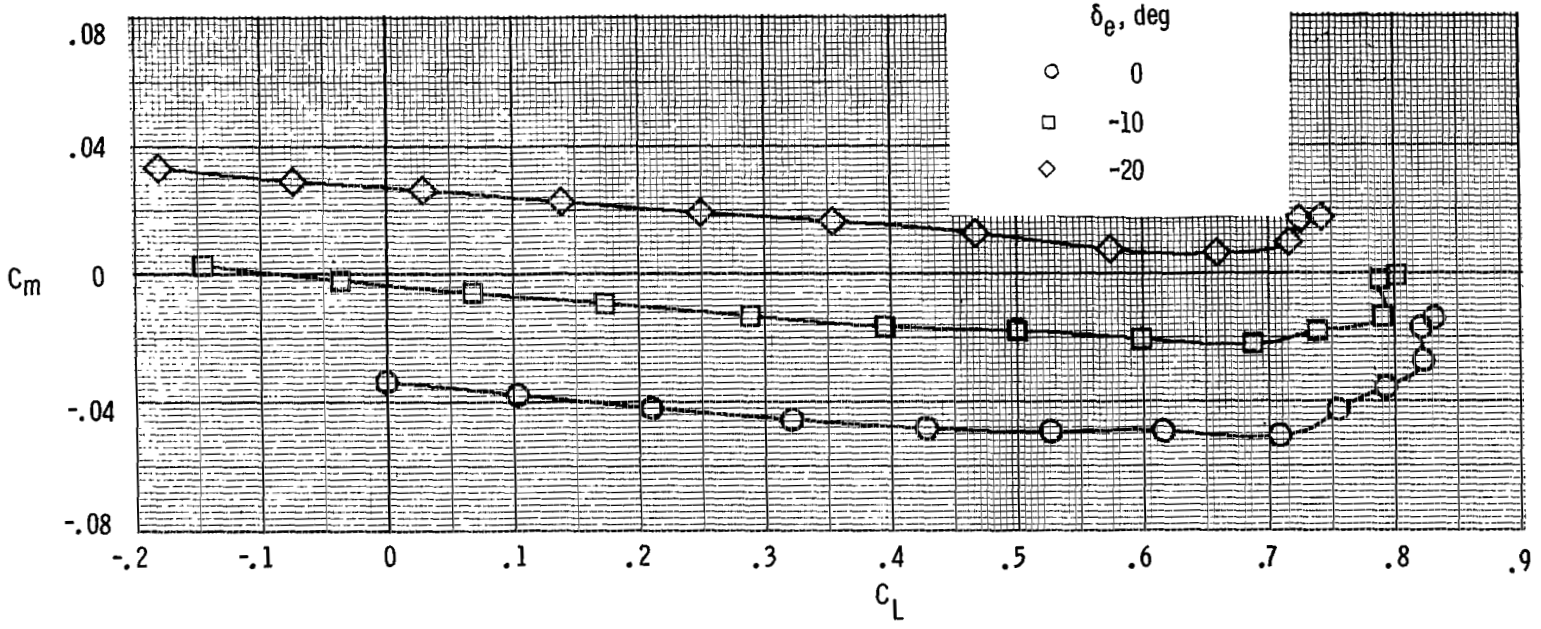

(e) C_m as a function of C_L.

Figure 12.- Concluded.

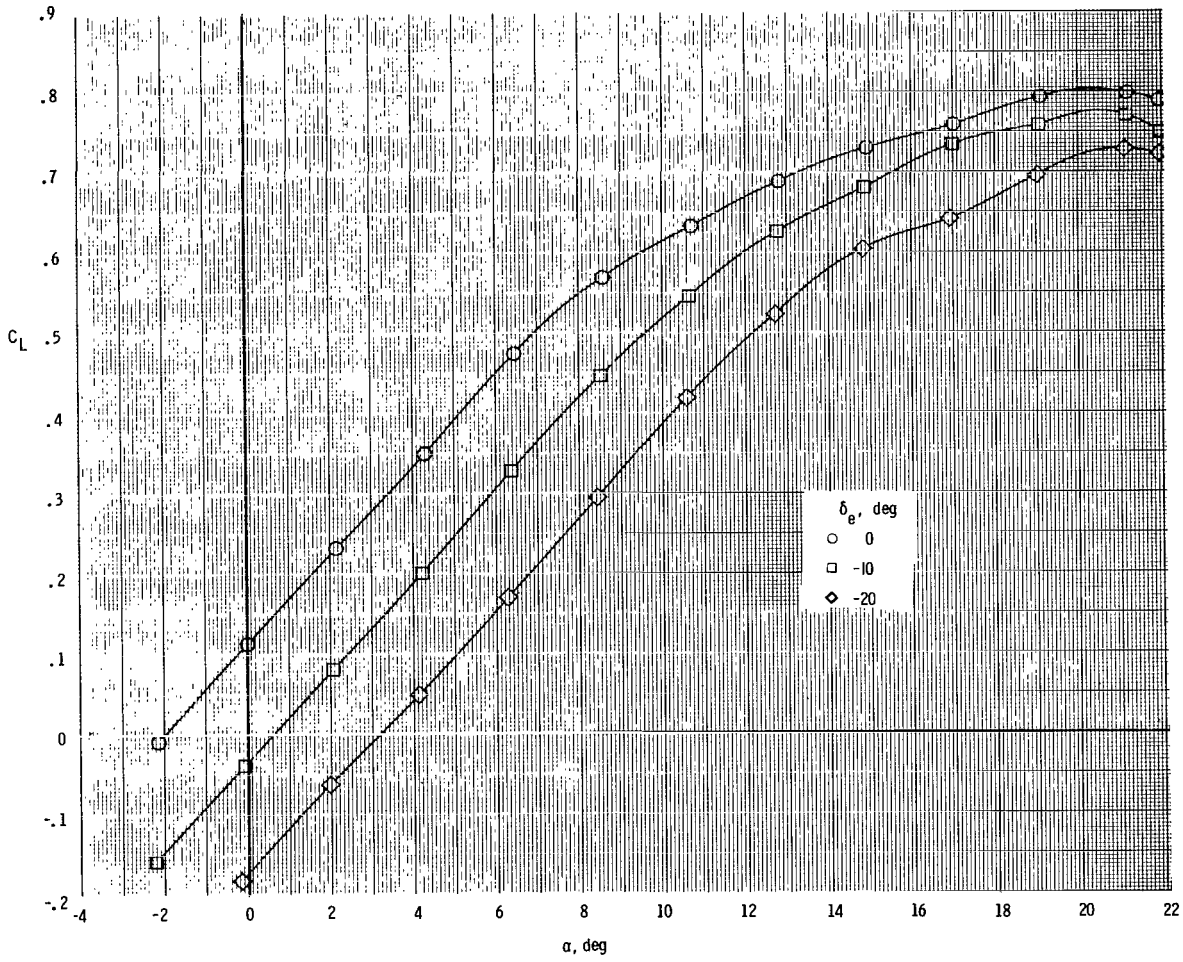

(a) C_L as a function of α.

Figure 13.- Elevon effectiveness of the model at M = 0.6.

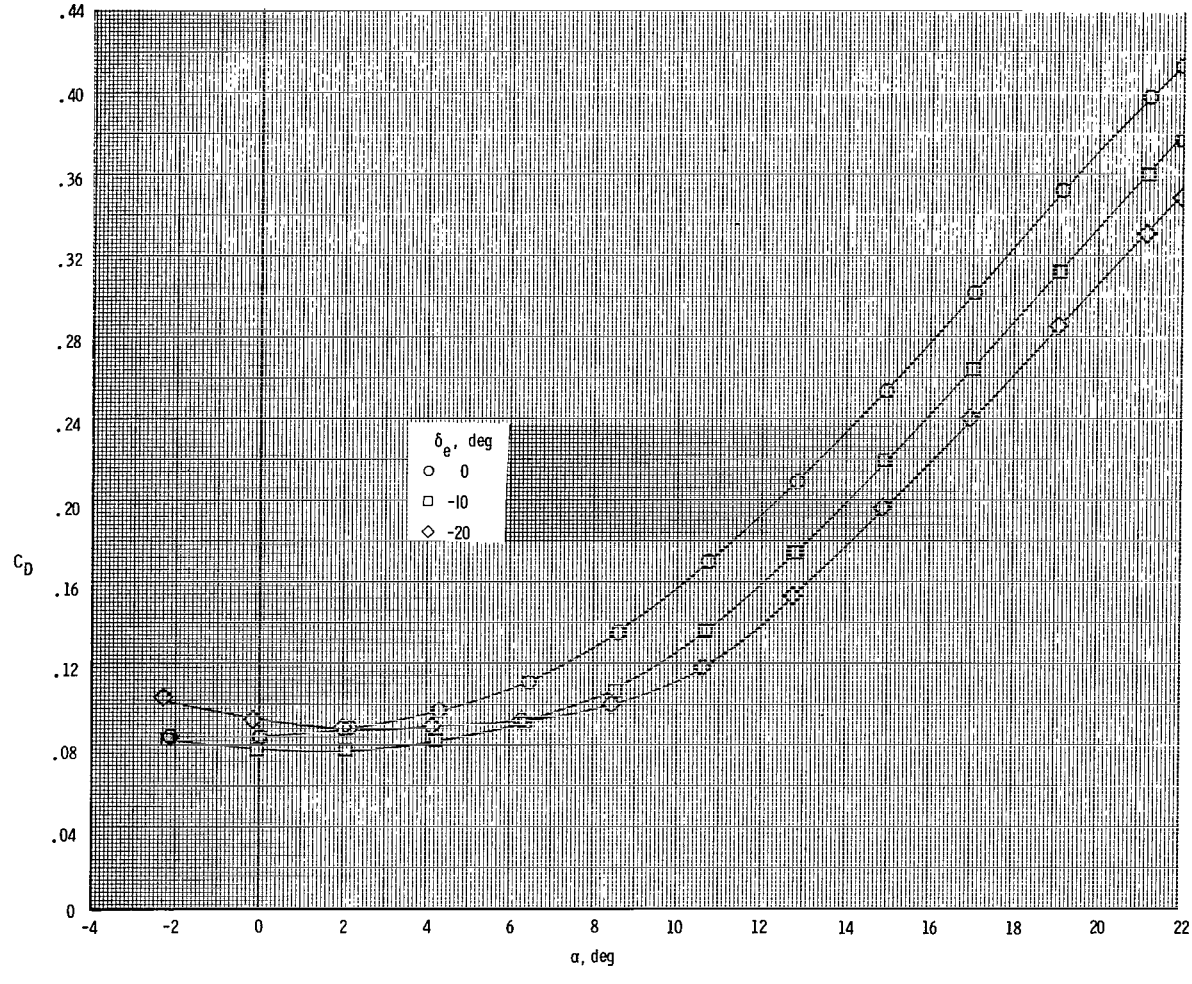

(b) C_D as a function of α.

Figure 13.- Continued.

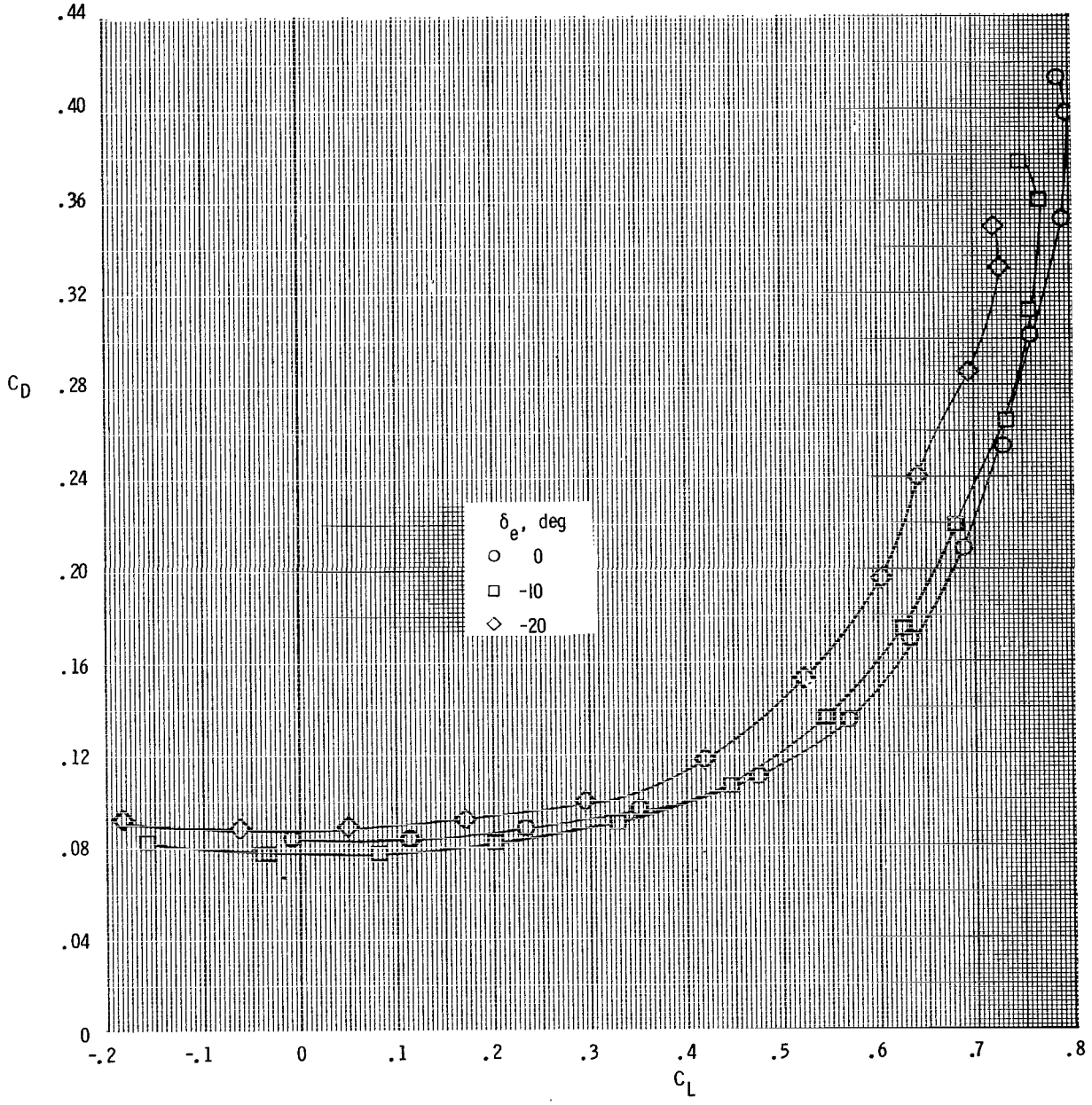

(c) C_D as a function of C_L.

Figure 13.- Continued.

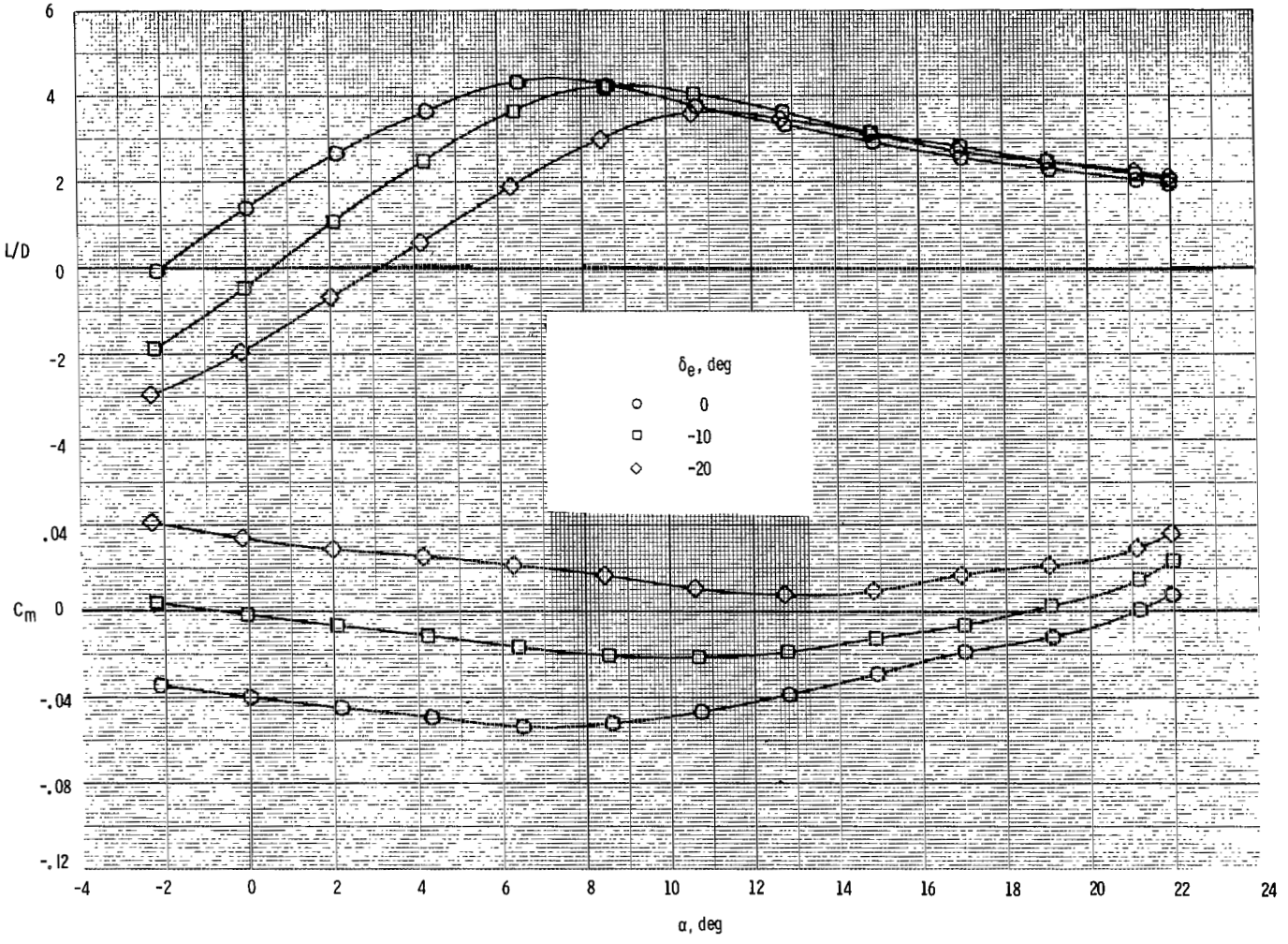

(d) C_m and L/D as a function of α.

Figure 13.- Continued.

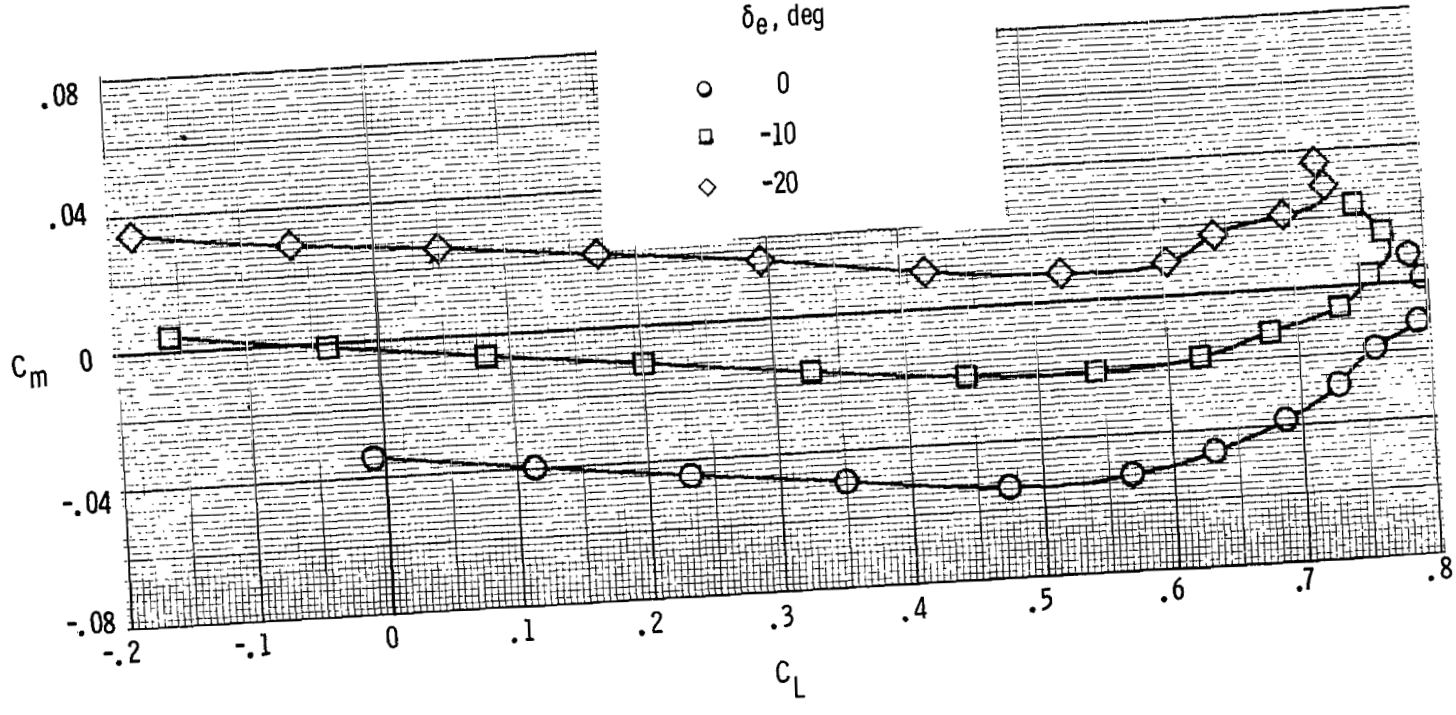

(e) C_m as a function of C_L.

Figure 13.- Concluded.

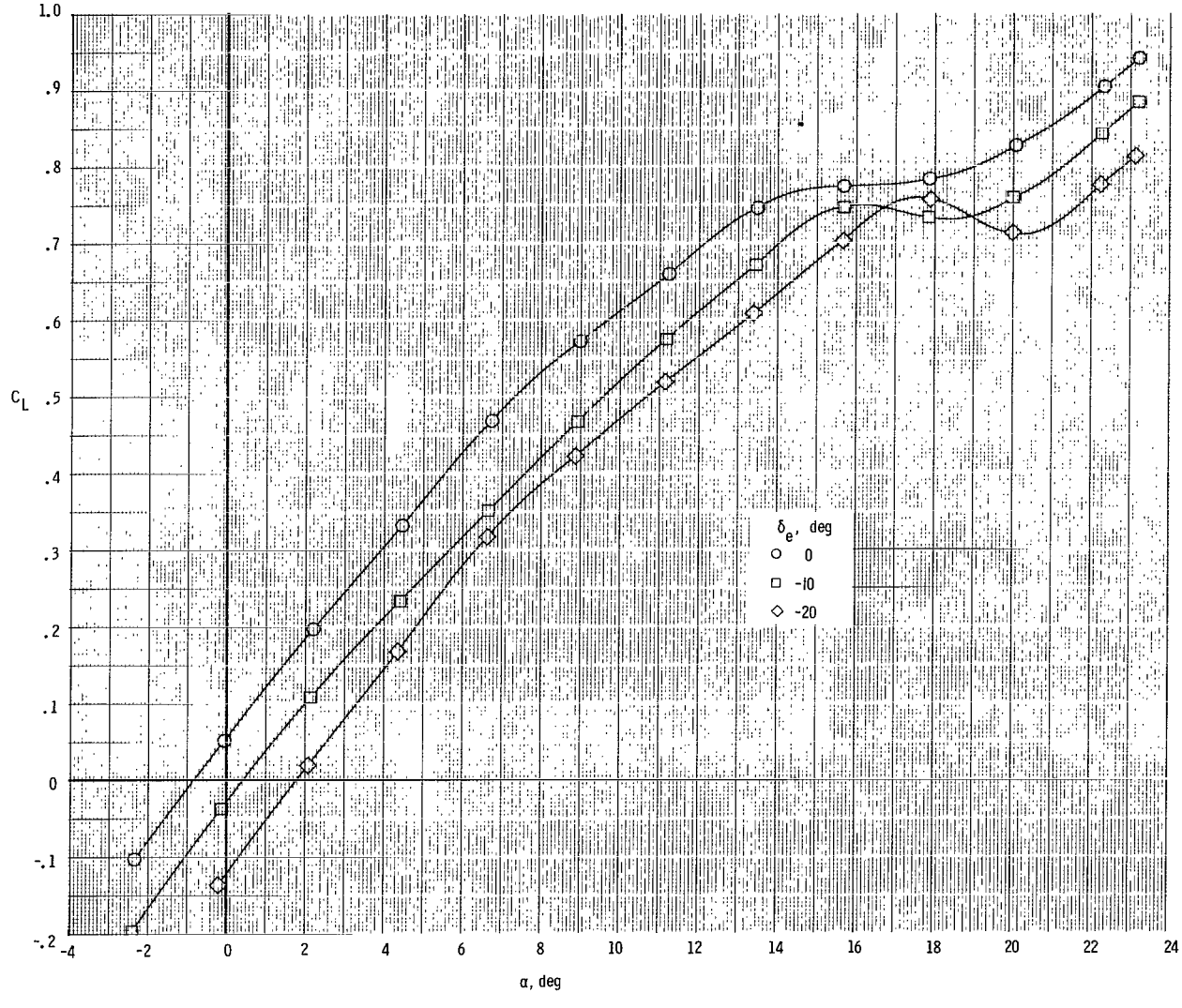

(a) C_L as a function of α.

Figure 14.- Elevon effectiveness of the model at M = 0.9.

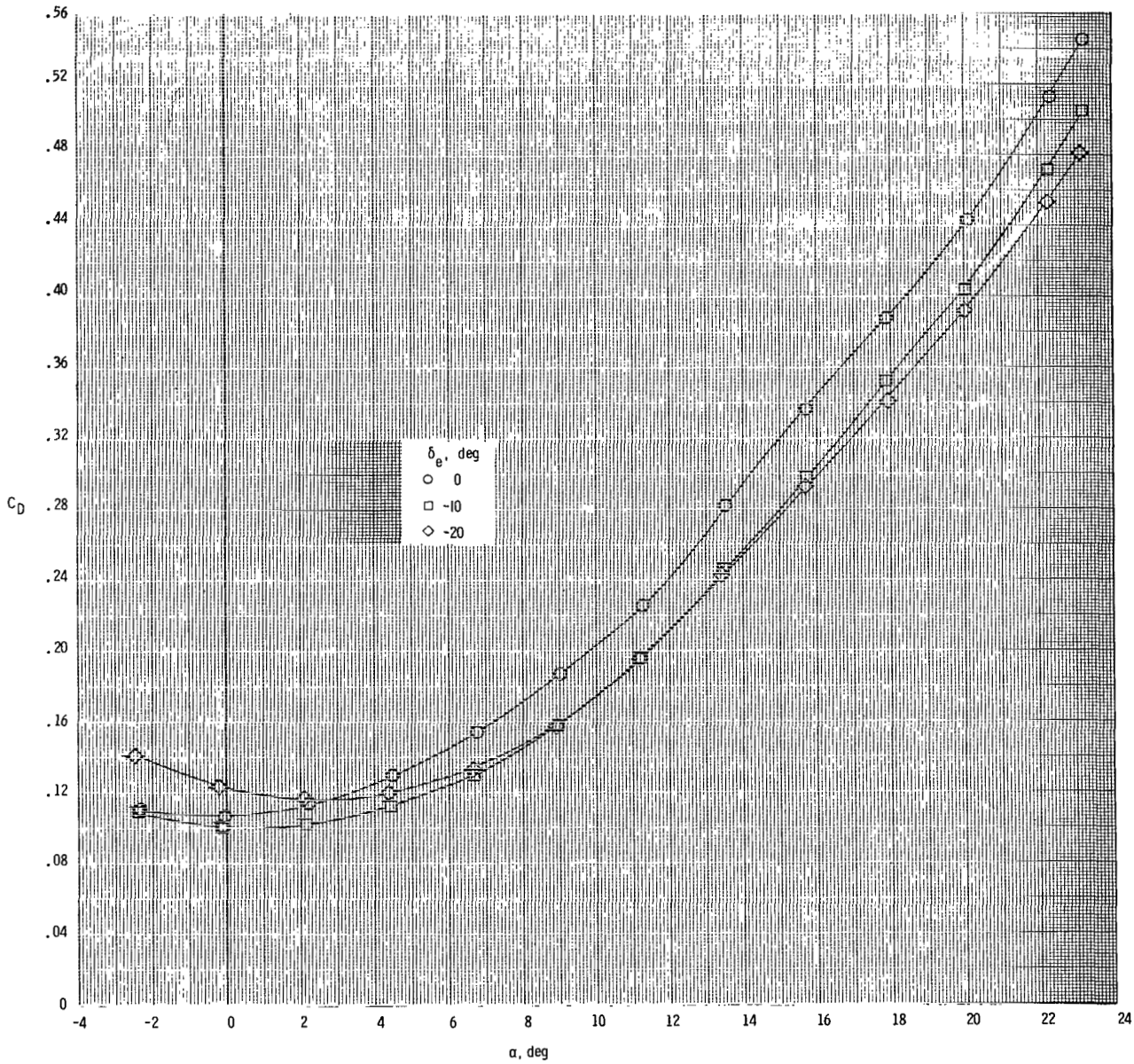

(b) C_D as a function of α.

Figure 14.- Continued.

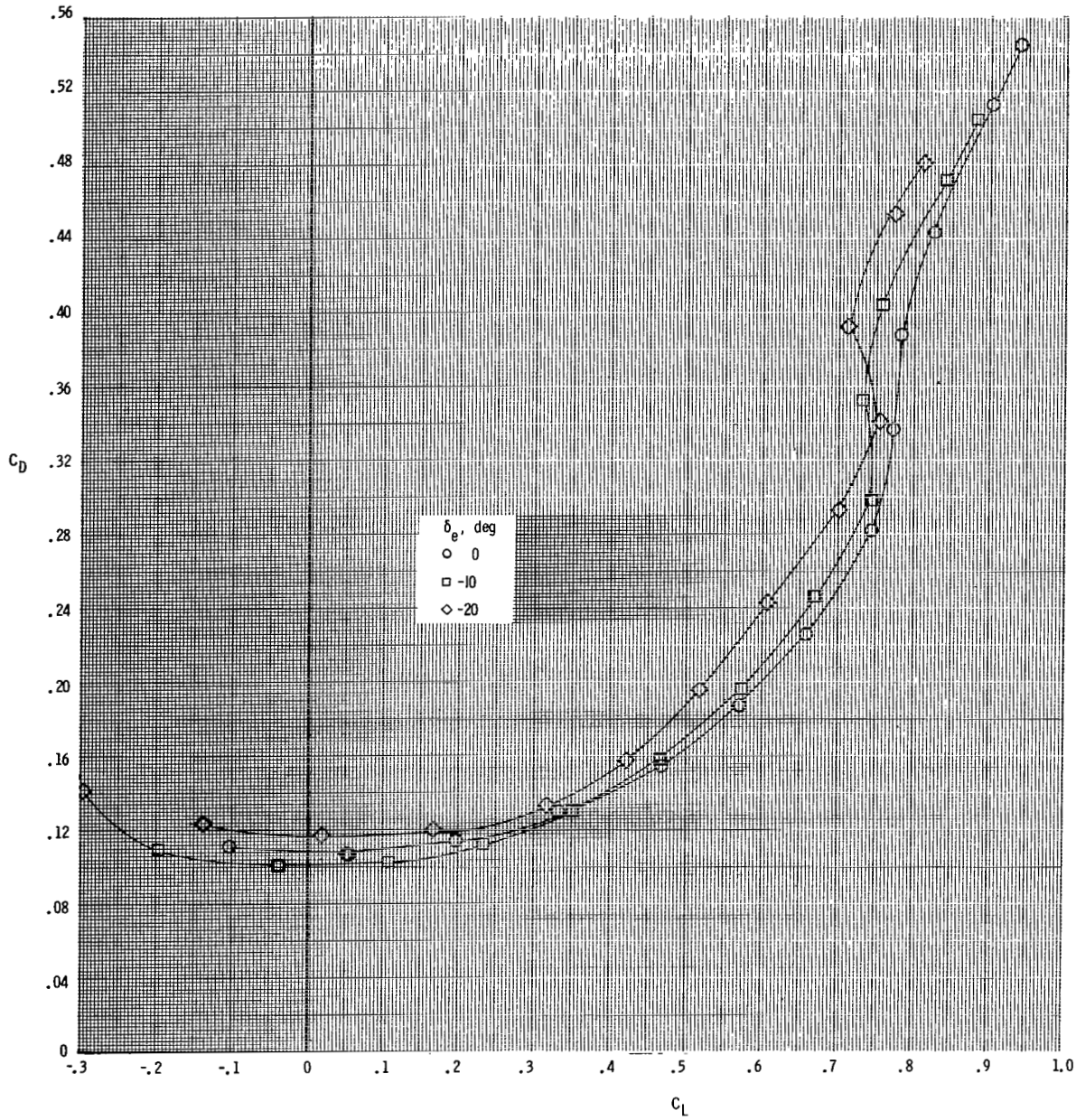

(c) C_D as a function of C_L.

Figure 14.- Continued.

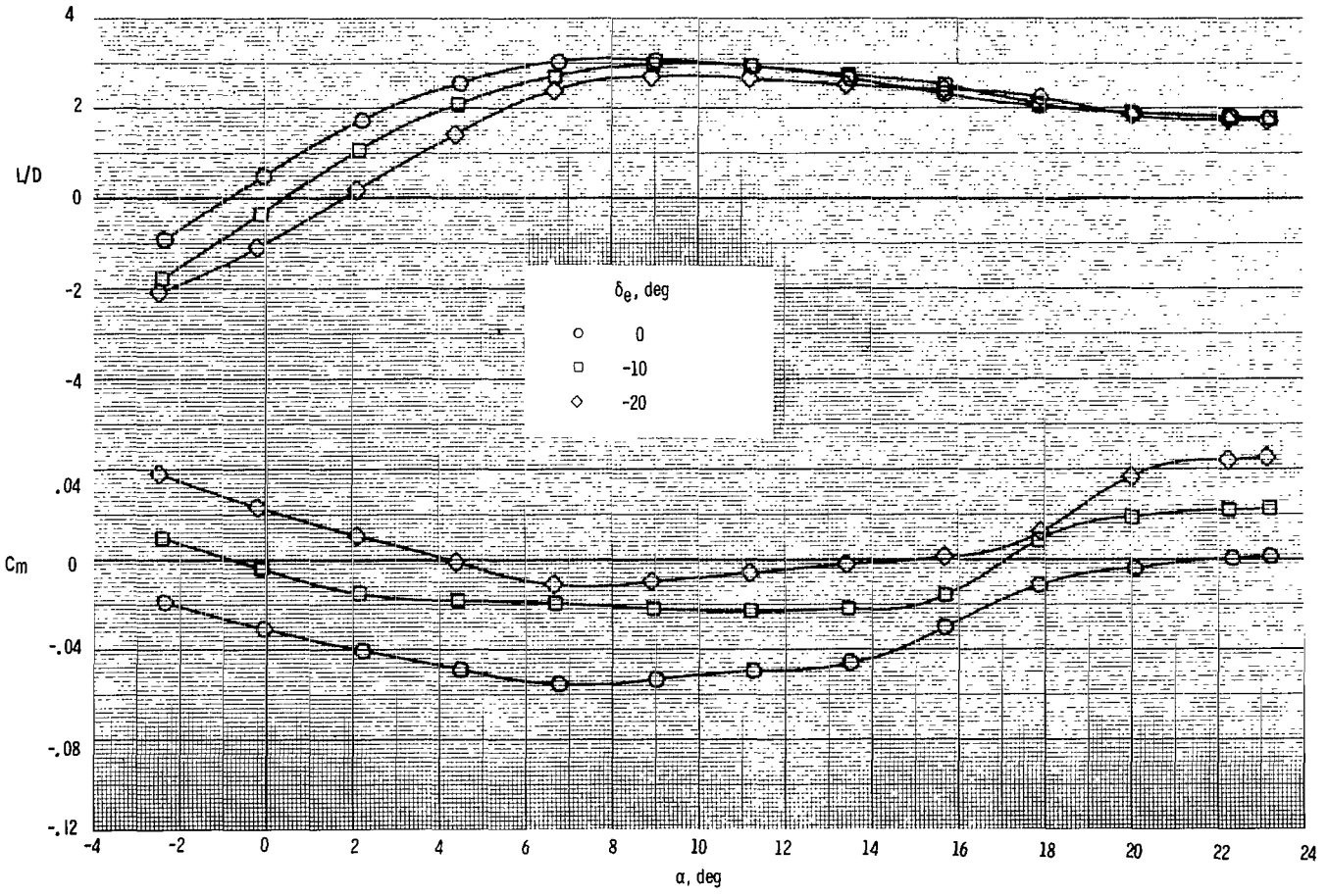

(d) C_m and L/D as a function of α.

Figure 14.- Continued.

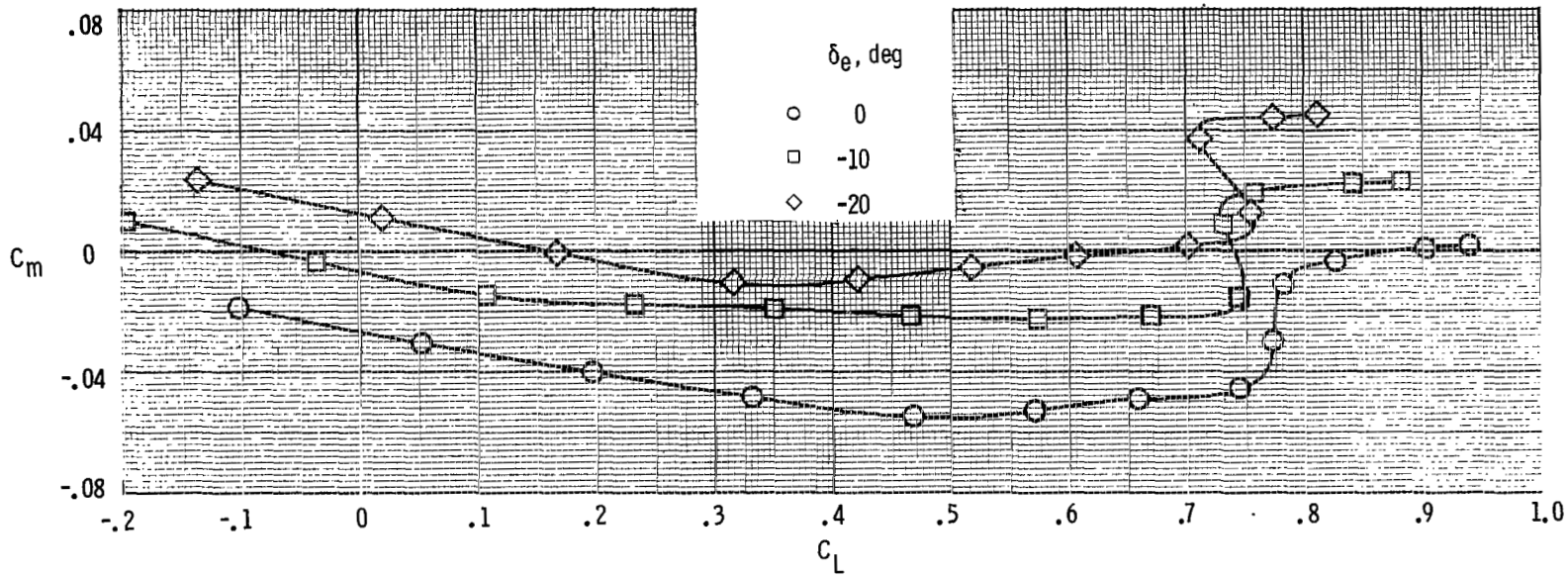

(e) C_m as a function of C_L.

Figure 14.- Concluded.

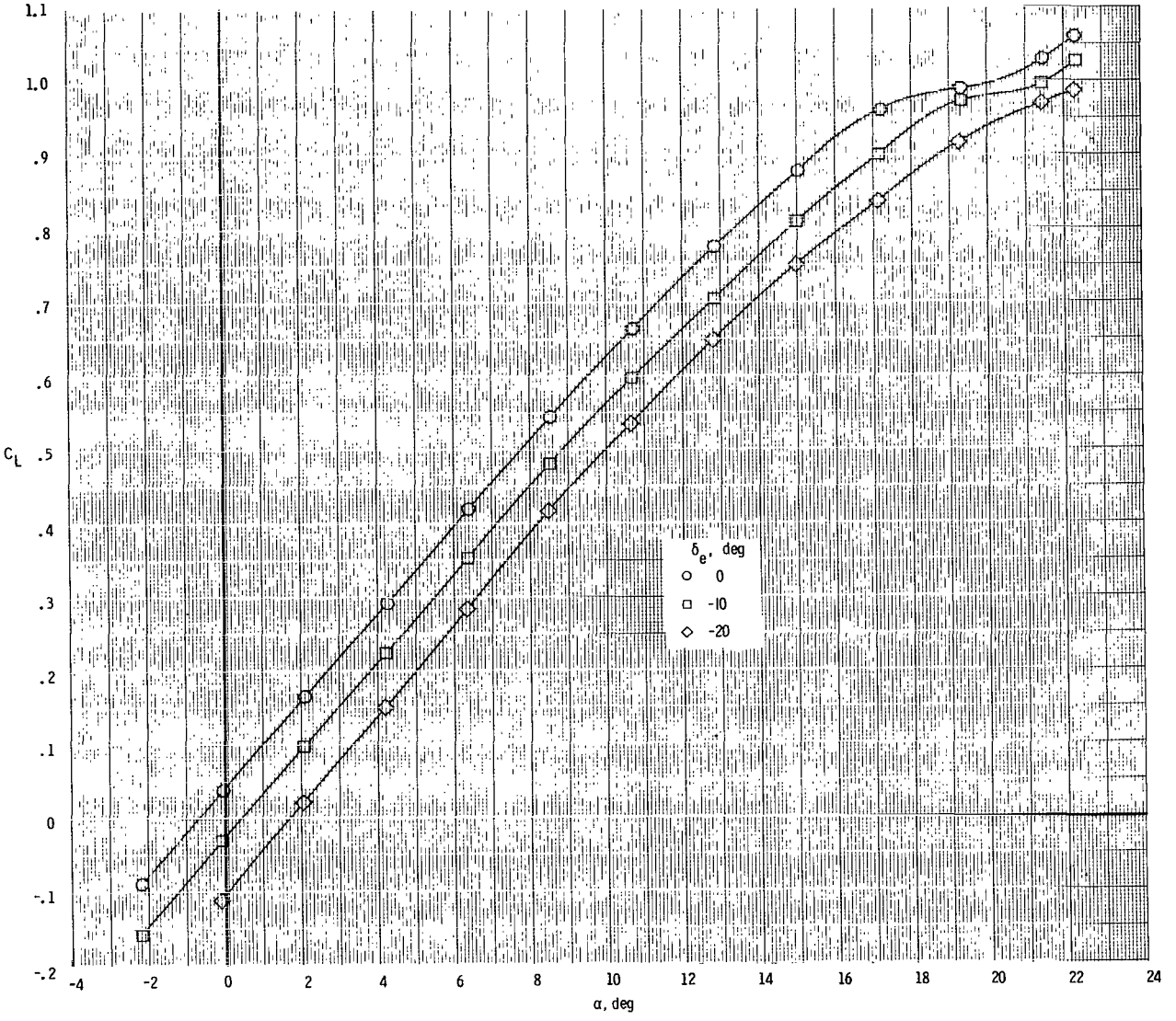

(a) C_L as a function of α.

Figure 15.- Elevon effectiveness of the model at M = 1.2.

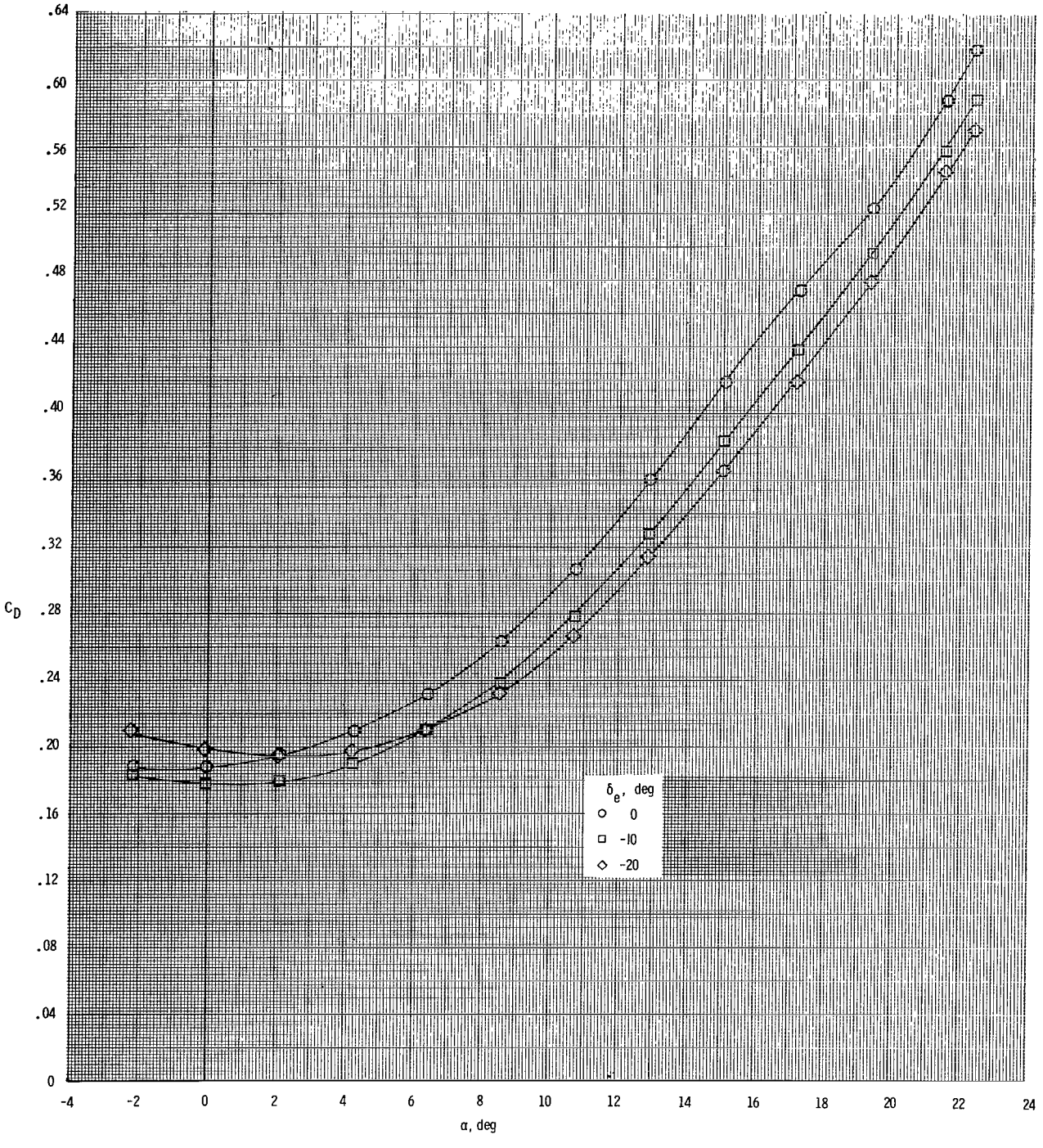

(b) C_D as a function of α.

Figure 15.- Continued.

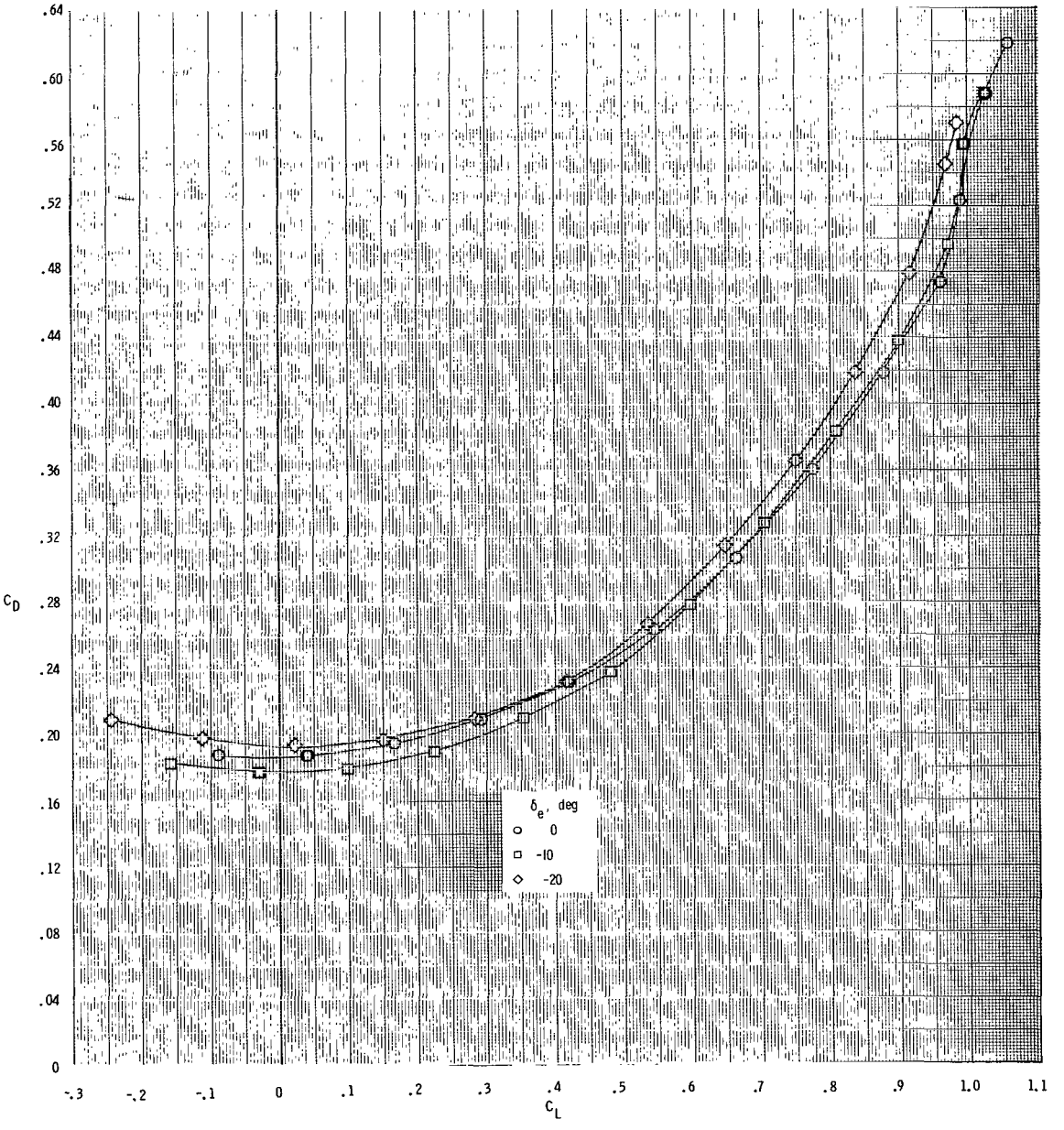

(c) C_D as a function of C_L.

Figure 15.- Continued.

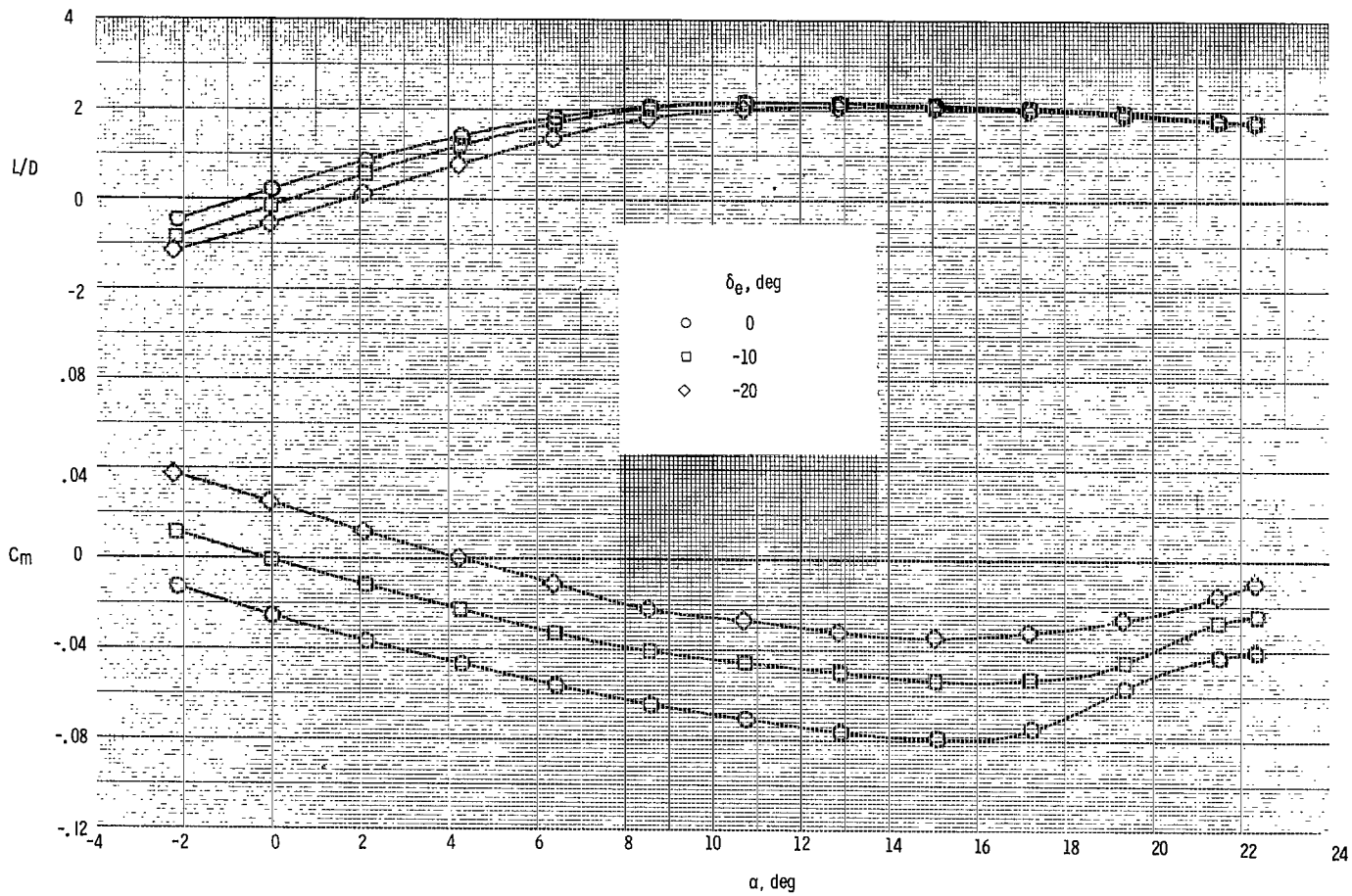

(d) C_m and L/D as a function of α.

Figure 15.- Continued.

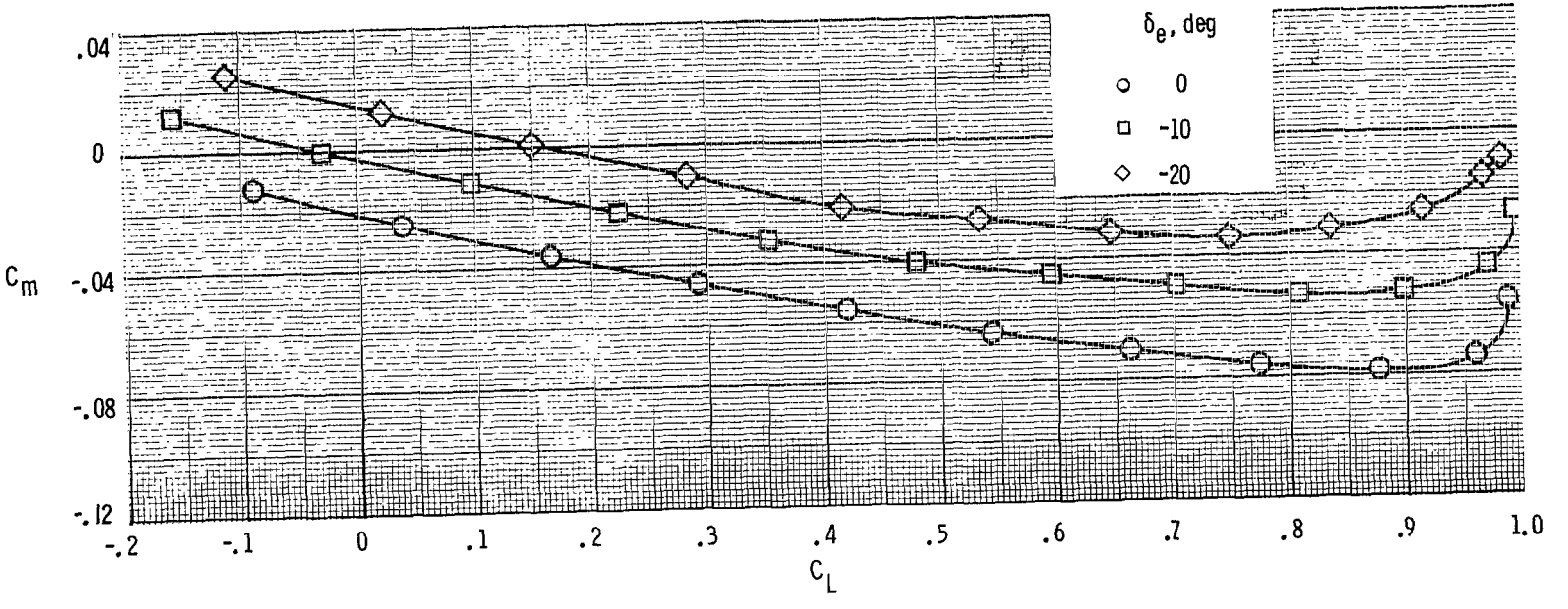

(e) C_m as a function of C_L.

Figure 15.- Concluded.

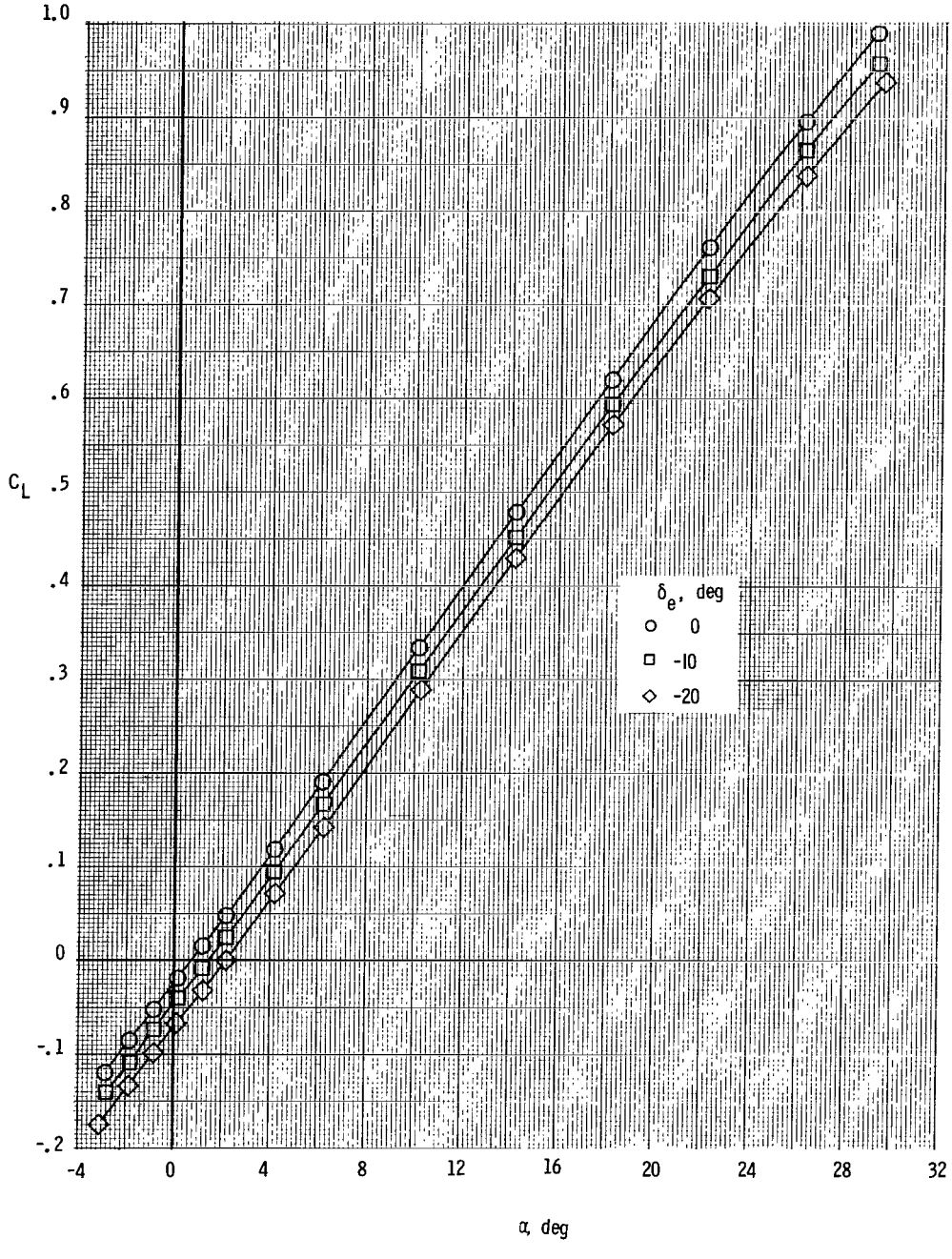

(a) C_L as a function of α.

Figure 16.- Elevon effectiveness of the model at M = 2.36.

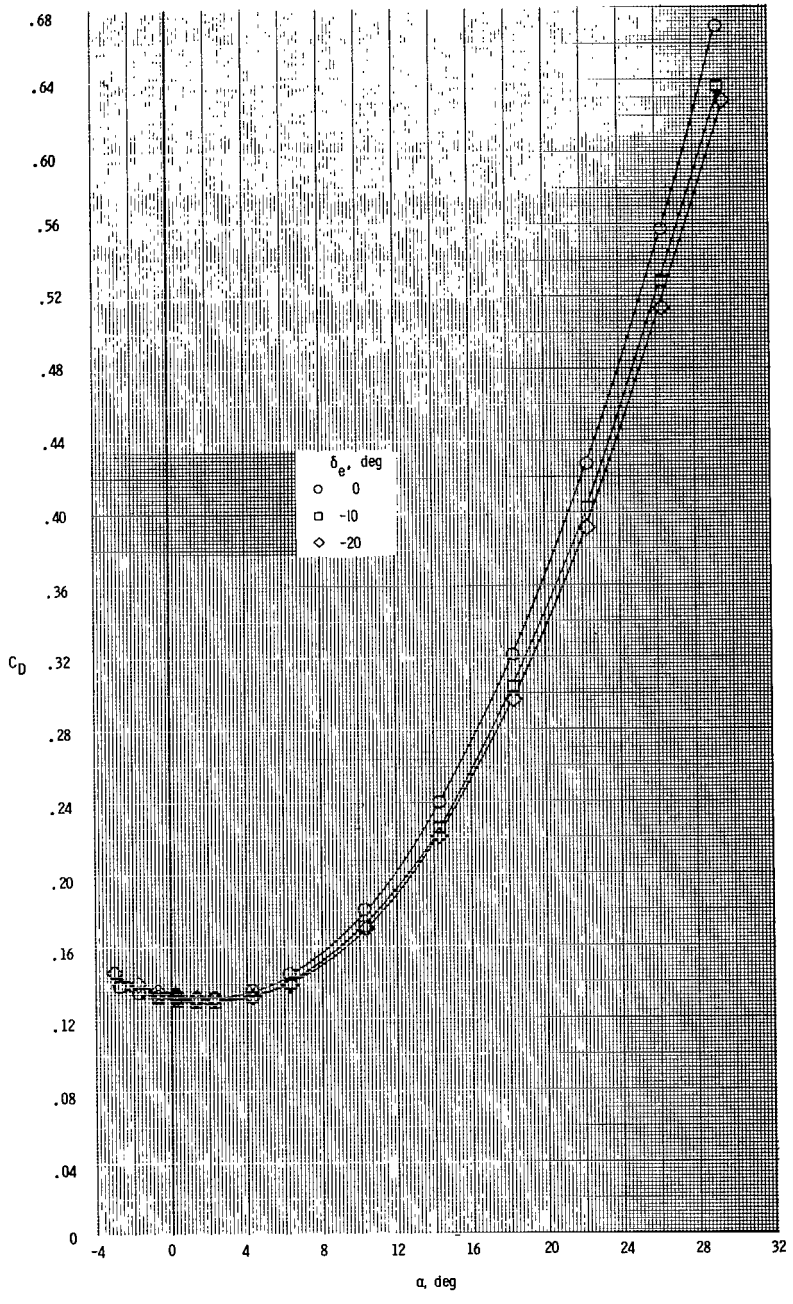

(b) C_D as a function of α.

Figure 16.- Continued.

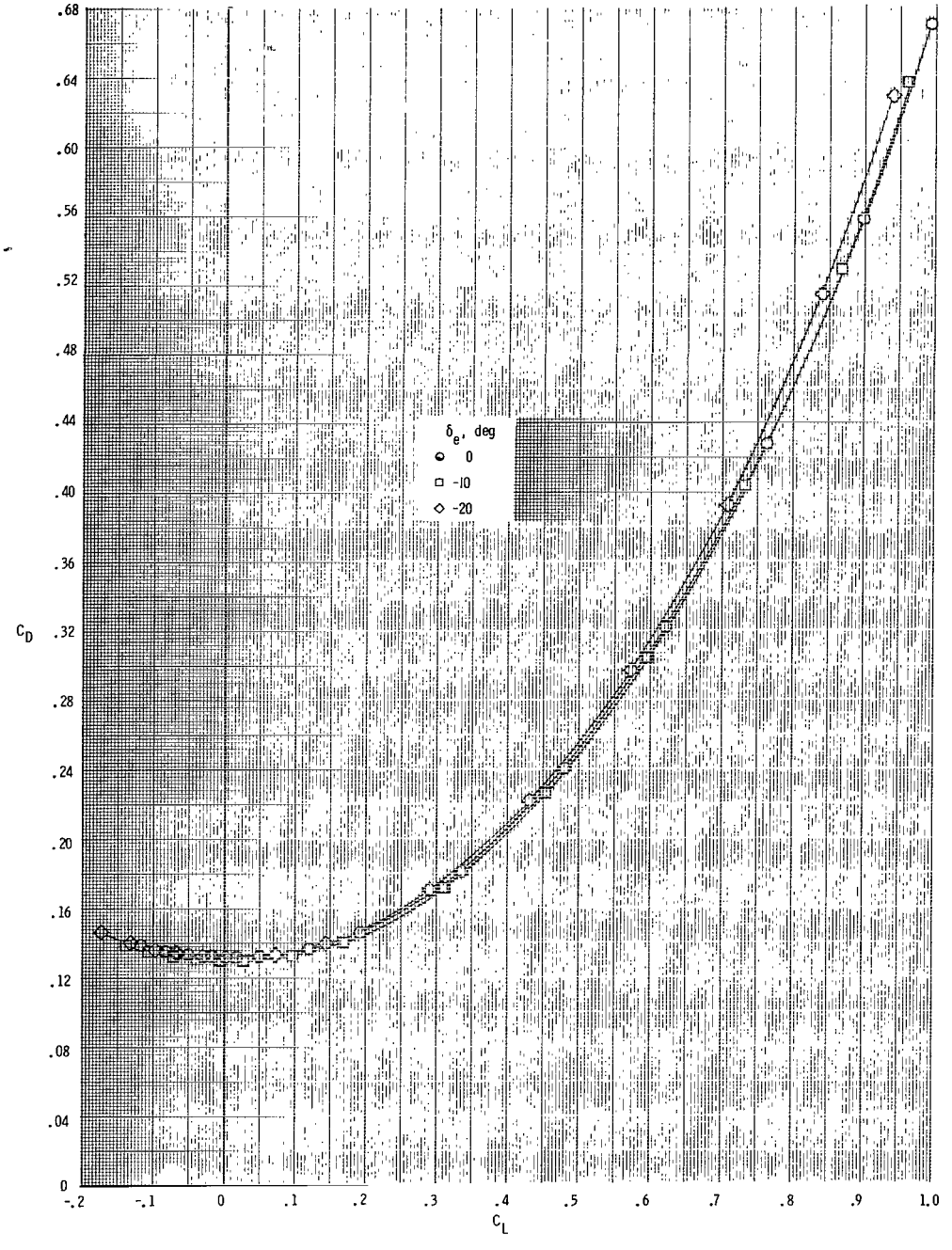

(c) C_D as a function of C_L.

Figure 16.- Continued.

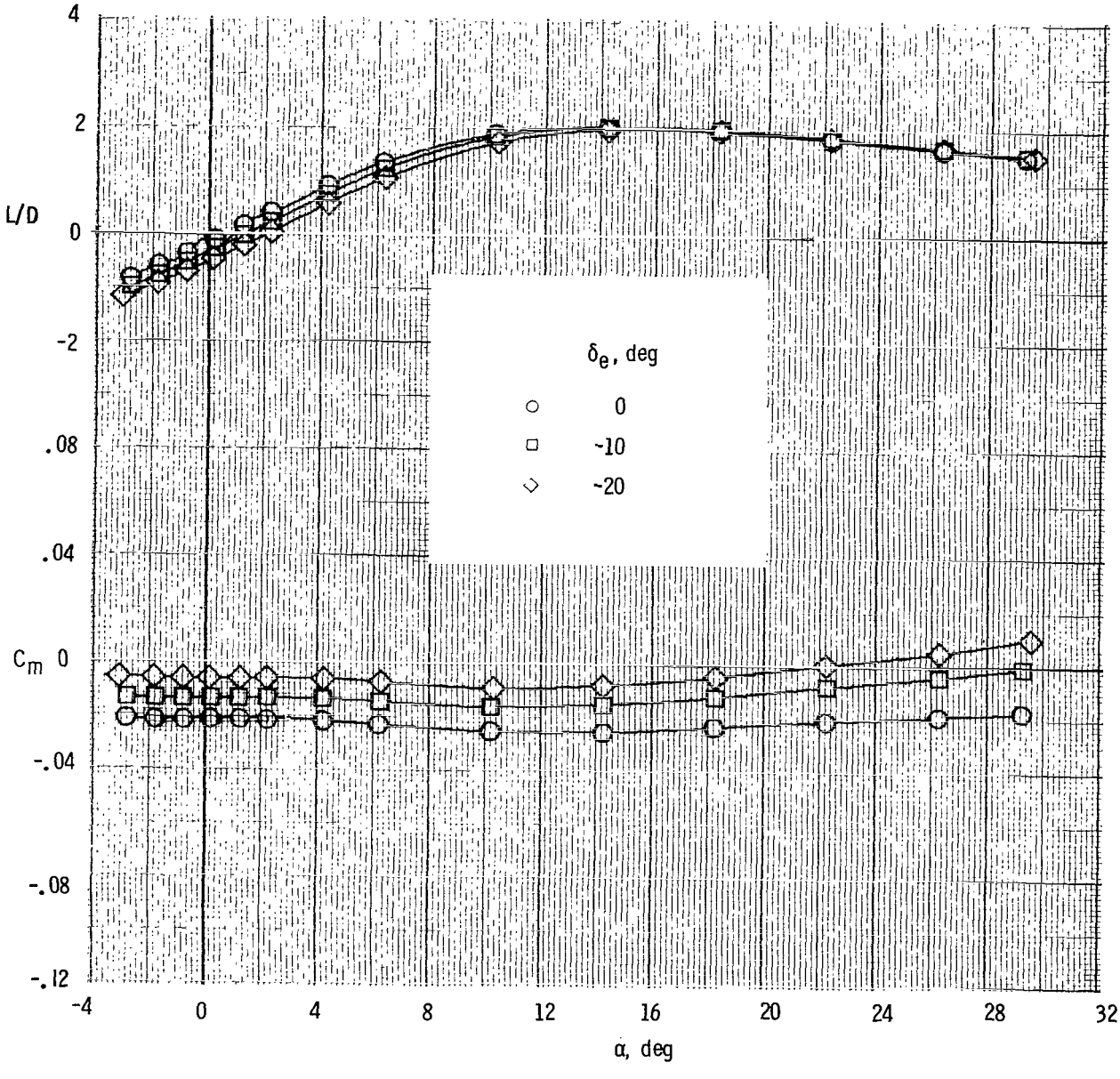

(d) C_m and L/D as a function of α.

Figure 16.- Continued.

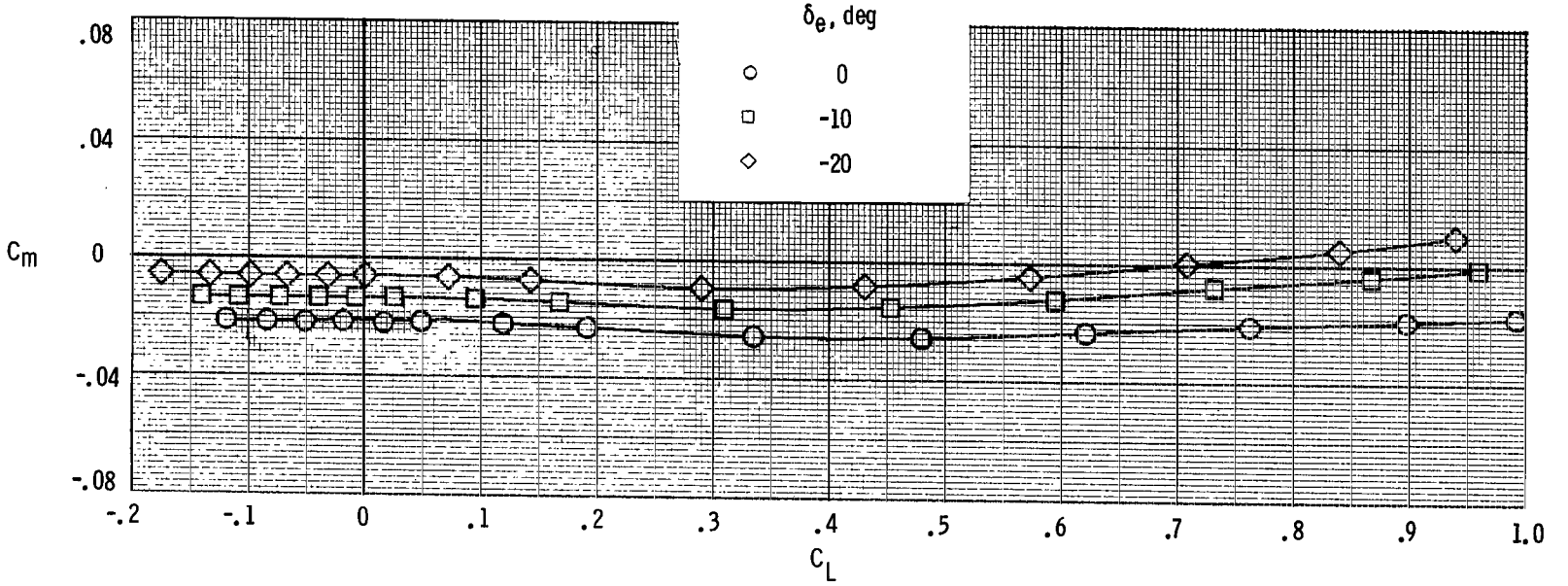

(e) C_m as a function of C_L.

Figure 16.- Concluded.

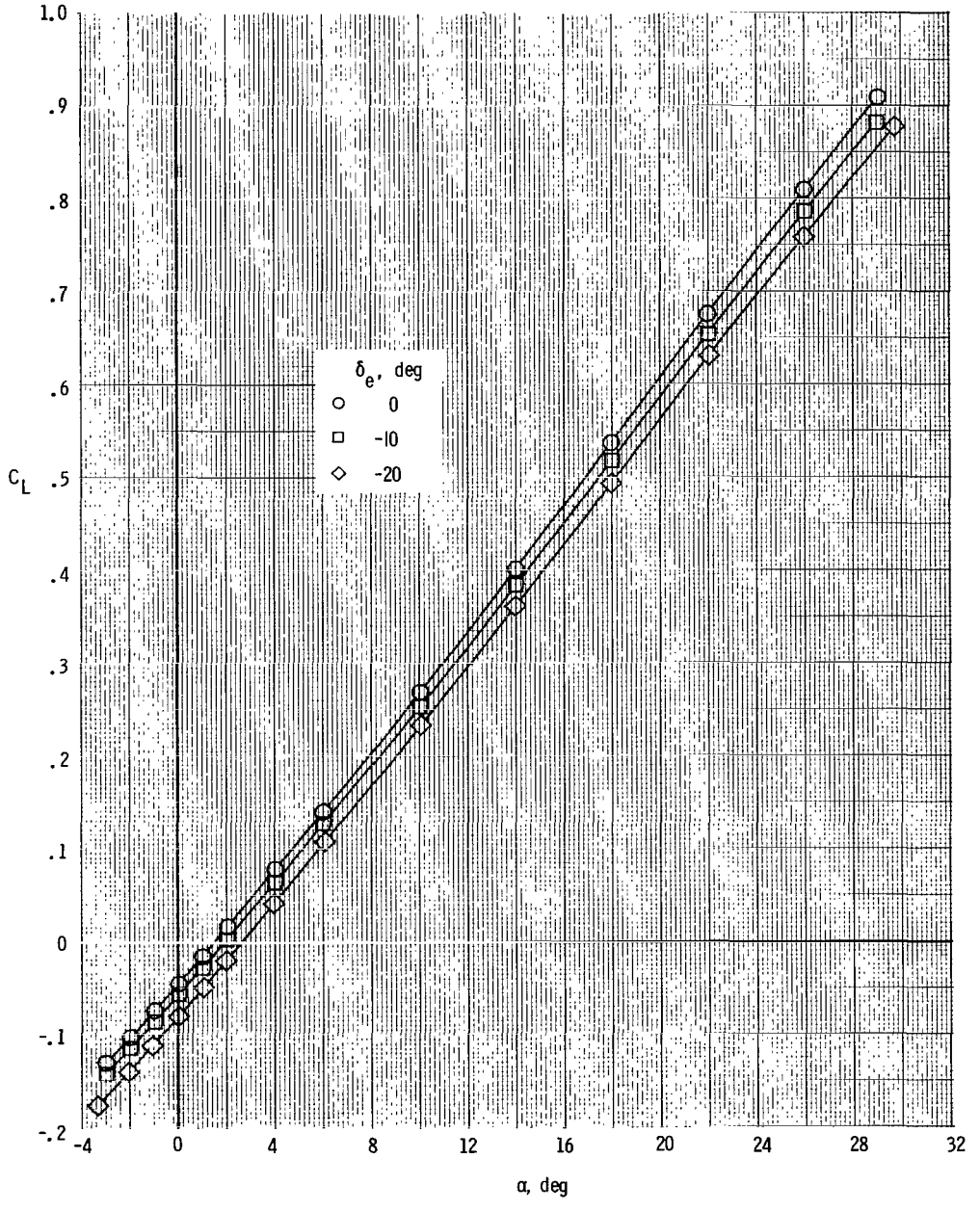

(a) C_L as a function of α.

Figure 17.- Elevon effectiveness of the model at M = 2.86.

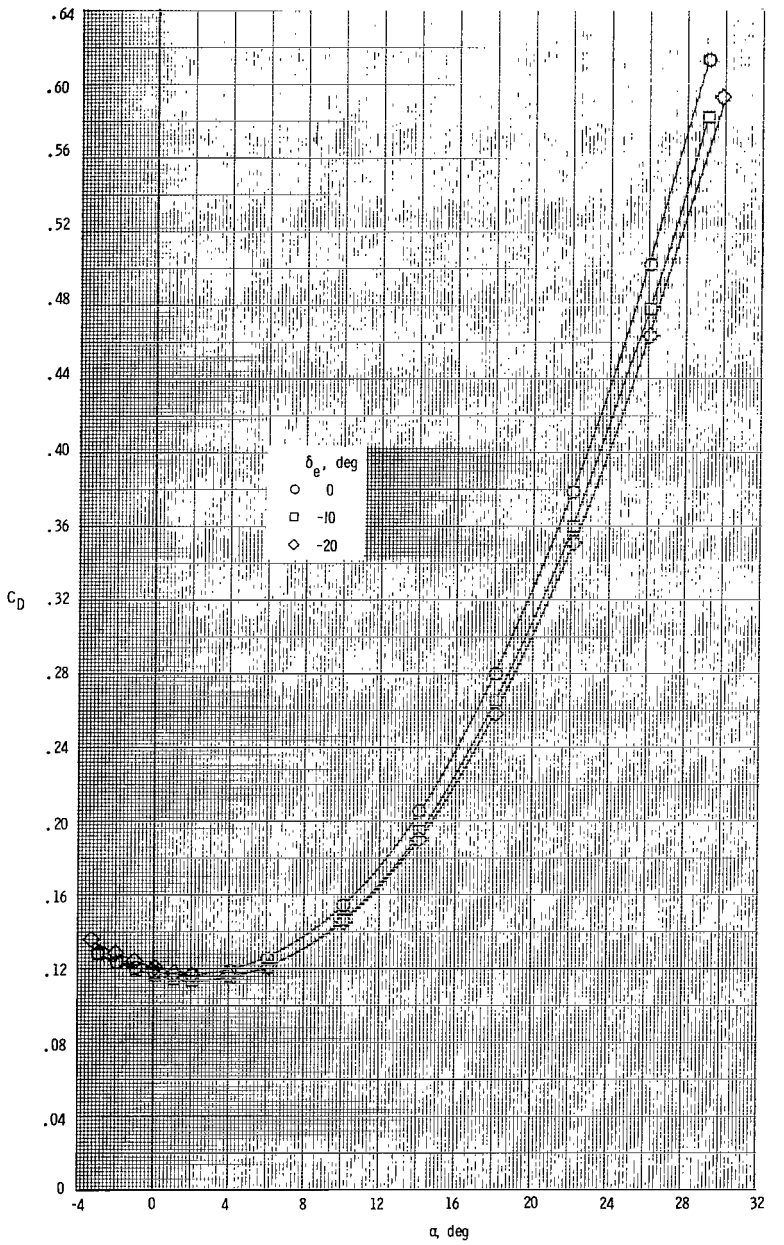

(b) C_D as a function of α.

Figure 17.- Continued.

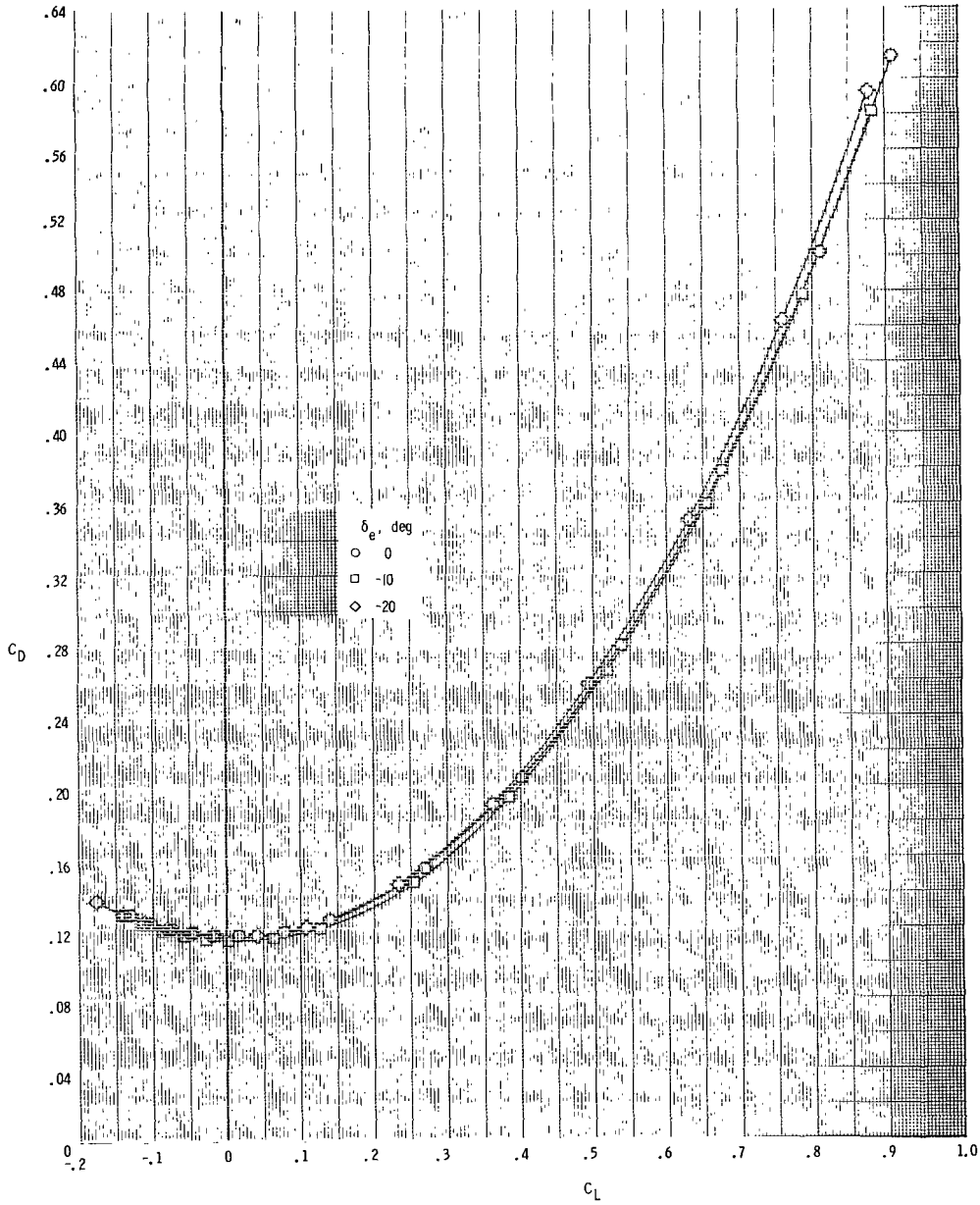

(c) C_D as a function of C_L.

Figure 17.- Continued.

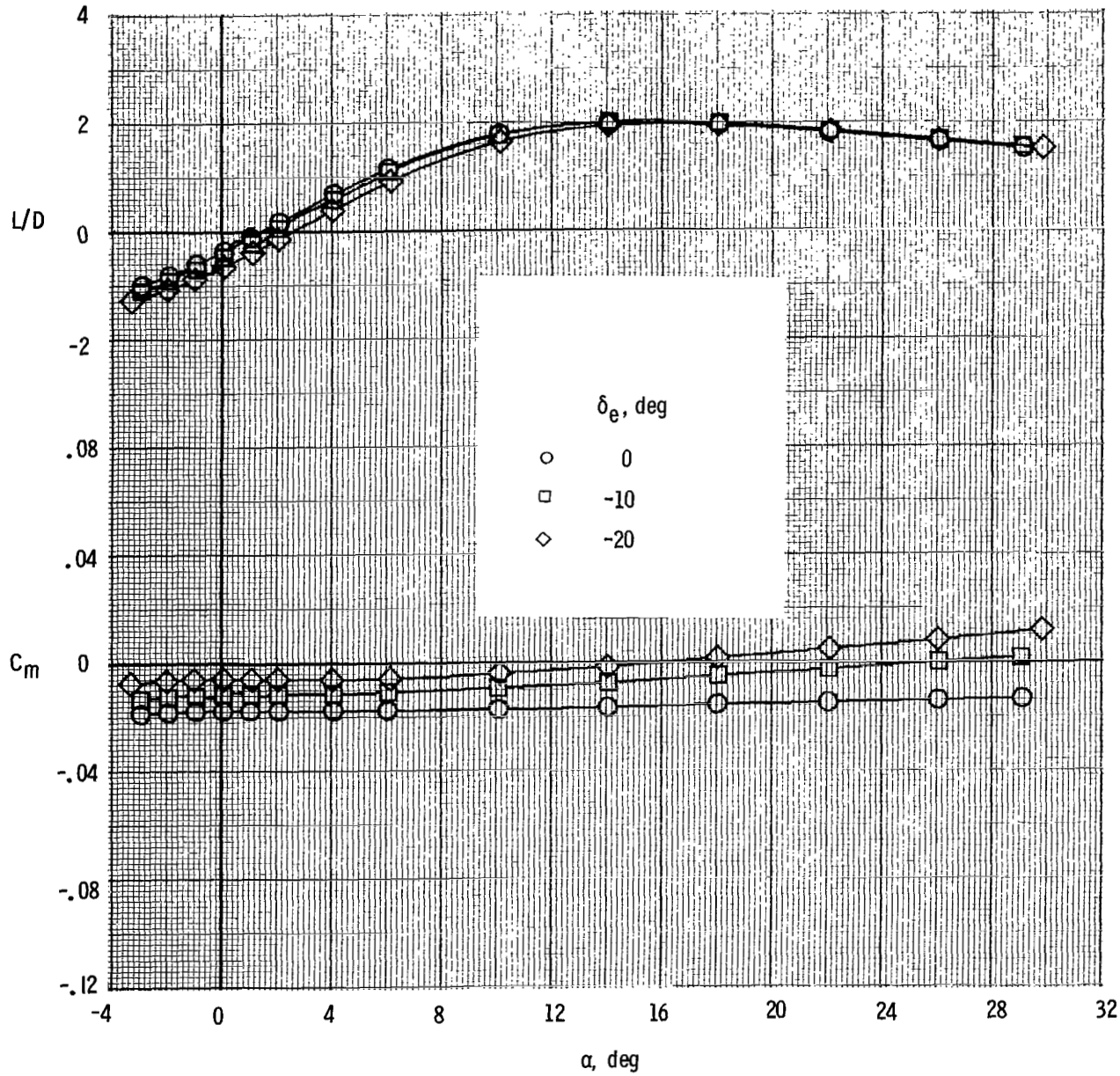

(d) C_m and L/D as a function of α.

Figure 17.- Continued.

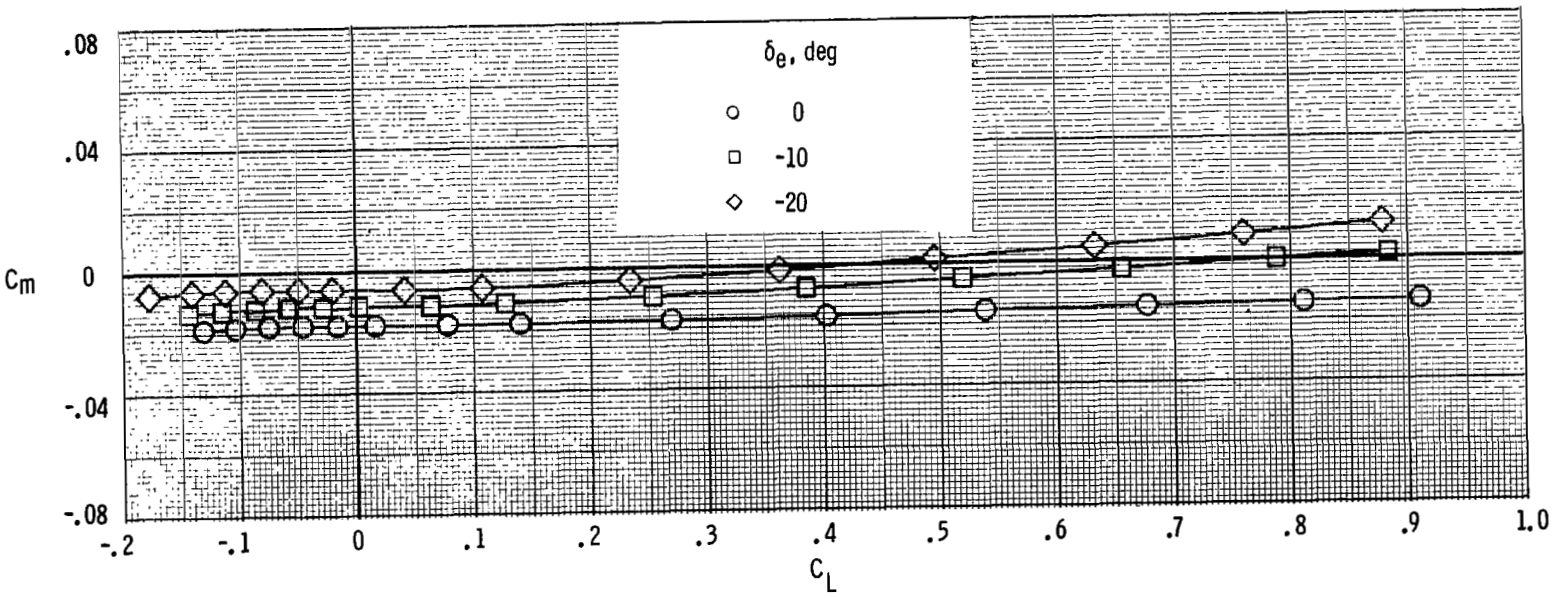

(e) C_m as a function of C_L.

Figure 17.- Concluded.

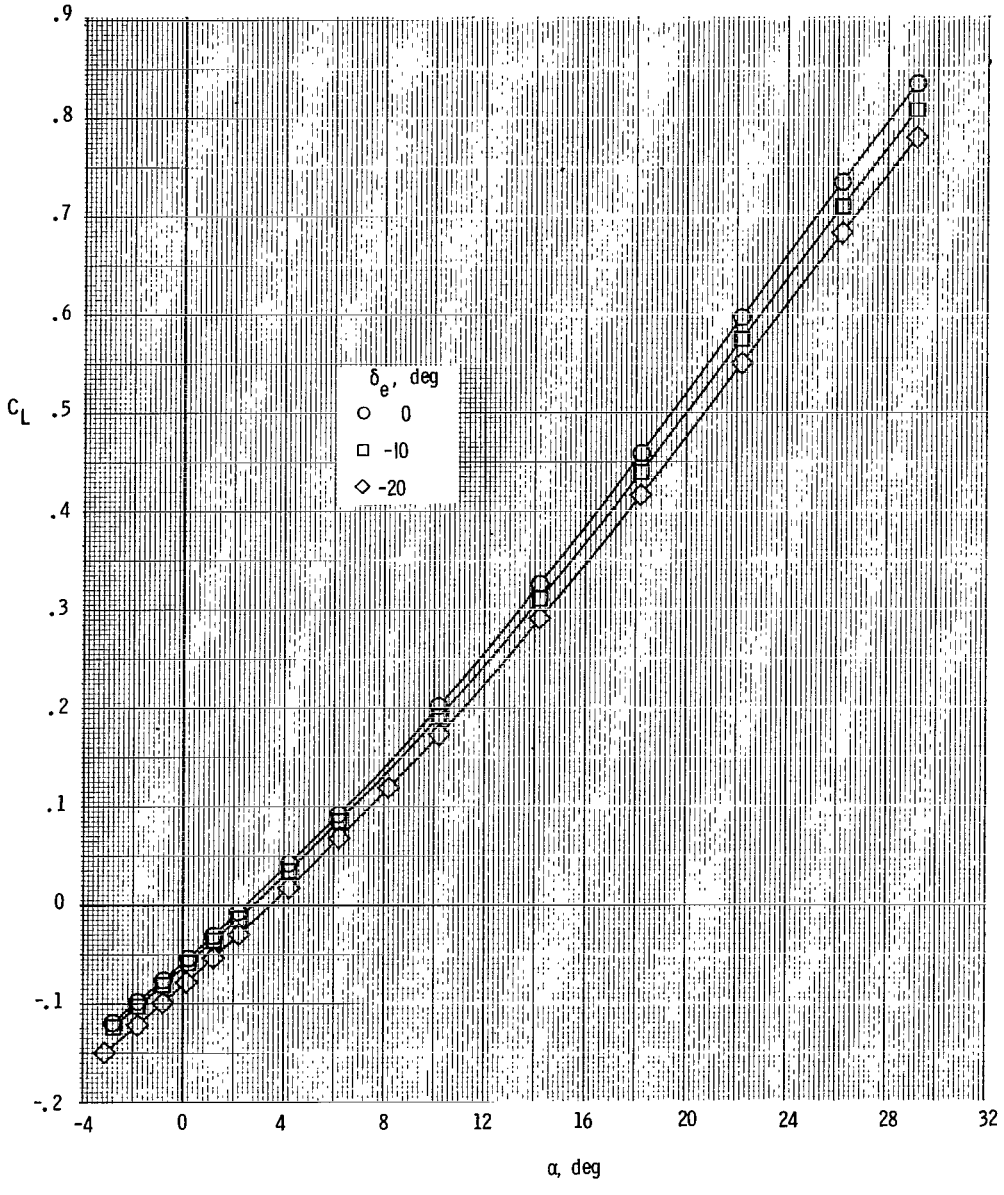

(a) C_L as a function of α.

Figure 18.- Elevon effectiveness of the model at M = 3.95.

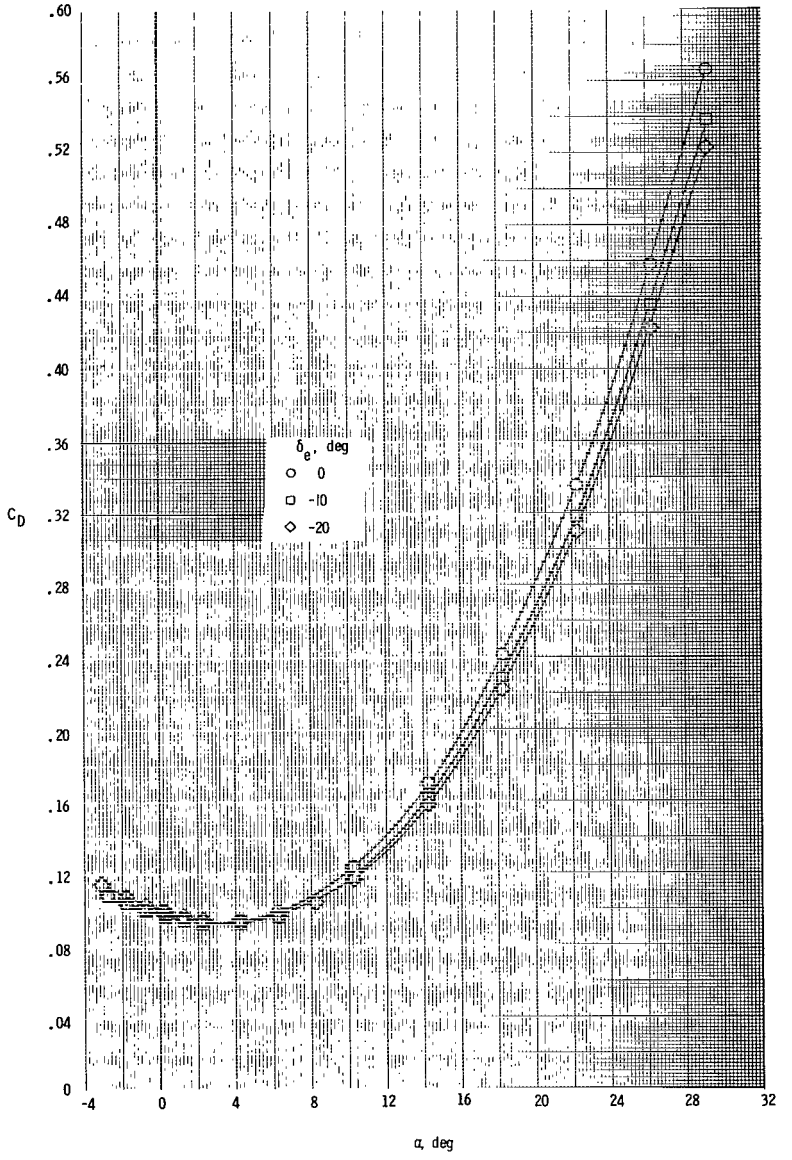

(b) C_D as a function of α.

Figure 18.- Continued.

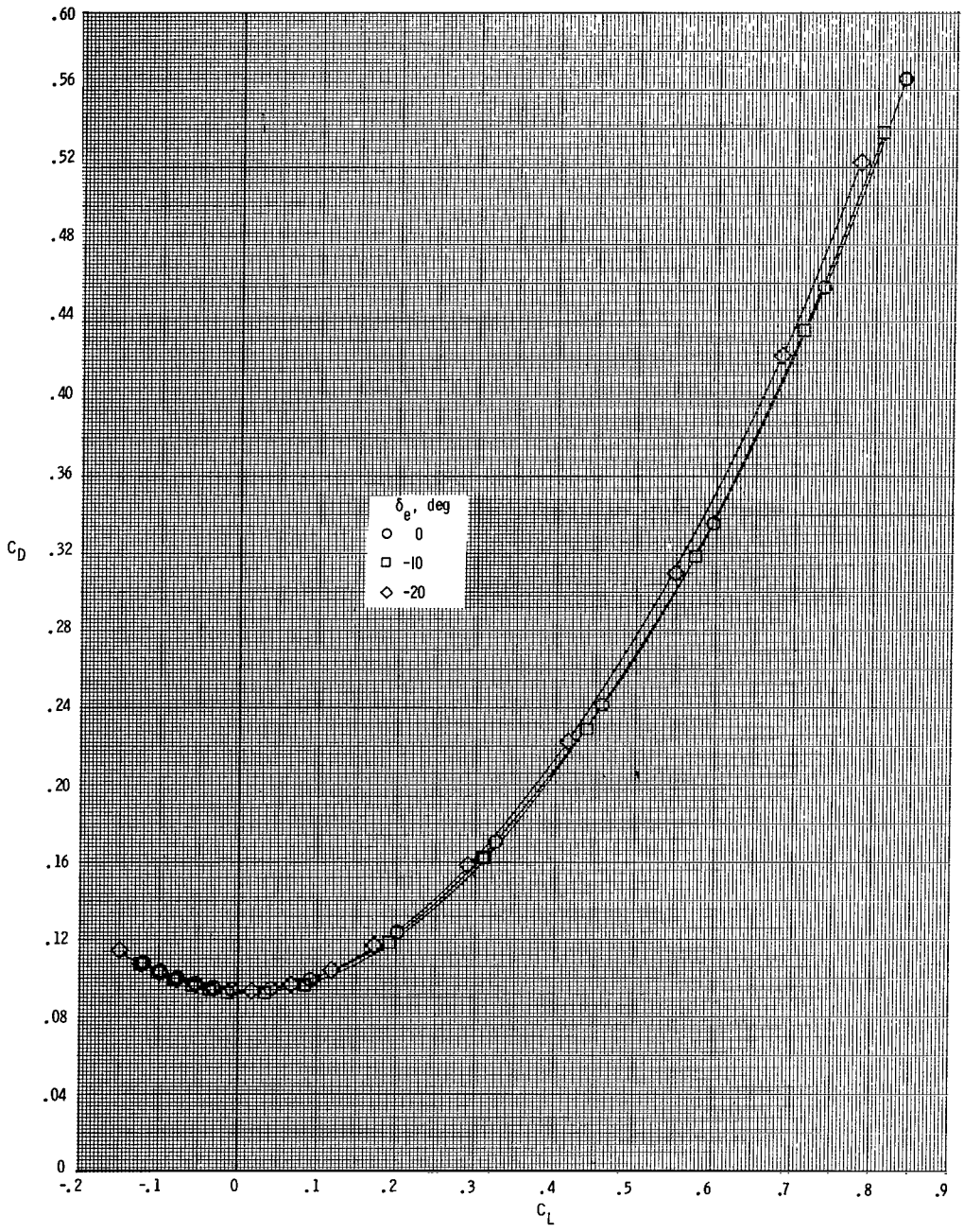

(c) C_D as a function of C_L.

Figure 18.- Continued.

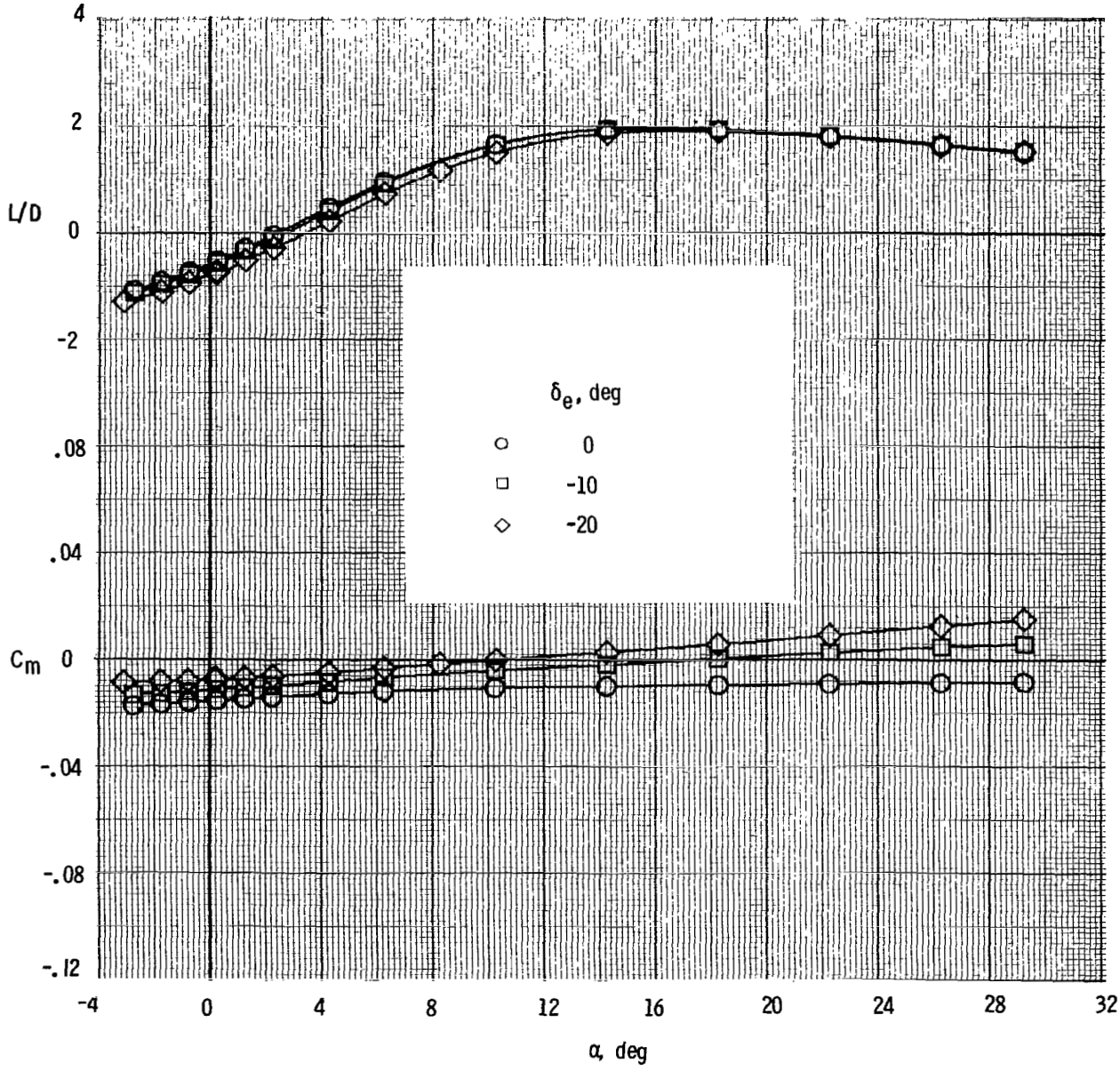

(d) C_m and L/D as a function of α.

Figure 18.- Continued.

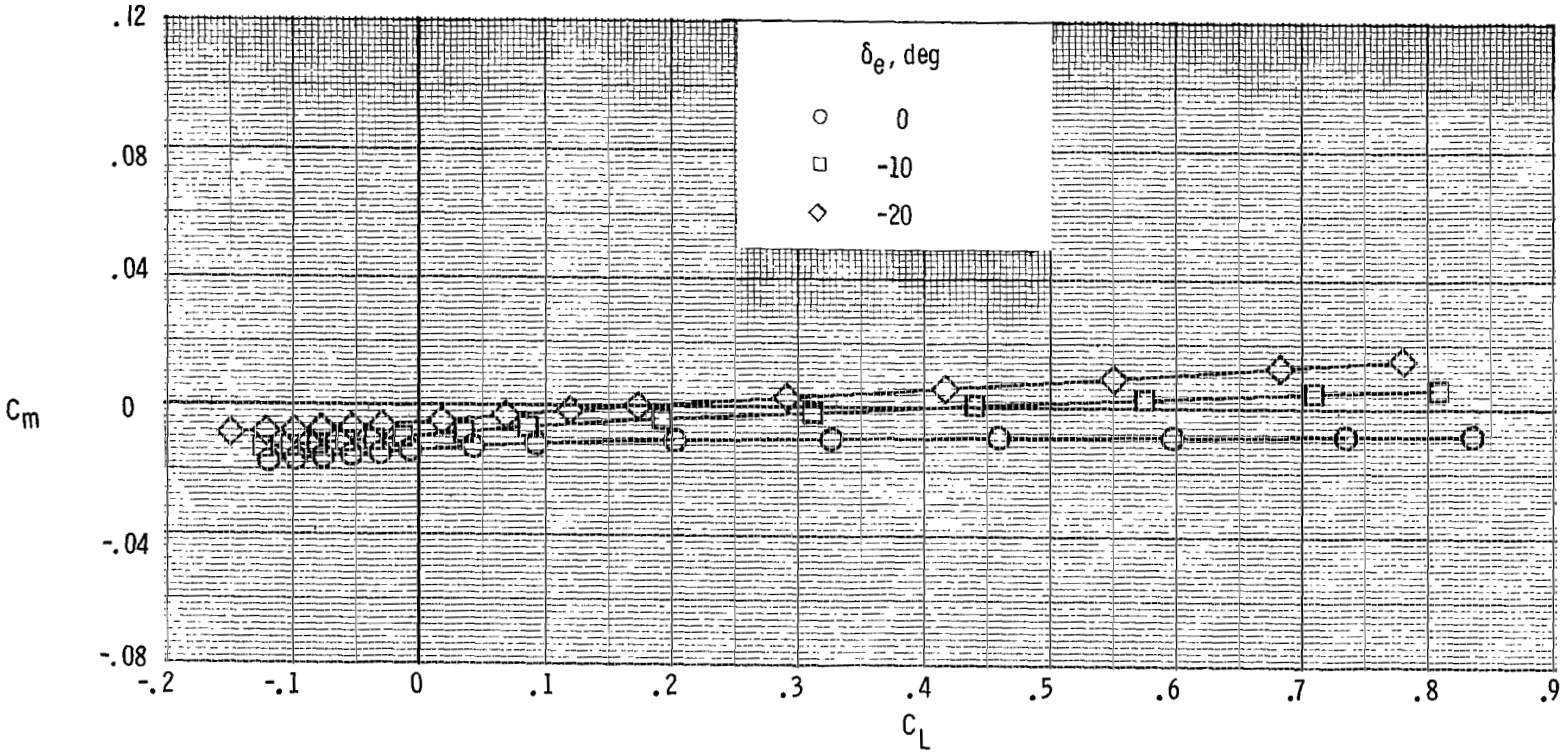

(e) C_m as a function of C_L.

Figure 18.- Concluded.

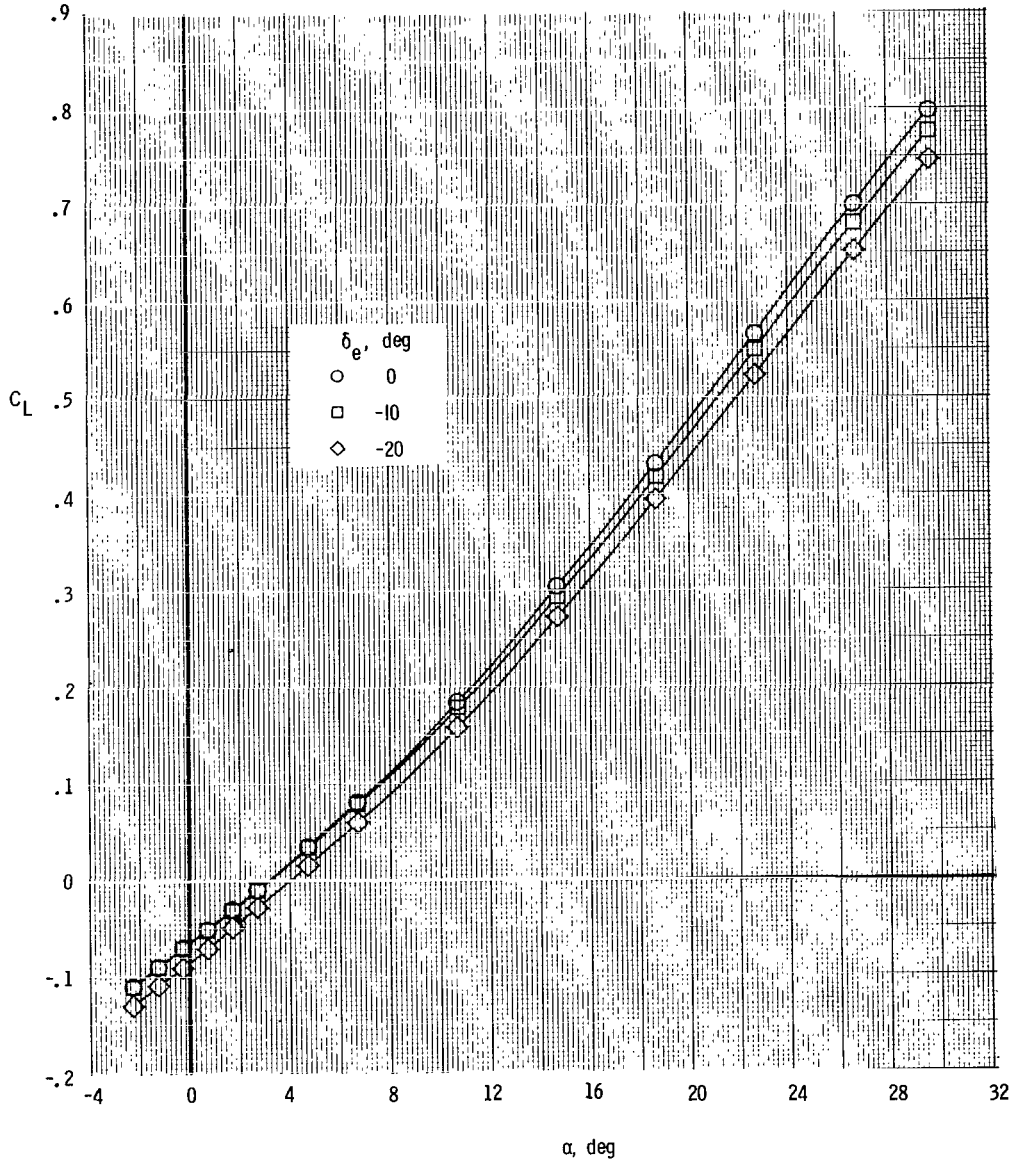

(a) C_L as a function of α.

Figure 19.- Elevon effectiveness of the model at M = 4.63.

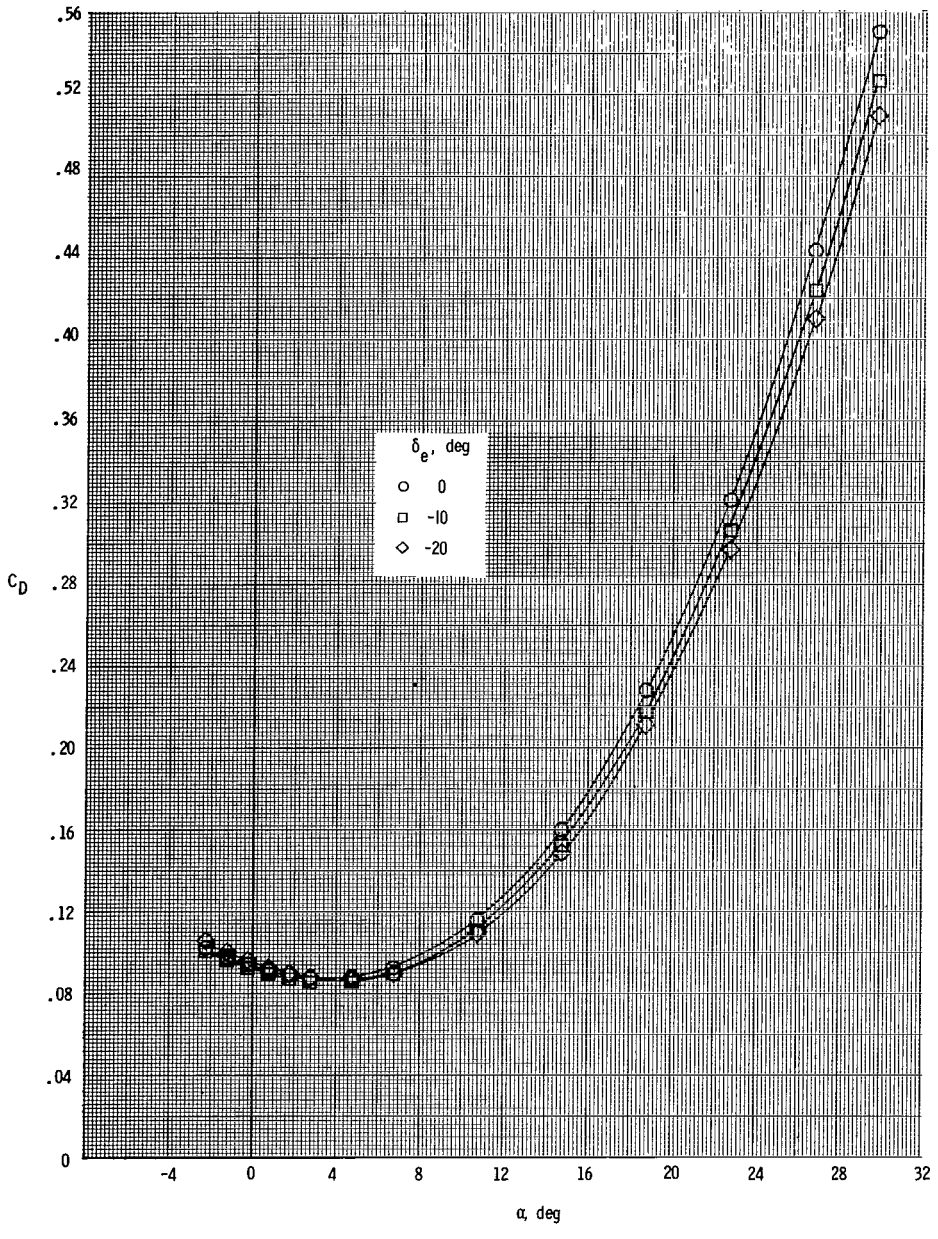

(b) C_D as a function of α.

Figure 19.- Continued.

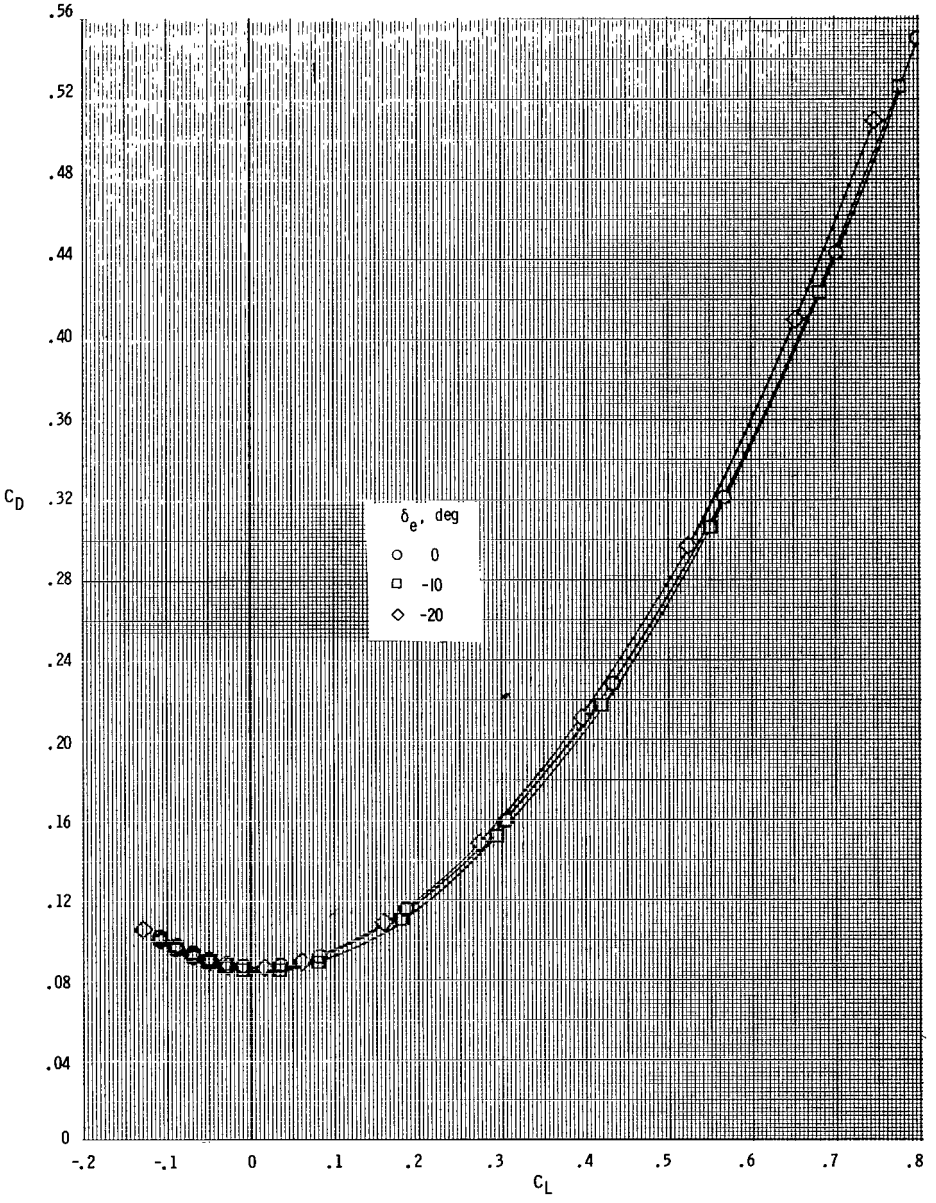

(c) C_D as a function of C_L.

Figure 19.- Continued.

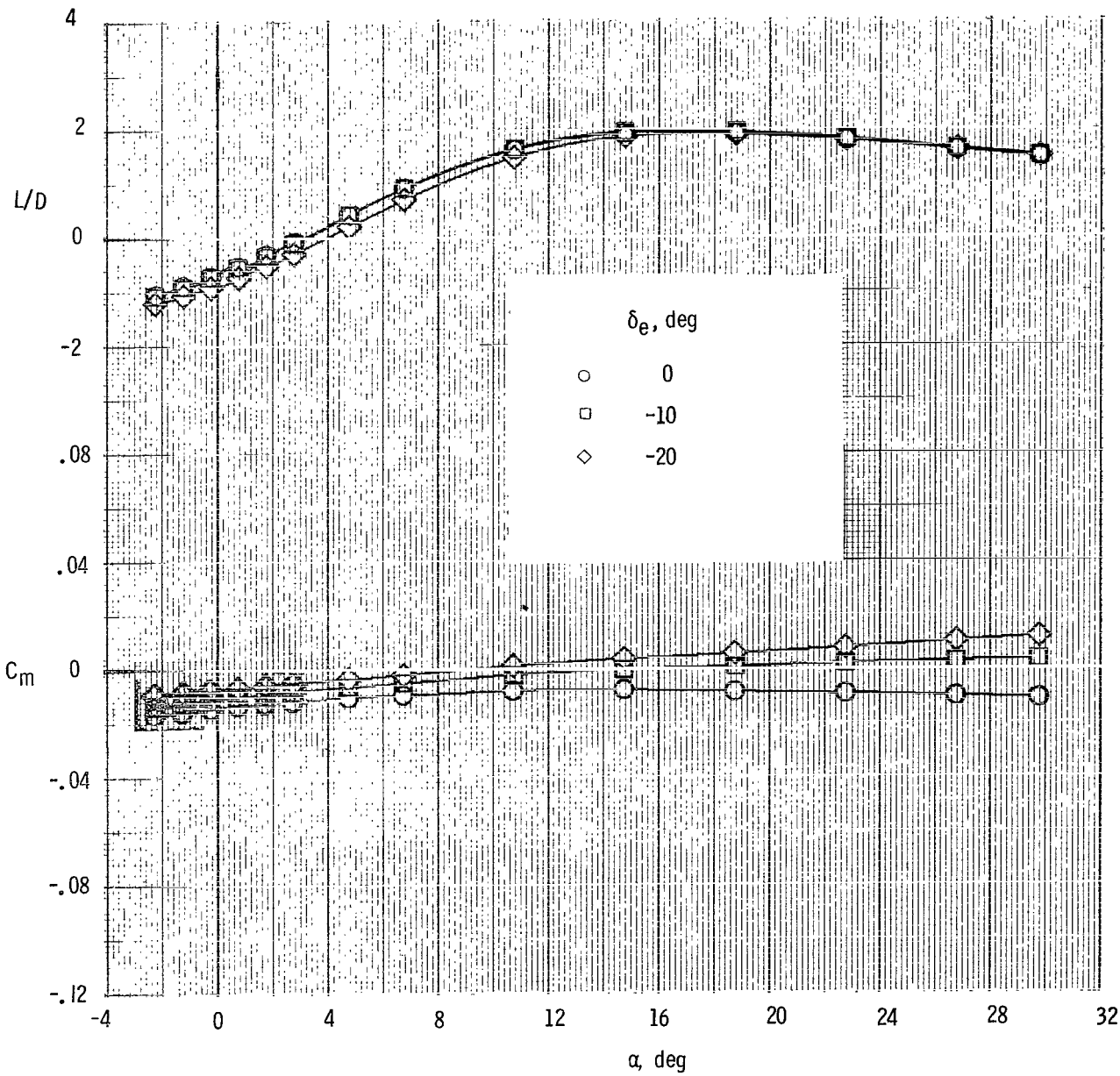

(d) C_m and L/D as a function of α.

Figure 19.- Continued.

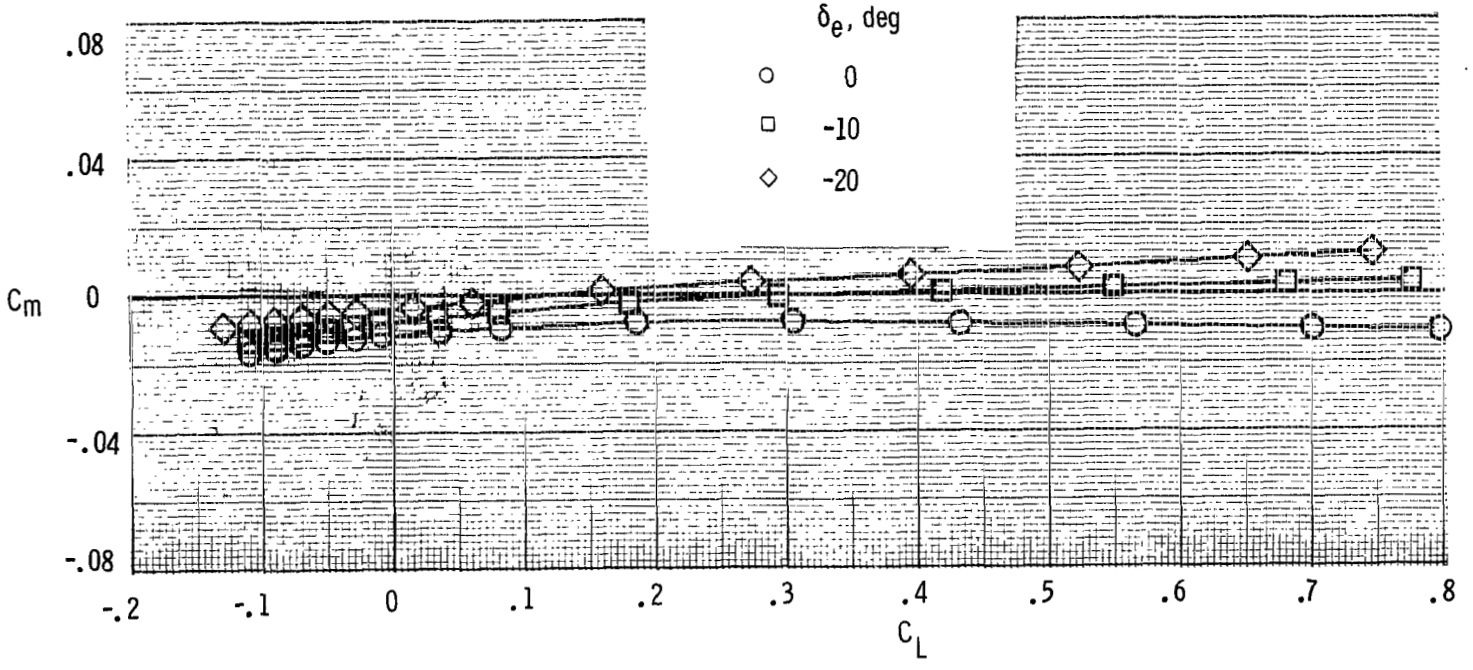

(e) C_m as a function of C_L.

Figure 19.- Concluded.

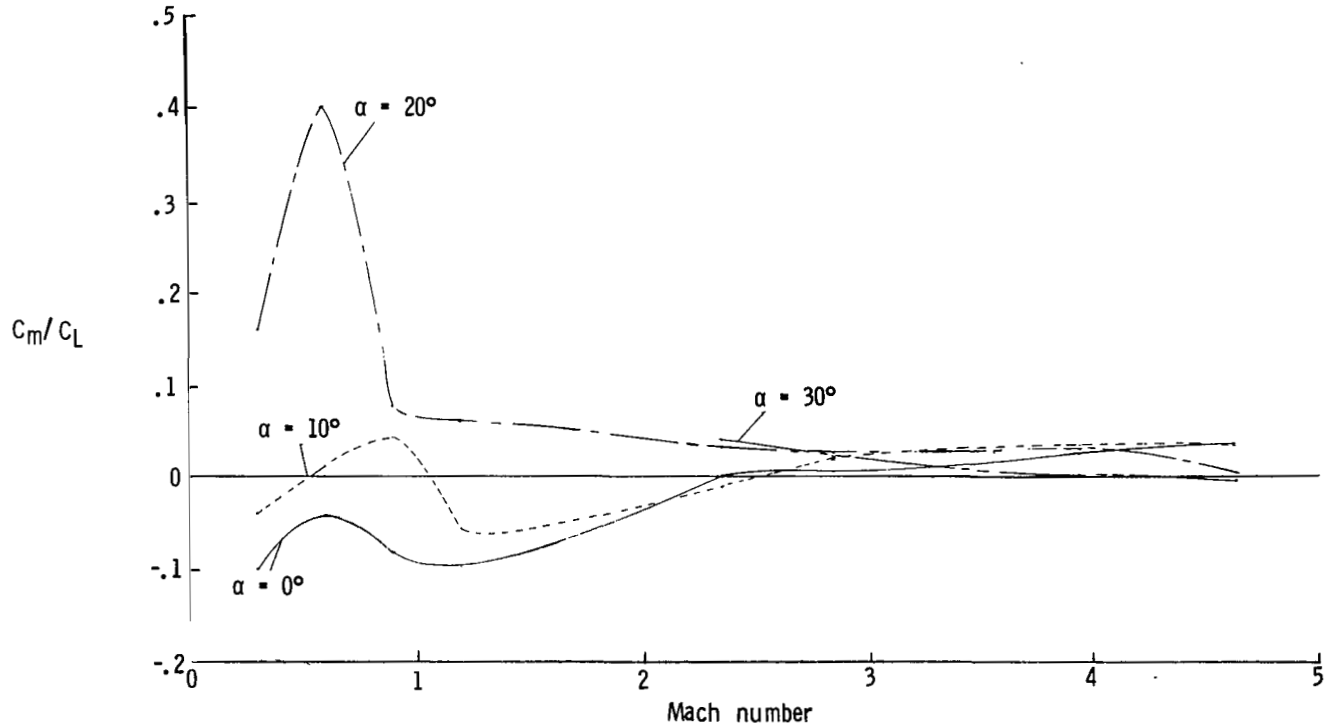

(a) C_m/C_L as a function of Mach number.

Figure 20.- Summary of longitudinal trim characteristics.

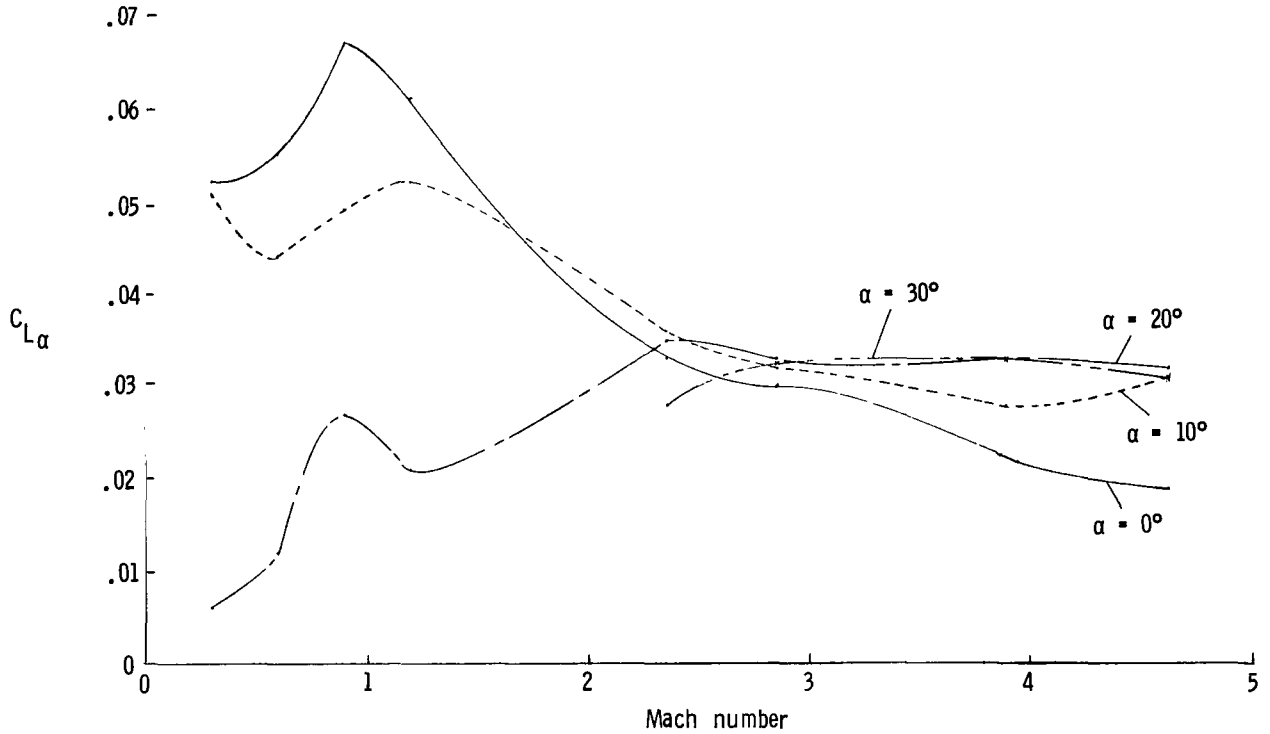

(b) C_{L_α} as a function of Mach number.

Figure 20.- Continued.

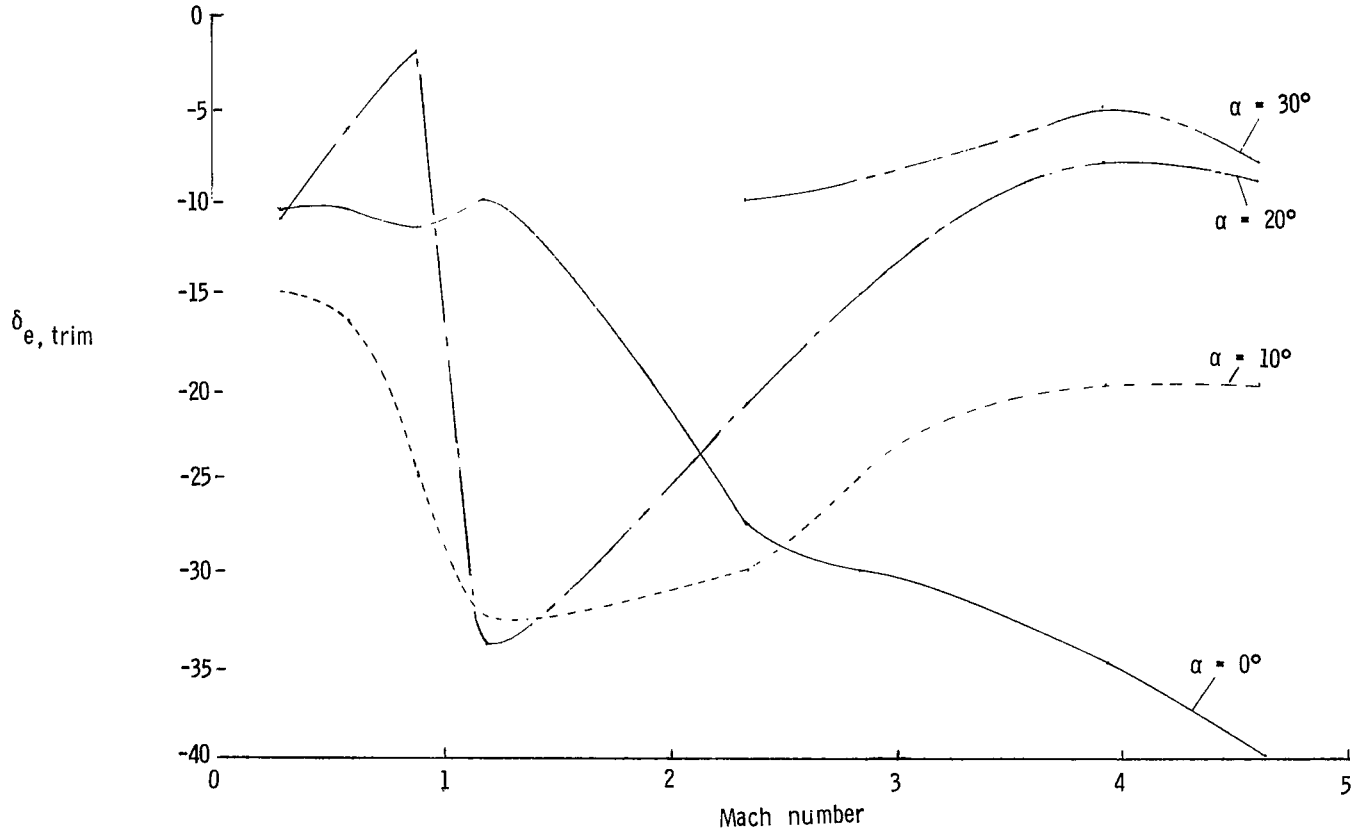

(c) $\delta_{e,trim}$ as a function of Mach number.

Figure 20.- Continued.

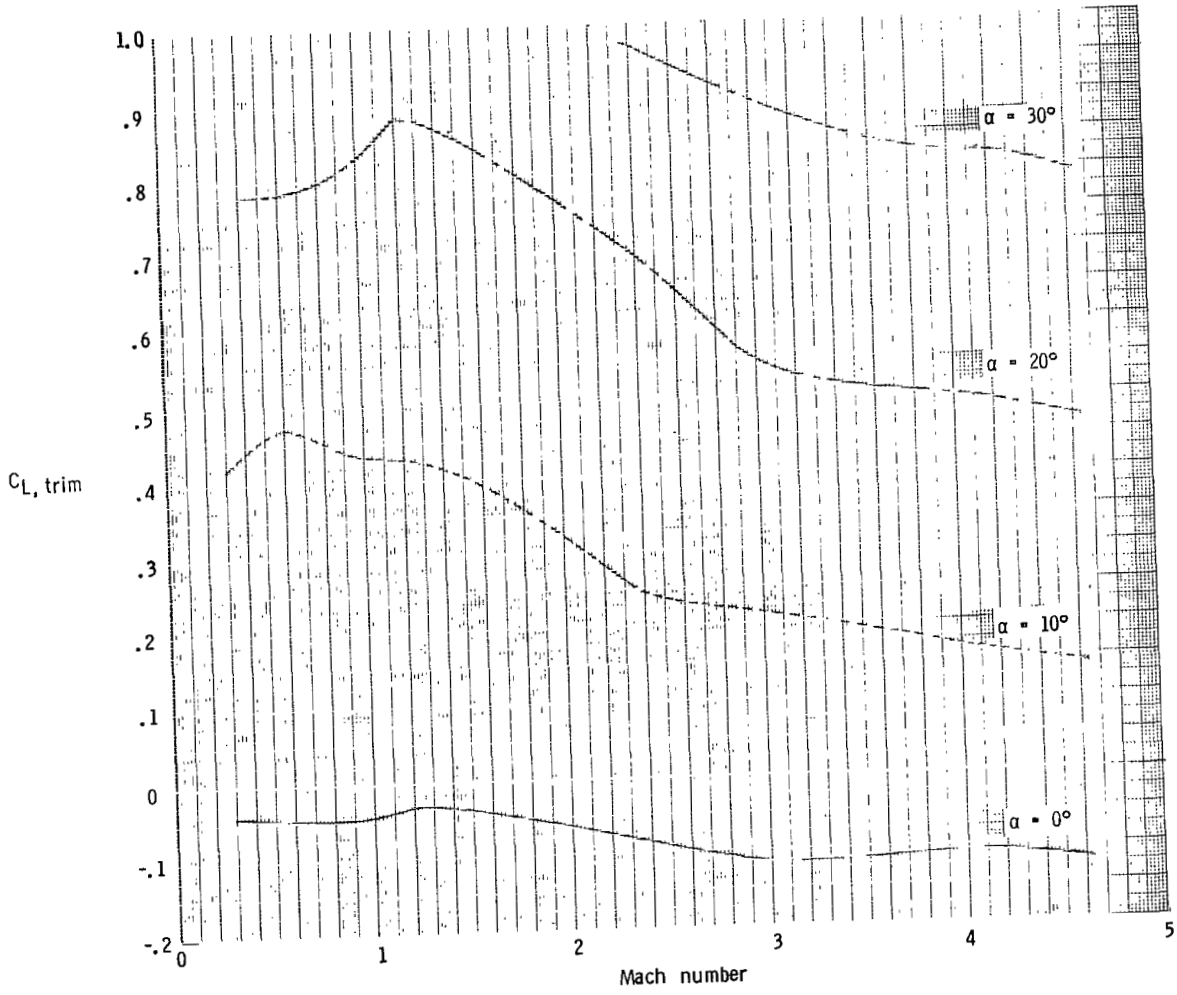

(d) $C_{L,trim}$ as a function of Mach number.

Figure 20.- Continued.

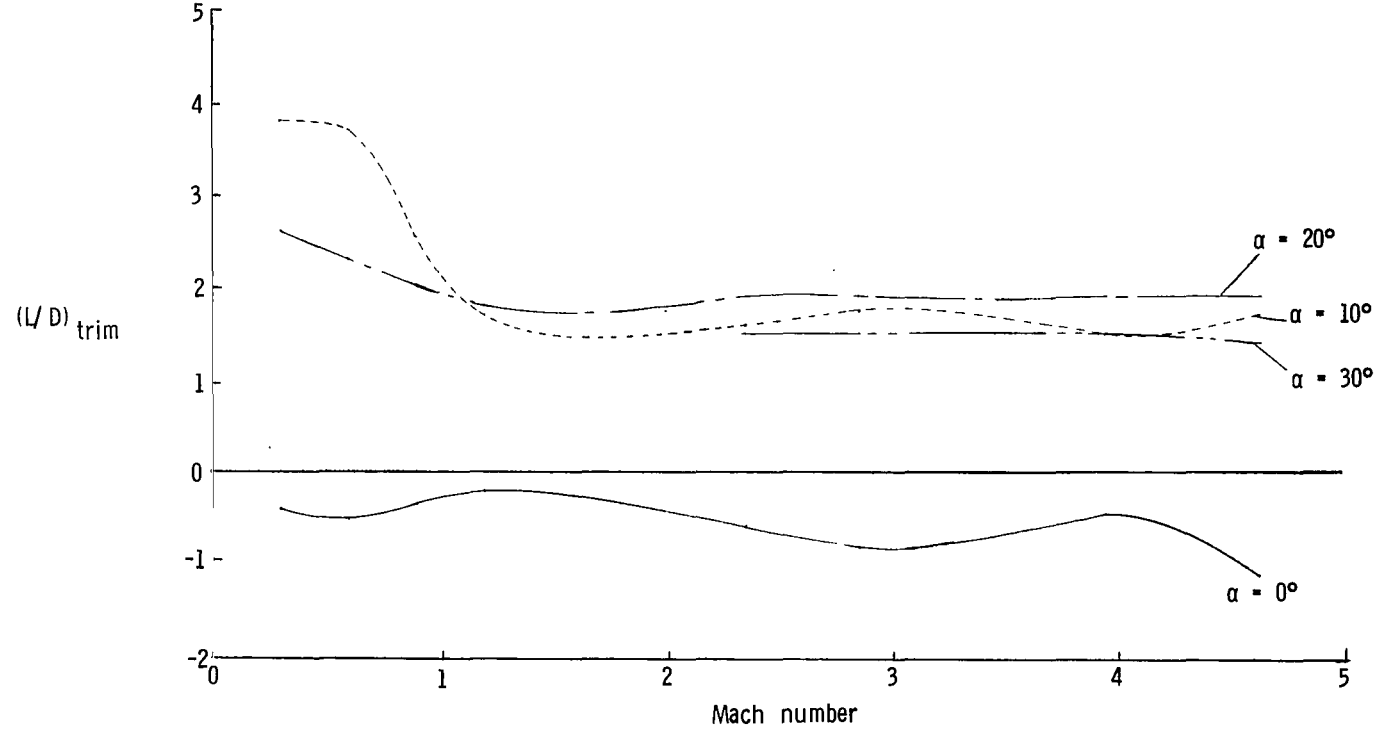

(e) $(L/D)_{trim}$ as a function of Mach number.

Figure 20.- Concluded.

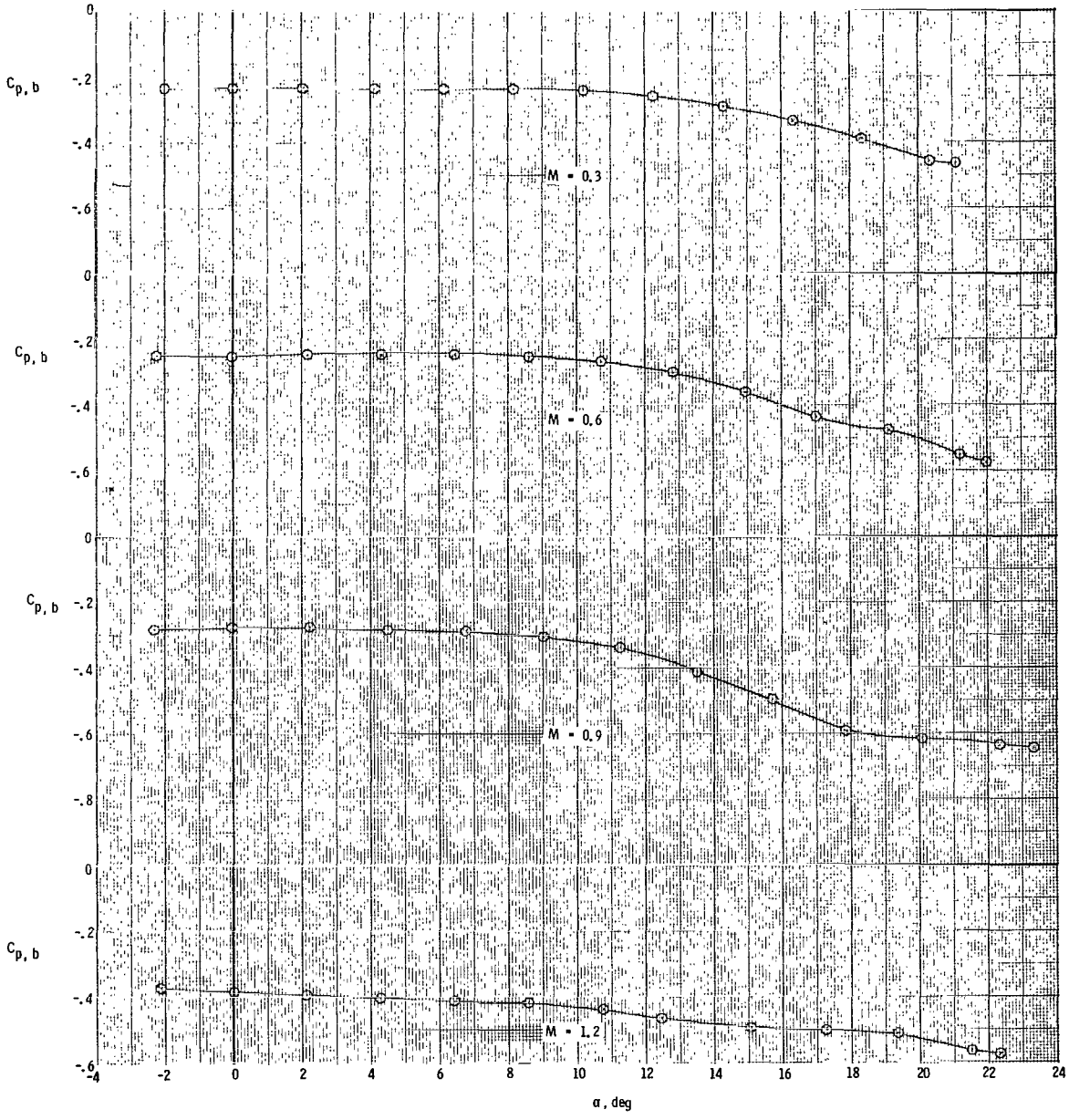

(a) M = 0.3 to 1.2.

Figure 21.- Base-pressure data measured during the tests.

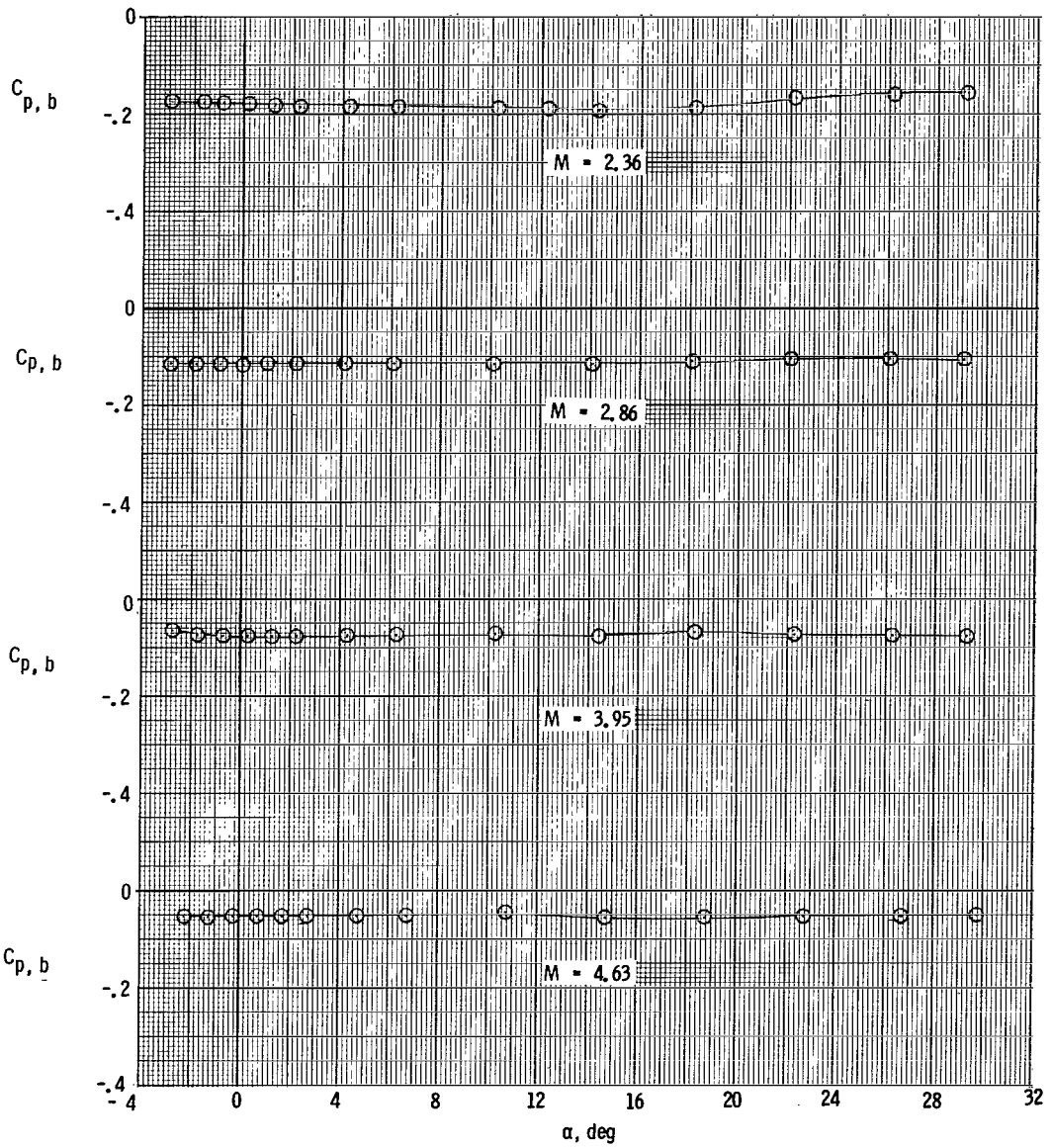

(b) M = 2.36 to 4.63.

Figure 21.- Concluded.

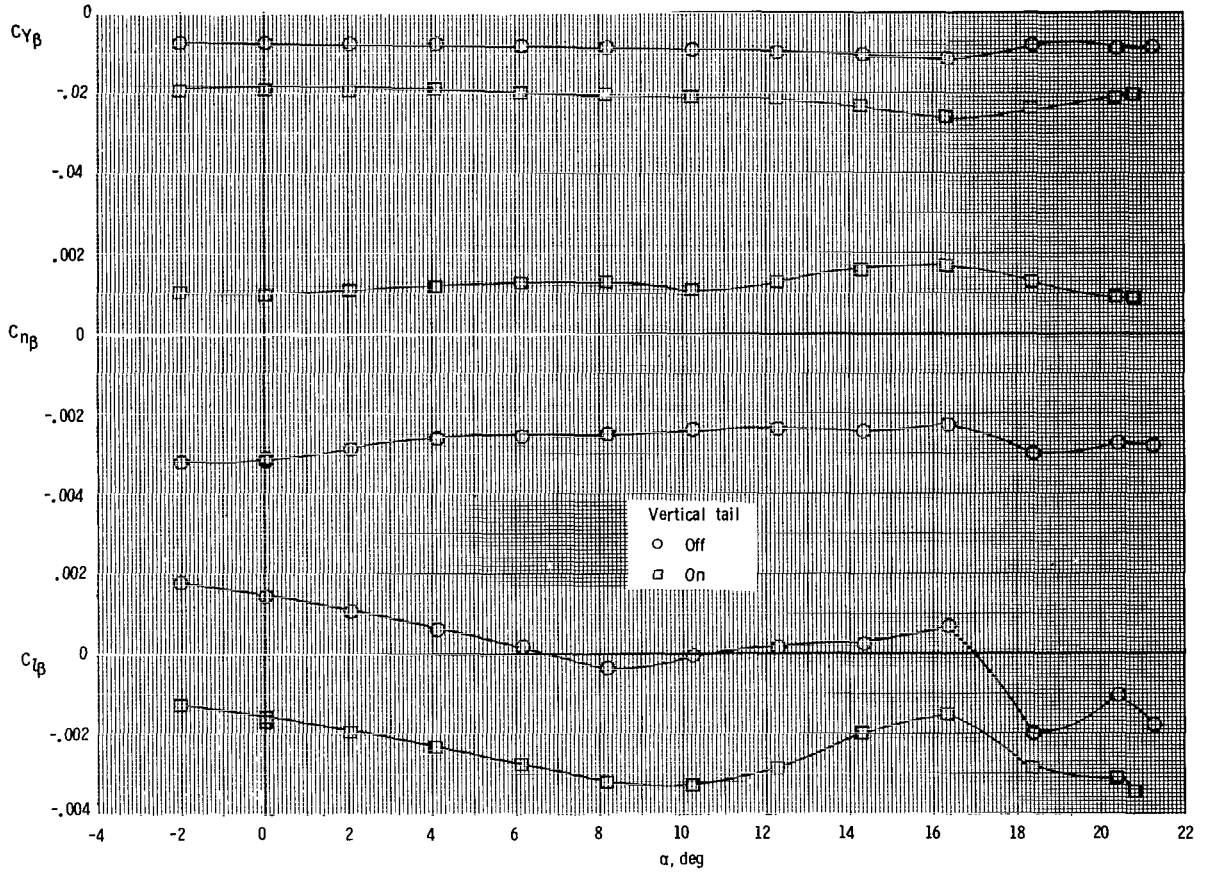

(a) M = 0.3.

Figure 22.- Static lateral-directional stability characteristics of the model.

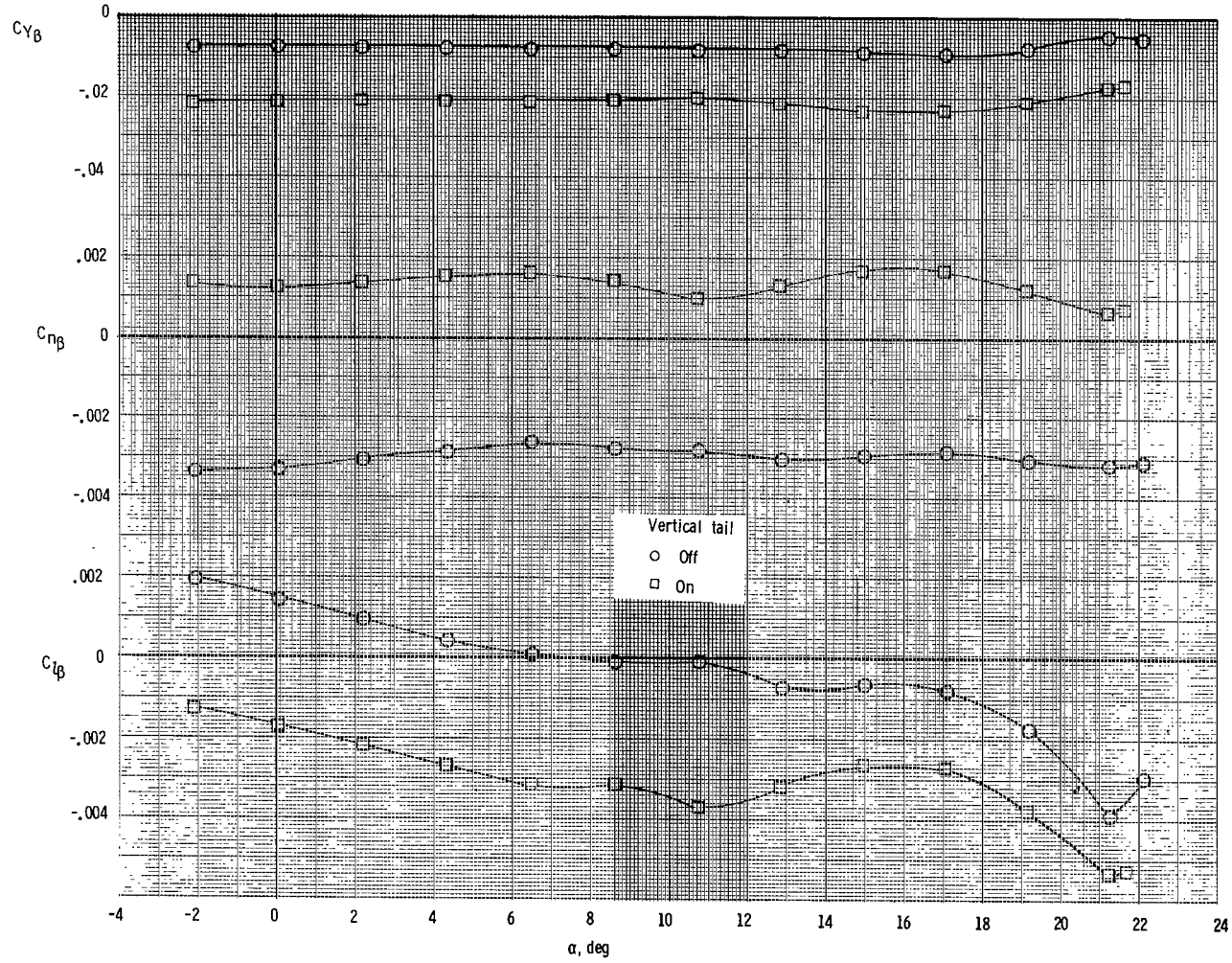

(b) M = 0.6.

Figure 22.- Continued.

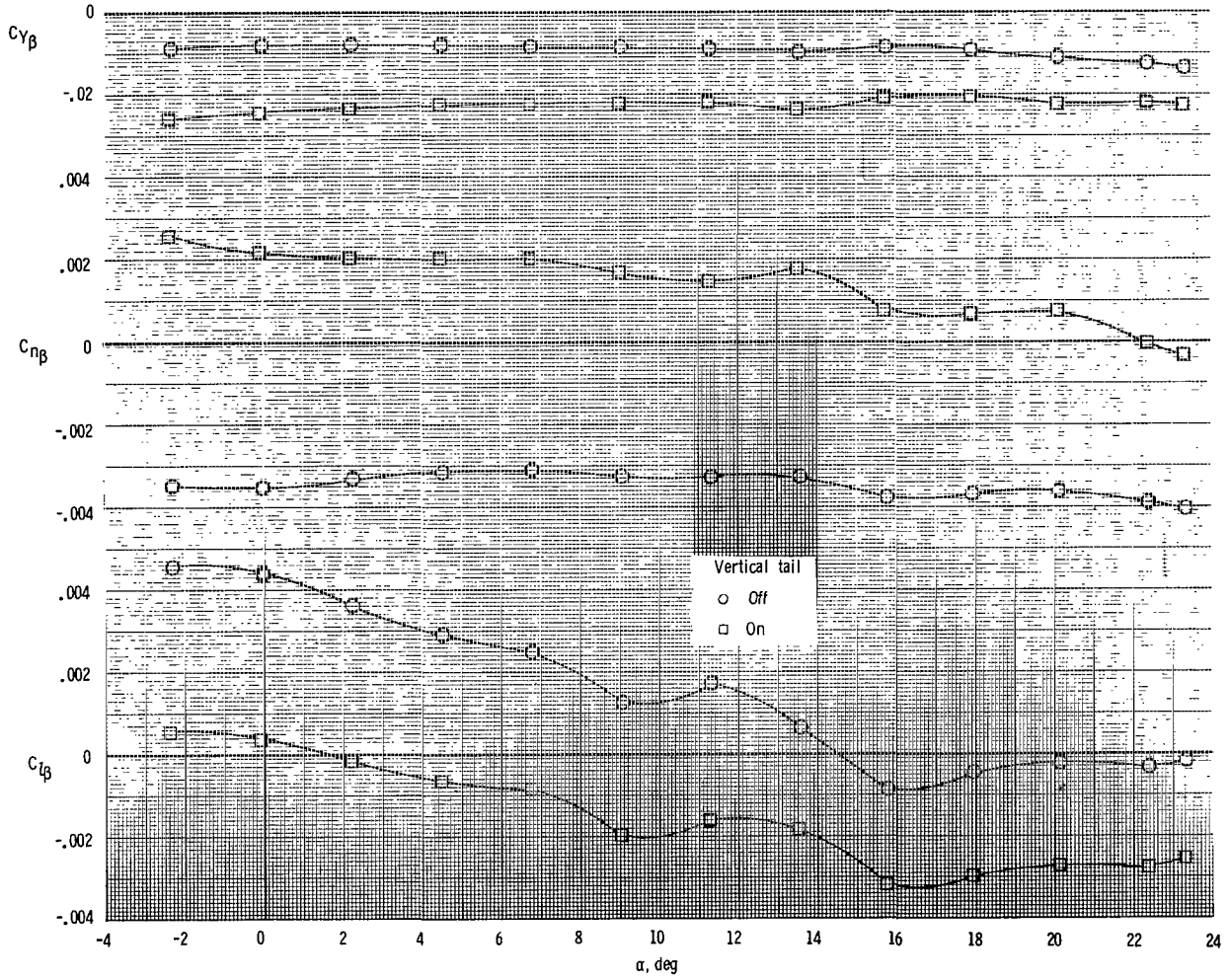

(c) M = 0.9.

Figure 22.- Continued.

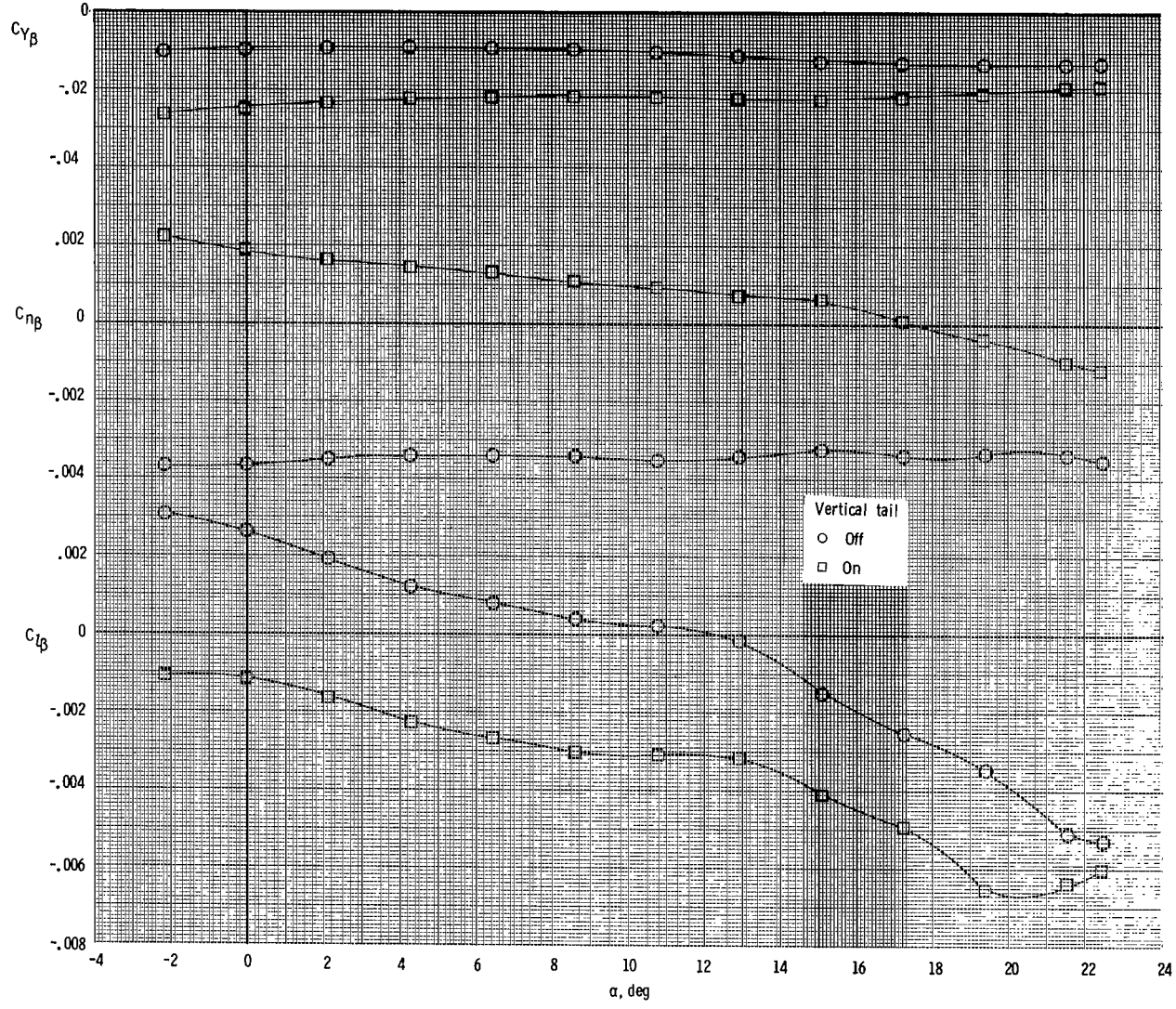

(d) M = 1.2.

Figure 22.- Continued.

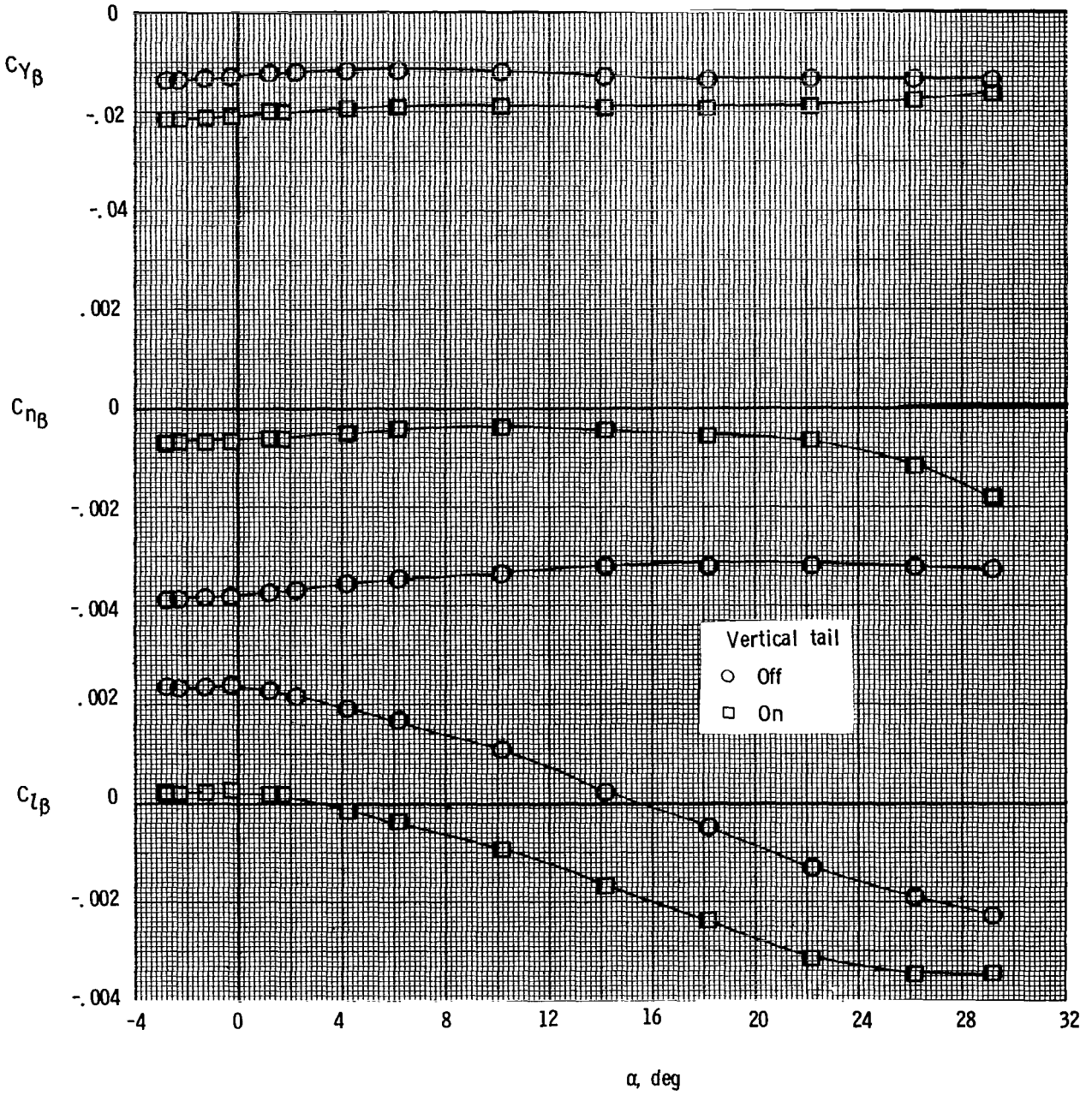

(e) M = 2.36.

Figure 22.- Continued.

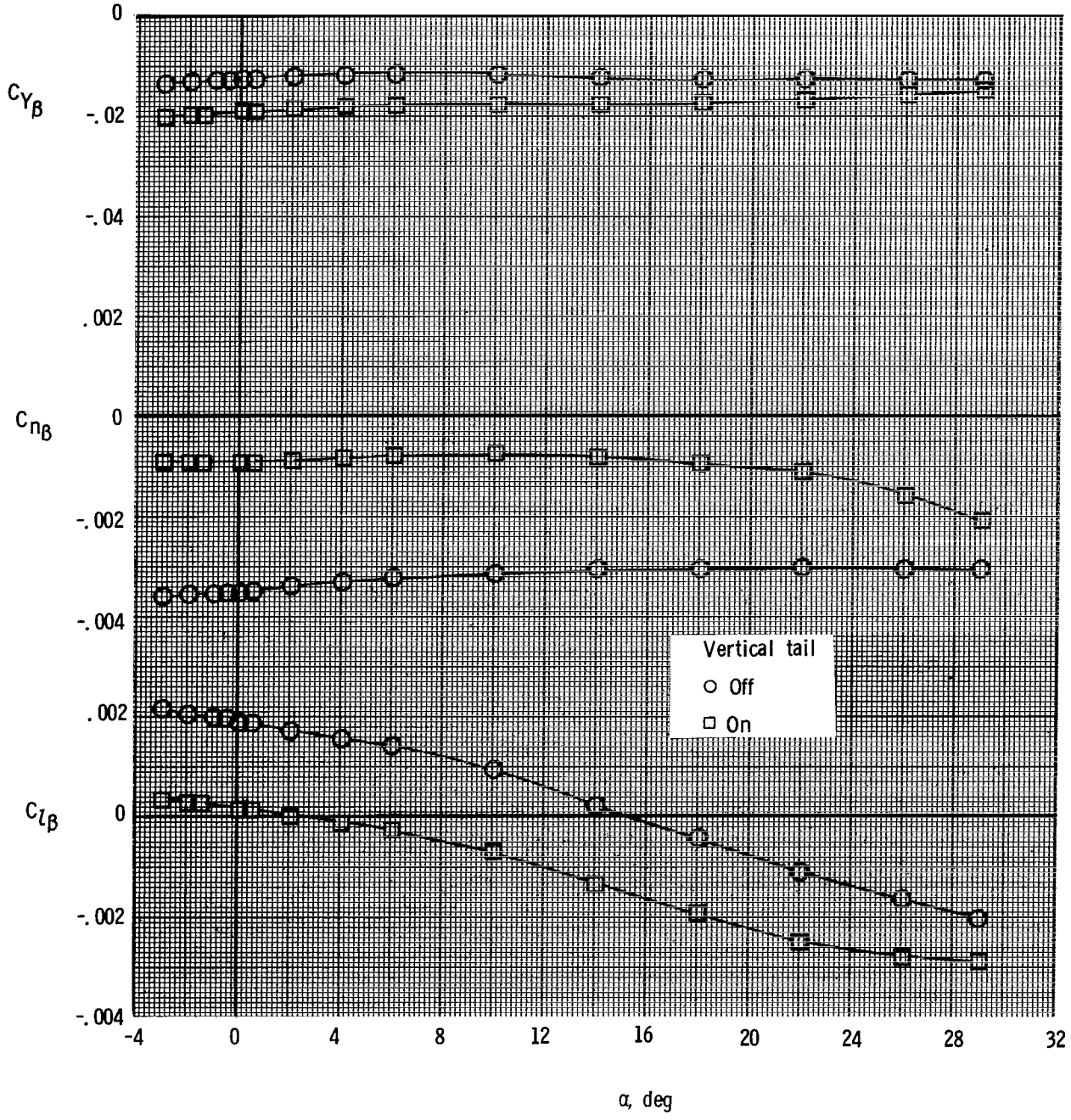

(f) M = 2.86.

Figure 22.- Continued.

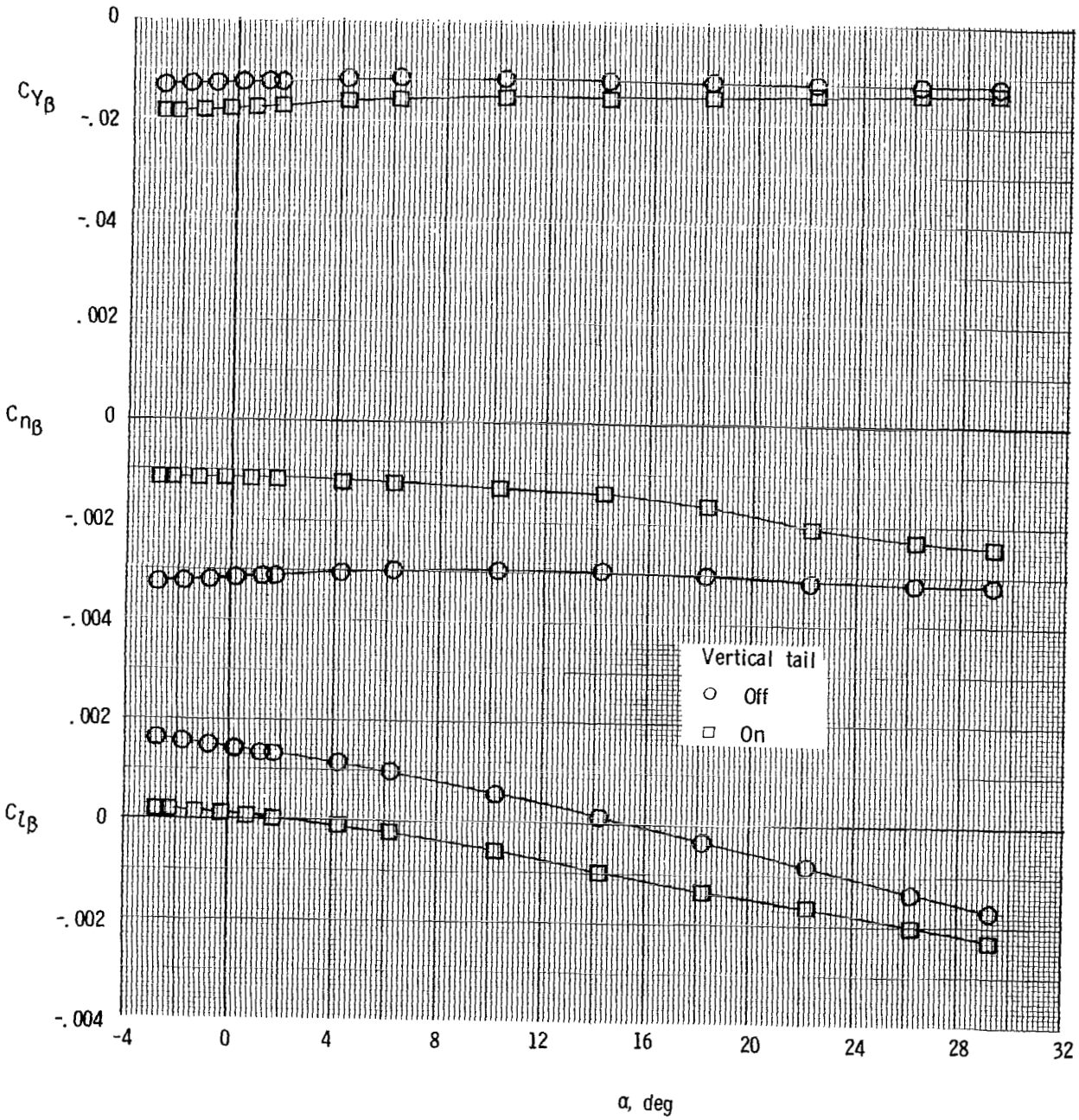

(g) M = 3.95.

Figure 22.- Continued.

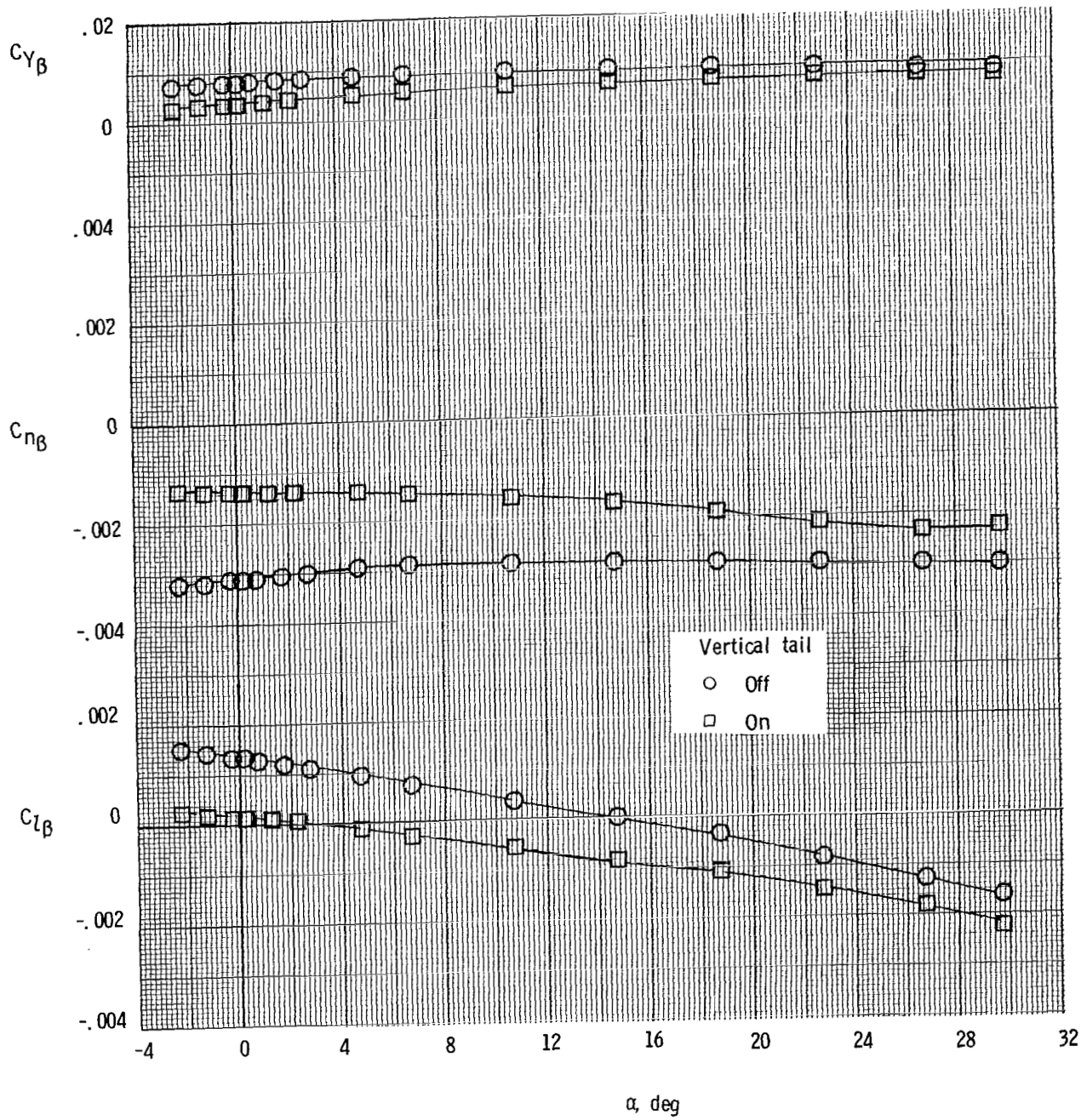

(h) M = 4.63.

Figure 22.- Concluded.

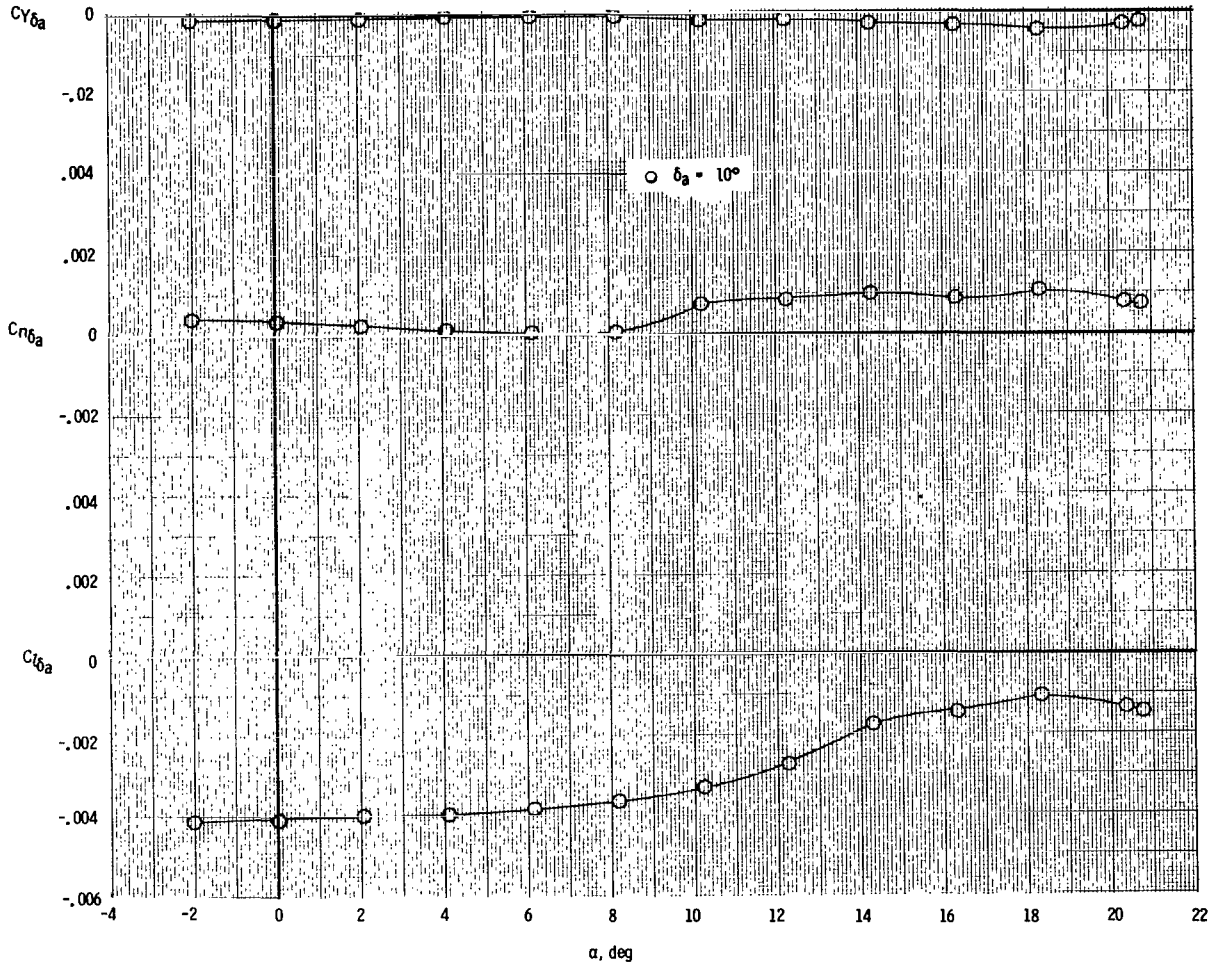

(a) M = 0.3.

Figure 23.- Aileron control effectiveness.

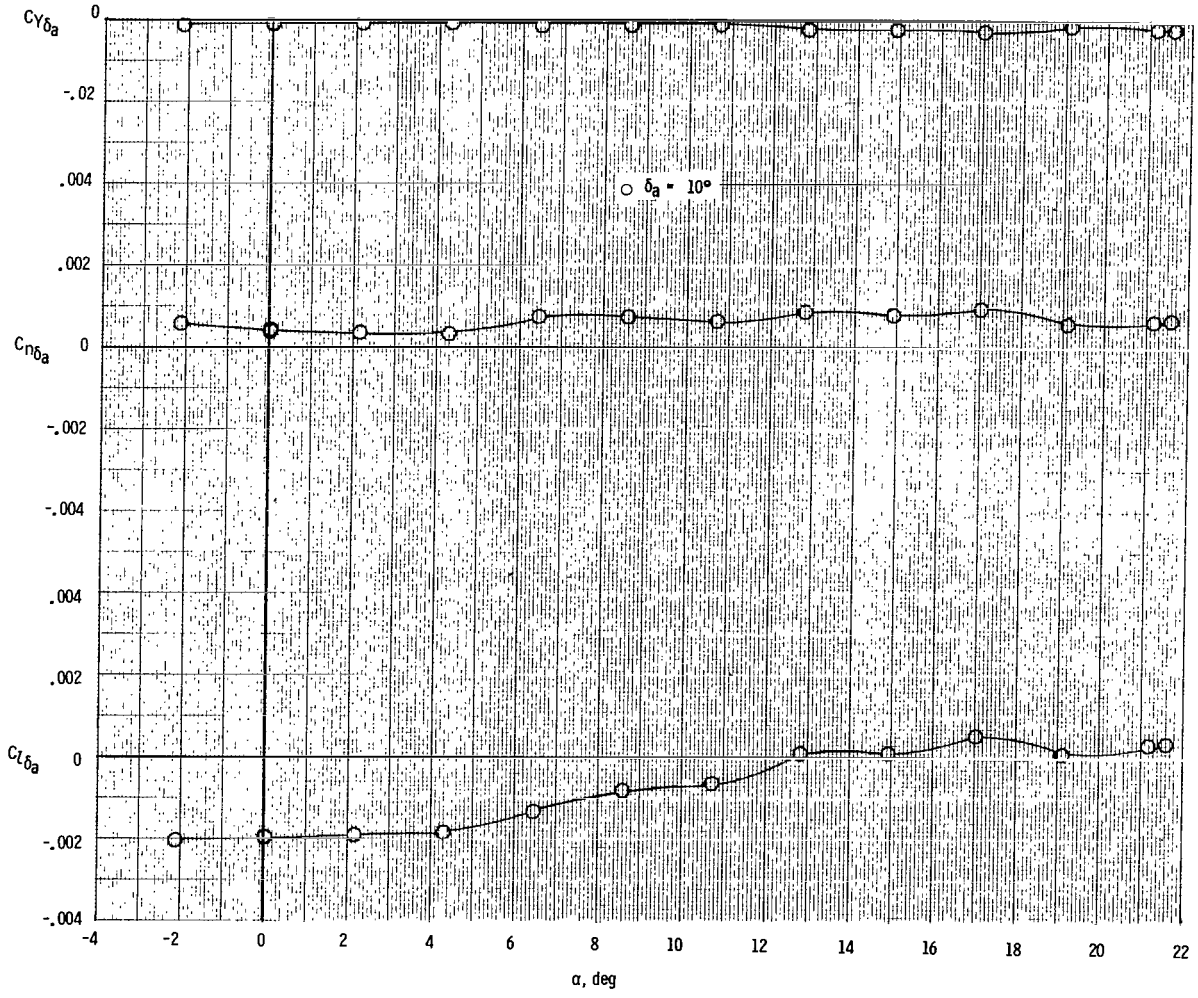

(b) M = 0.6.

Figure 23.- Continued.

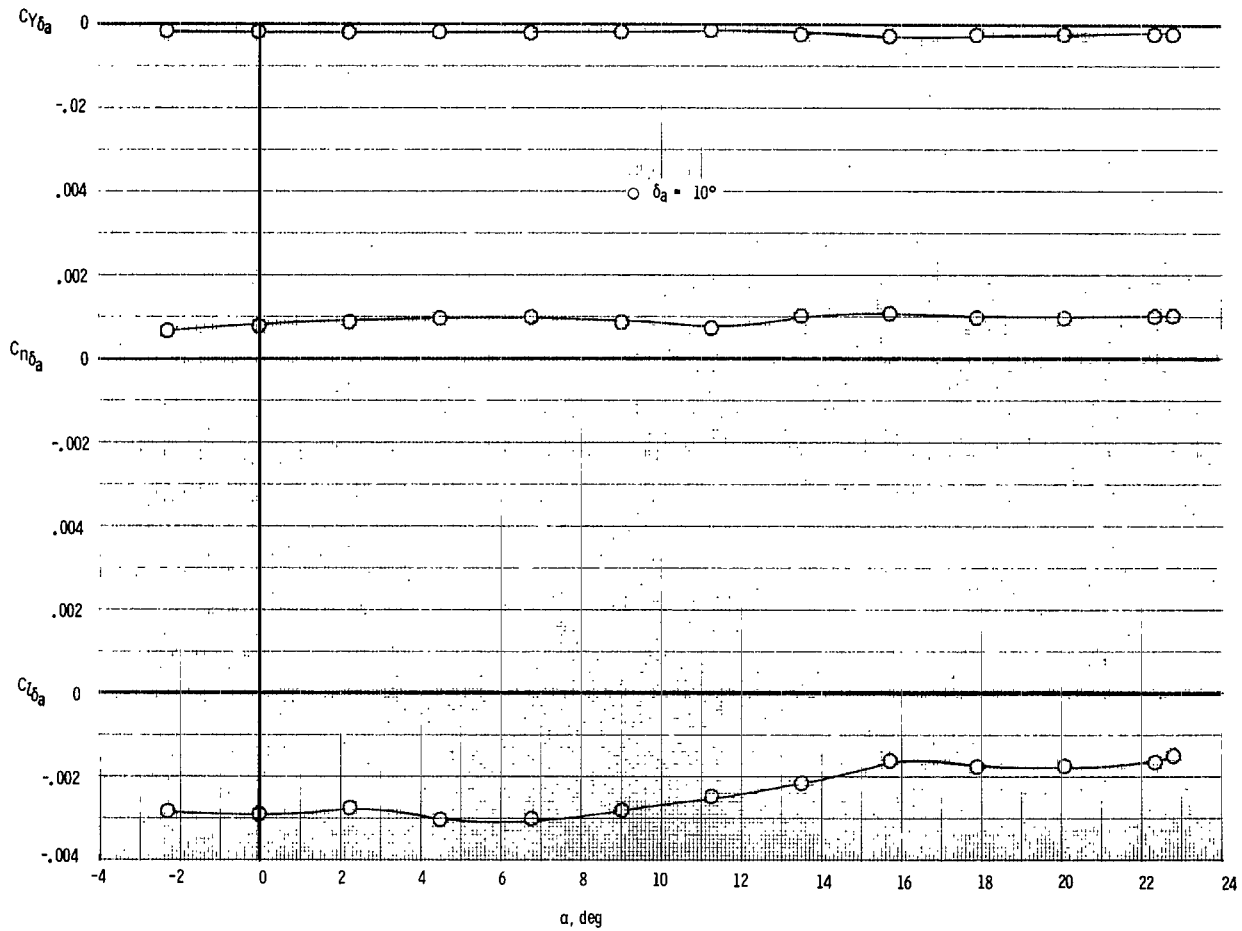

(c) M = 0.9.

Figure 23.- Continued.

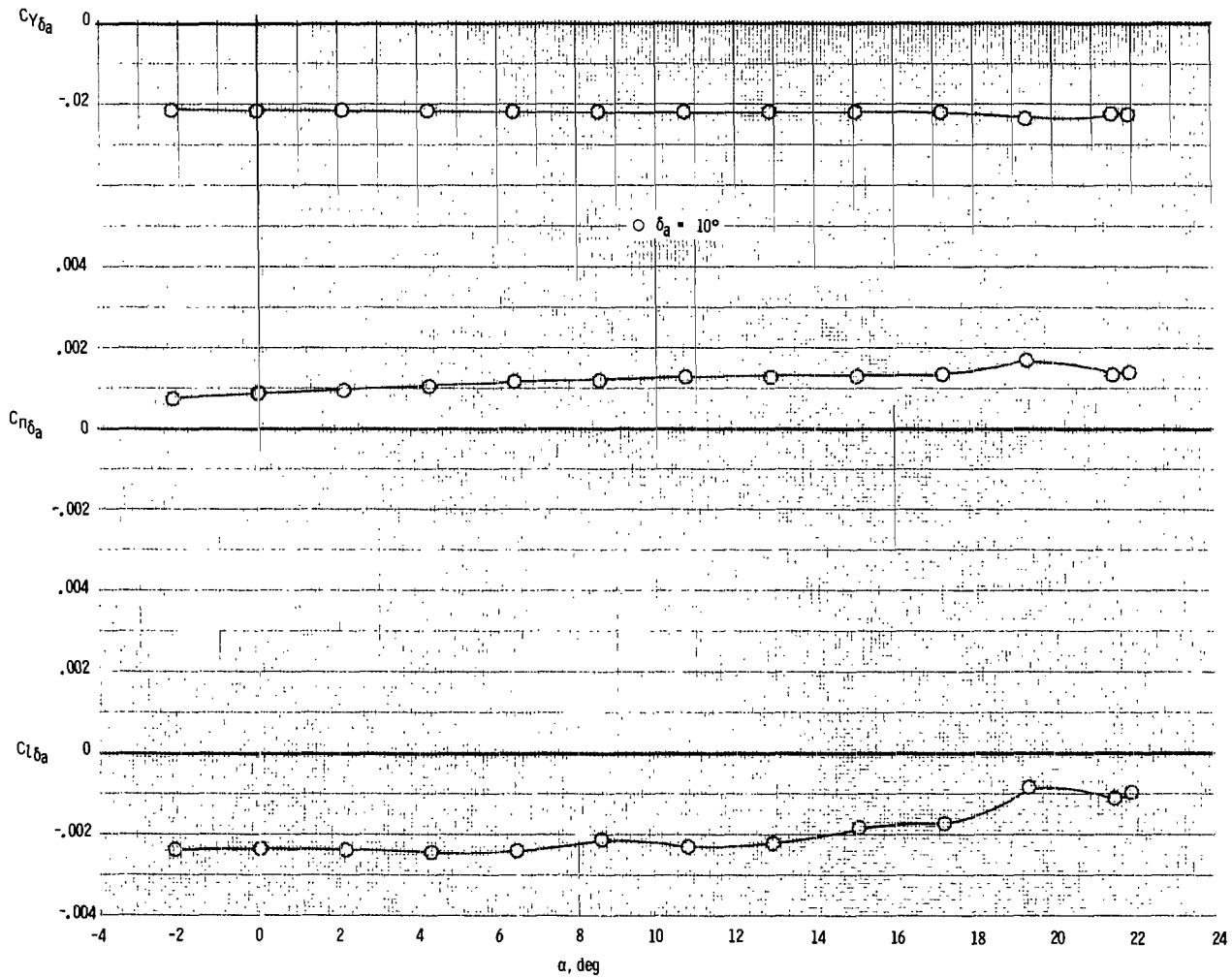

(d) M = 1.2.

Figure 23.- Continued.

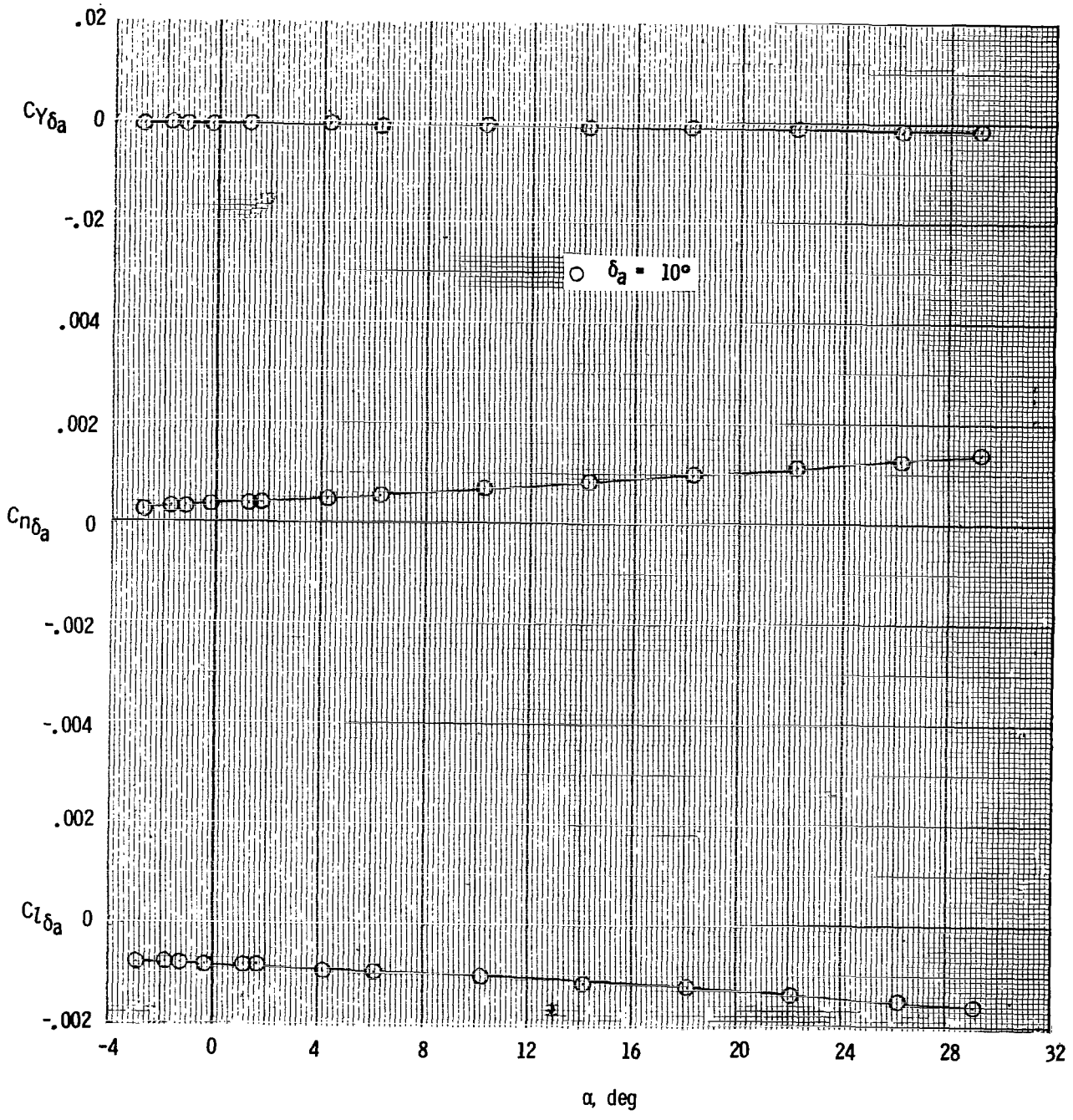

(e) M = 2.36.

Figure 23.- Continued.

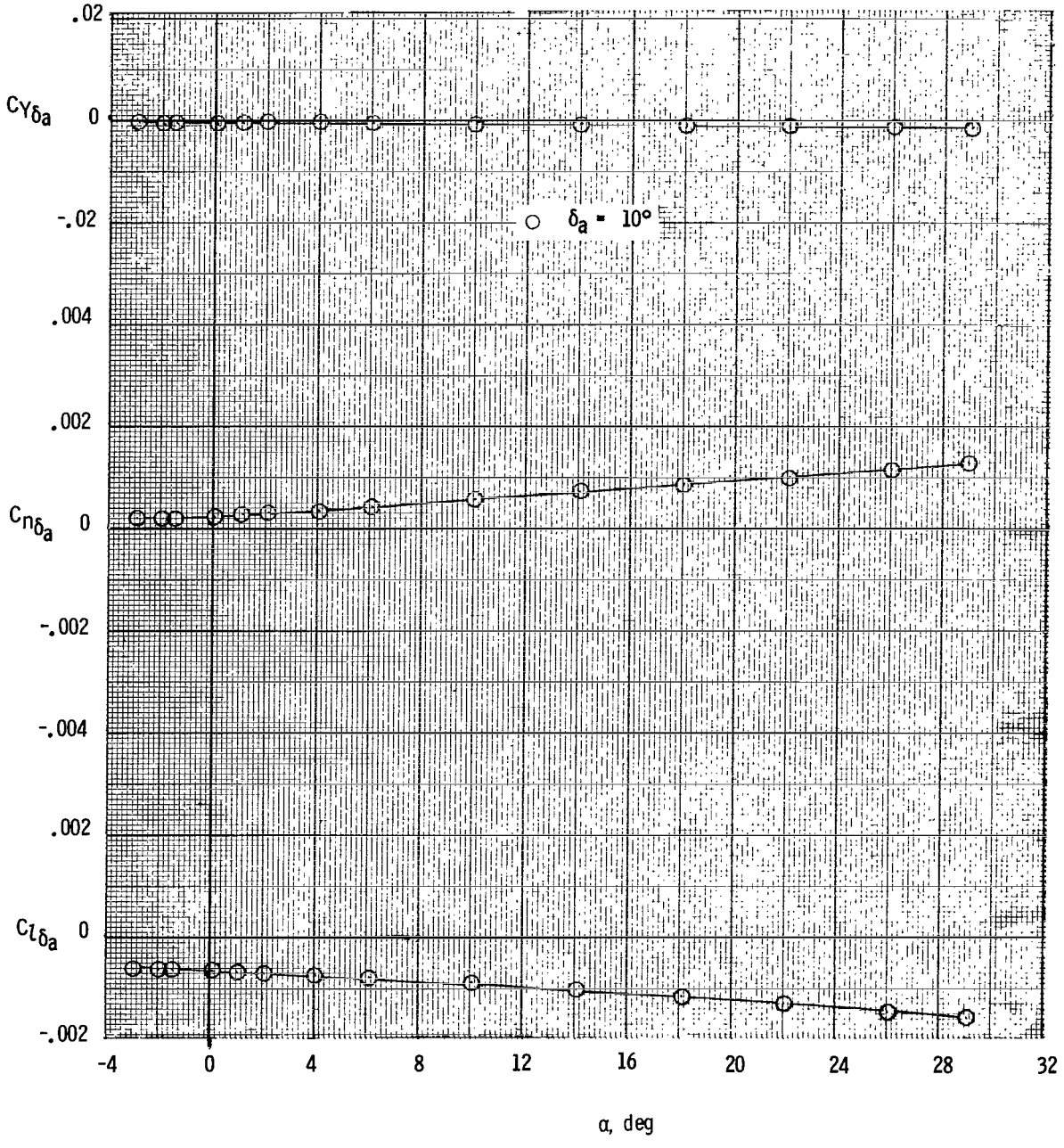

(f) M = 2.86.

Figure 23.- Continued.

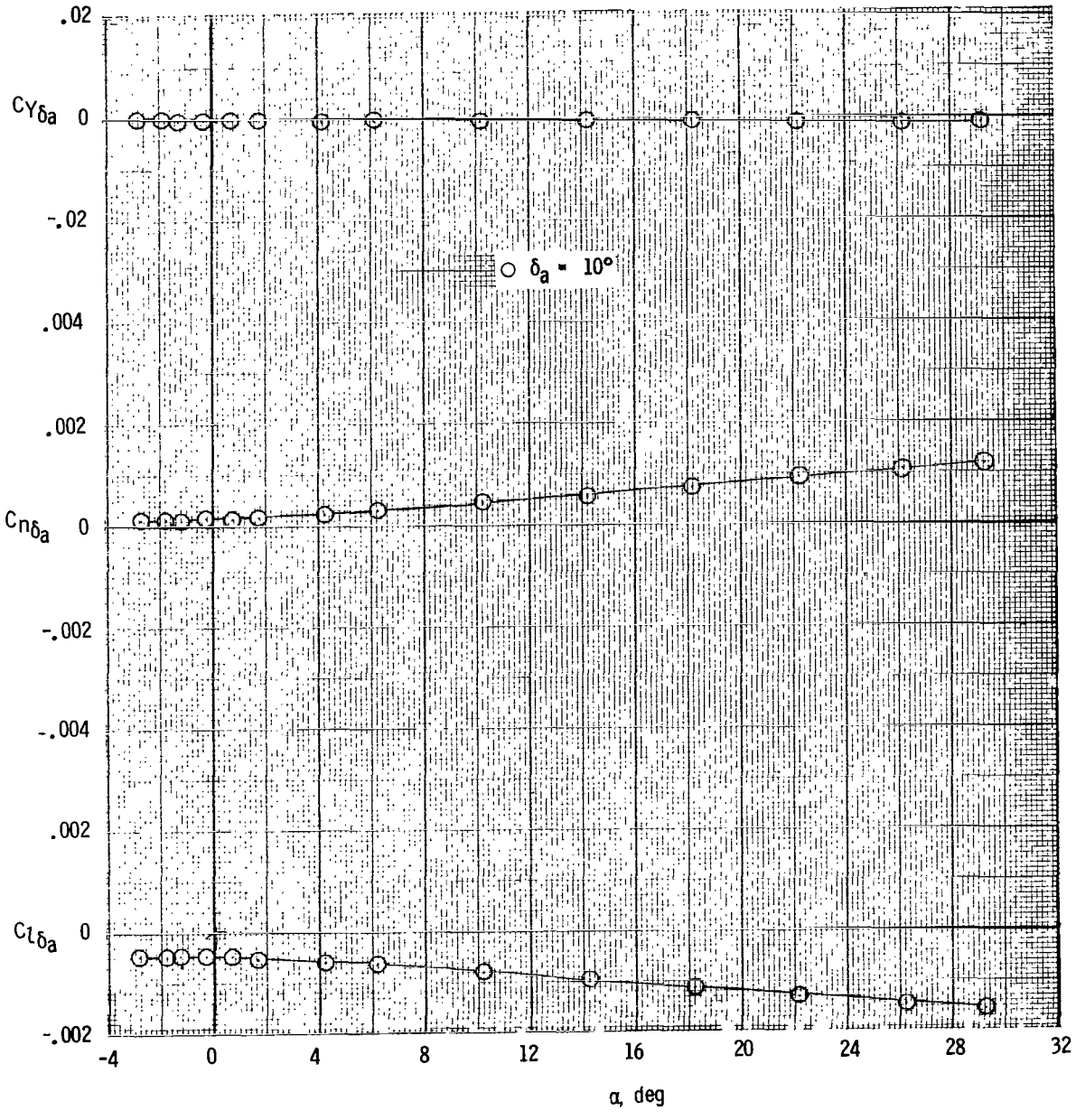

(g) M = 3.95.

Figure 23.- Continued.

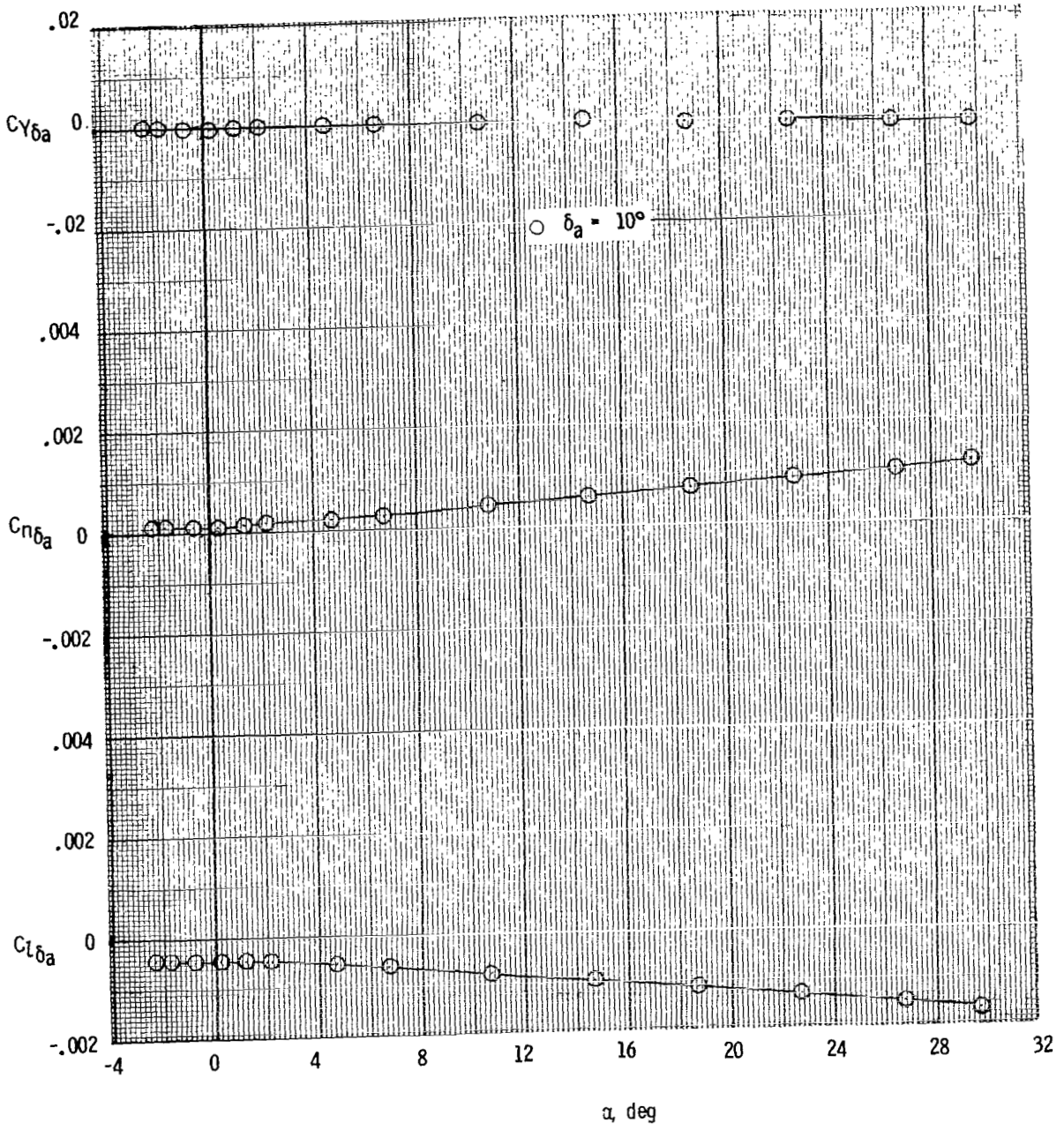

(h) M = 4.63.

Figure 23.- Concluded.

1. Report No.	2. Government Accession No.	3. Recipient's Catalog No.
NASA TP-1233		

4. Title and Subtitle
STATIC AERODYNAMIC CHARACTERISTICS OF A WINGED SINGLE-STAGE-TO-ORBIT VEHICLE AT MACH NUMBERS FROM 0.3 TO 4.63

5. Report Date
August 1978

6. Performing Organization Code

7. Author(s)
Delma C. Freeman, Jr., and Roger H. Fournier

8. Performing Organization Report No.
L-12200

9. Performing Organization Name and Address
NASA Langley Research Center
Hampton, VA 23665

10. Work Unit No.
506-26-33-03

11. Contract or Grant No.

12. Sponsoring Agency Name and Address
National Aeronautics and Space Administration
Washington, DC 20546

13. Type of Report and Period Covered
Technical Paper

14. Sponsoring Agency Code

15. Supplementary Notes

16. Abstract

An investigation has been conducted in the Langley 8-foot transonic pressure tunnel and the Langley Unitary Plan wind tunnel to determine the longitudinal and lateral-directional aerodynamic characteristics of a winged single-stage-to-orbit vehicle. The model was tested over a Mach number range from 0.3 to 4.63 for an angle-of-attack range from -4° to 30° at both 0° and 5° sideslip.

17. Key Words (Suggested by Author(s))
Entry-vehicle aerodynamics
Space transportation systems
Aerodynamics

18. Distribution Statement
Unclassified – Unlimited

Subject Category 02

19. Security Classif. (of this report)	20. Security Classif. (of this page)	21. No. of Pages	22. Price*
Unclassified	Unclassified	116	$6.50

*For sale by the National Technical Information Service, Springfield, Virginia 22161

NASA-Langley, 1978

National Aeronautics and
Space Administration

Washington, D.C.
20546

Official Business
Penalty for Private Use, $300

THIRD-CLASS BULK RATE

Postage and Fees Paid
National Aeronautics and
Space Administration
NASA-451

3 1 1U,A, 072178 S00903DS
DEPT OF THE AIR FORCE
AF WEAPONS LABORATORY
ATTN: TECHNICAL LIBRARY (SUL)
KIRTLAND AFB NM 87117

NASA

POSTMASTER: If Undeliverable (Section 158 Postal Manual) Do Not Return